Simultaneous electrochemical detection of serotonin and ascorbic acid at MWCNT- antimony oxide nanocomposite modified electrode

P.C MOTSAATHEBE

orcid.org/0000-0002-4235-9850

Dissertation submitted in fulfilment of the requirements for the degree *Master of Science in Chemistry* at the North-West University

Supervisor: Prof O.E Fayemi

Examination: 2021

Student number: 27242412

DECLARATION

I, Pholoso Calvin Motsaathebe, hereby state solemnly that the work undertaken in this dissertation entitled "Simultaneous electrochemical detection of serotonin and ascorbic acid at MWCNT-antimony oxide nanocomposite modified electrode" was submitted to the Department of Chemistry, North-West University, Mafikeng Campus in fulfilment of the requirements for the degree of Masters of Science in Chemistry was written by me under the supervision of Professor O.E Fayemi and has not been previously submitted at the North-West University or any other University. All external sources used in this work are acknowledged as a reference list.

.....

Pholoso Calvin Motsaathebe

ACKNOWLEDGMENTS

I would like to thank God Almighty for granting me the wisdom, gift of life, and patience to conclude this work. Furthermore, I would like to thank my sponsors, namely the National Research Foundation (NRF), Sasol Inzalo bursary foundation, and the North-West University Master's bursary. My greatest appreciation to my supervisor Prof Omolola E. Fayemi, for her continuous support, guidance, and encouragement. To my family, I am grateful to have such a supportive and caring family, which has always played an active role in my academic journey. To our sisters who became our mother, Mpho A. Motsaathebe, Mmatsela F. Motsaathebe, Rapelang G. Motsaathebe, and Onkutlwile T. Motsaathebe, I dedicate this work to all of you. To our late mother, Oronamang A. Motsaathebe, I also dedicate this work to her memory. To my twin brother, Poloko C. Motsaathebe, thank you for being there and for your moral support. To my nieces, Phemelo Motsaathebe, Gontle Motsaathebe, and Lethabo Motsaathebe thank you for always checking up on me, and I hope this serves as enough motivation for all of you. I would like to extend my warm and deepest appreciation to the Faculty of Natural and Agricultural Sciences, particularly at the Department of Chemistry. The Dean, Prof. Helen P. Drummond; the director, Prof. Lebogang Katata-Seru; and the HoD, Dr. Zimbili Mkhize. To my colleagues and friends at the MaSIM Research group and staff members in the Department of Chemistry at the North-West University. I was blessed to have such talented and goal-driven individuals like you around me. These include Mr Peter Mahlangu, Mr Sizwe Loyilane, Mr Michael Nengwekhulu, Ms Murendeni Ravele, Ms Mogomotsi Ranku, Ms Paula Maseko, Ms Othukile, Ms Sasha Mariki, Dr Gloria Uwaya, Dr Chimaijem Okpara, Mr Sheriff Balogun, Mr Elugoke Saheed, Mr Tsholofelo Mosalashuping, Mr Onkarabile G Pooe, and Mr Seleke P Mokole.

Pula Barolong!

ABSTRACT

Abnormal neurotransmitters (NTs) levels have been reported to cause various neurological diseases and disorders such as bipolar disorder, borderline personality disorder, social phobia, schizotypal personality disorder, attention deficit hyperactivity disorder (ADHD), Alzheimer's disease and Parkinson's disease, etc. Therefore, a simple, affordable, user-friendly, quick, and highly sensitive detection method is required. Electrochemical techniques offer such advantages, henceforth; this work describes the fabrication of an electrochemical sensor made-up of multi-walled carbon nanotube- antimony oxide (MWCNT-AONP) nanocomposite embedded on screen-printed carbon electrodes (SPCEs) to simultaneously detect ascorbic acid (AA) and serotonin (5-HT). Various spectroscopic and microscopic techniques were used to confirm the successful synthesis of the nanomaterials, including fourier transform infrared (FTIR) spectroscopy, ultraviolet-visible (UV-Vis) spectroscopy, x-ray diffractogram (XRD) spectroscopy, transmission electron microscopy (TEM), scanning electron microscopy (SEM), and energy-dispersive x-ray (EDX) spectroscopy. Cyclic voltammetry (CV) and square wave voltammetry (SWV) techniques were used to investigate the electrochemical properties of the electrodes. Compared to other electrodes tested, the MWCNT-AONP electrode demonstrated better electron transport and improved electrocatalytic response towards 5-HT and AA detection. For 5-HT detection, the SPCE@AONP-MWCNT electrode displayed the sensitivity, and limit of detection (LOD) of 0.2863 µA/µM, and 24 nM, with a linear range of 1.56×10^{-8} – 1.28×10^{-7} M respectively, and 0.4789 µA/µM, and 278 nM in the 1.60×10^{-8} – 6.40×10^{-7} M concentration range for AA detection using SWV. Three well-separated oxidation peaks were observed in a mixed system containing AA, 5-HT, and dopamine (DA); the 5-HT– DA and DA–AA potential separations were 170 and 250 mV, respectively, owing to the synergistic effect of multi-walled carbon nanotubes (MWCNTs), and antimony oxide nanoparticles (AONPs). Linear responses were obtained for 5-HT, and AA in the 35 – 205 µM ($R^2 = 0.9940$), and 45 – 190 µM ($R^2 = 0.9927$) concentration ranges, with detection limits of 24 and 17 µM, respectively. Compared to the literature, the acquired LOD values for detecting AA and 5-HT were better. The proposed electrode exhibited excellent selectivity and outstanding anti-interference behaviour. The applicability of the sensor to detect AA and 5-HT in oranges and tomatoes exhibited outstanding recoveries above 99.12 and 91.32 %, with RSD (relative standard deviation) values of 3.52 and 2.57 %, respectively. The obtained results underpin the fabricated sensor's potential applicability to determine AA and 5-HT simultaneously in bodily fluids.

Keywords: serotonin, ascorbic acid, multi-walled carbon nanotubes, antimony oxide nanoparticles, electrochemical detection.

LIST OF ABBREVIATIONS

AA	Ascorbic acid
AONPs	Antimony oxide nanoparticles
Ag/AgCl	Silver/silver chloride reference electrode
ADHD	Attention deficit hyperactivity disorder
AMP	Amperometry
Arb	Absorbance
AE	Auxiliary electrode
CE	Capillary electrophoresis
CV	Cyclic voltammetry
CNTs	Carbon nanotubes
DA	Dopamine
DWCNTs	Double-walled carbon nanotubes
D	Dimensions
EP	Epinephrine
EIS	Electrochemical impedance spectroscope
EDX	Energy dispersive X-ray
FTIR	Fourier transformed infrared spectroscope
GABA	Gamma-aminobutyric acid
LOQ	Limit of quantification
LOD	Limit of detection
MWCNTs	Multi-walled carbon nanotubes
MOFs	Metal-organic frameworks
MO	Metal oxide
MONPs	Metal oxide nanoparticles
NTs	Neurotransmitters

NPs	Nanoparticles
DMF	N,N-dimethylformamide
PBS	Phosphate-buffered saline
pH	Potential of hydrogen
RSD	Relative standard deviation
R.E	Reference electrode
SPEs	Screen-printed electrodes
SPCEs	Screen-printed carbon electrodes
SWV	Square wave voltammetry
SWCNTs	Single walled carbon nanotubes
5-HT	Serotonin
SEM	Scanning electron microscope
TEM	Transmission electron microscope
WO_3NPs	Tungsten trioxide nanoparticles
UA	Uric acid
UV-Vis	Ultraviolet-visible spectroscope
XRD	X-ray diffraction spectroscope
ZnONPs	Zinc oxide nanoparticles

LIST OF SYMBOLS

A	Active surface area
E_{pa}	Anodic peak potential
I_{pa}	Anodic peak current
E_{pc}	Cathodic peak potential
I_{pc}	Cathodic peak current
c	Constant
D	Diffusion coefficient
F	Faraday's constant
$E_{1/2}$	Half-wave potential
K	Kelvin
μ	Micro
nM	Nanomolar
n	Number of electrons
v	Scan rate
E^o	Standard potential
V	Voltage
E	Potential
R	Universal gas constant
λ	Wavelength

LIST OF FIGURES

LIST OF TABLES

LIST OF SCHEMES

TABLE OF CONTENTS

CHAPTER 1: Introduction and problem statement

1.1. Neurotransmitters

Neurotransmitters (NTs) are important endogenous chemical messengers that control and facilitate communication between nerve cells and the body [1, 2]. Acetylcholine was the first neurotransmitter discovered in 1921 by a Noble Prize-winning German pharmacologist, Otto Loewi [3]. His discovery-helped scientists better understand the role and effects of NTs on biological and physiological processes in human beings. Since then, many other NTs have been discovered, which include serotonin (5-HT), dopamine (DA), glutamate, opioids, endorphins, norephedrine (NE), adrenaline (Epi), gamma-aminobutyric acid (GABA), histamine, and several others. Catecholamines (5-HT, DA, NE, and Epi) are the most important and widely studied class of NTs [4]. NTs aid in stress management, attitude, emotions, rest, cognition, memory, hunger, attention, and other cognitive functions. However, altered levels of NTs in the blood have been associated with depression, stress, schizophrenia, drug addictions, Alzheimer's disease, bipolar disorder, attention deficit hyperactivity disorder (ADHD), Parkinson's disease, and many more [3]. Factors such as stress, poor diet, medications (recreational or prescription), neurotoxins, genetic predisposition, alcohol and caffeine consumption have been noted as contributors to abnormal NTs levels in the body [4].

Since NTs in the blood can serve as biological markers of disease, scientists have used various analytical methods to detect them. These techniques include capillary electrophoresis (CE), high-pressure liquid chromatography (HPLC), microdialysis, and mass spectrometry (MS), in combination with imaging methods to enhance ultra-sensitivity and resolution [5, 6]. However, these methods have many disadvantages, including high cost, cumbersomeness, slow response, and difficulty in implementation, while some require trained laboratory personnel [7]. In contrast, electrochemical techniques are proven highly sensitive, easy to use, inexpensive, and offer rapid analysis in a short period allowing for real-time analysis of NTs in living organisms and *in vivo* assays [8].

Conversely, the presence of NTs with other compounds in bodily fluids with comparable oxidation potentials, called interfering compounds, presents a significant challenge for detecting NTs at bare electrodes (platinum, glassy carbon, and gold electrodes). These interfering compounds reduce the reproducibility and selectivity of the electrodes when used as NTs sensors in the blood. The second challenge is the availability of interfering compounds such as ascorbic acid (AA) and uric acid (UA) at concentrations higher than NTs. This causes surface electrode biofouling and reduces electrode sensitivity, resulting in a poor sensor. For instance, the AA concentration in the blood is reported to be 100 - 1000 times higher than 5-HT [9]. To solve the mentioned challenges, various nanomaterials such as conductive polymers, metal nanoparticles, metal oxide nanoparticles, organic and inorganic materials, and carbon nanotubes have been used to fabricate electrodes to produce enhanced sensors for NTs detection in living organisms [10, 11]. The electrodes are often fabricated with a nanocomposite material to enhance electron transfer kinetics and electro-catalytic response.

1.1.1. 5-HT and AA

Although a lot of work has been done to determine 5-HT and AA simultaneously using various sensors electrode modified with metal oxide nanoparticles, metal nanoparticles, nanofibers, conducting polymers, and carbon-based nanocomposite [12-21], however, no studies have reported on the simultaneous electrochemical detection of 5-HT and AA using multi-walled carbon nanotube- antimony oxide (MWCNT-AONP) nanocomposite embedded on screen-printed carbon electrodes (SPCEs). Therefore, this dissertation reports the synthesis and characterization of antimony oxide nanoparticles (AONPs), functionalized multi-walled carbon nanotubes (f-MWCNTs), and the construction of SPCE@MWCNT-AONP nanocomposite as a novel sensor for AA and 5-HT detection in oranges and tomatoes, respectively. The proposed novel sensor displayed excellent recoveries, low LOD values, enhanced sensitivity, and selectivity due to its excellent electron transfer kinetics and high surface area resulting from the synergy between the two nanomaterials.

1.2. Sensors

A sensor is a device that responds to an external stimulus, such as heat, light, pressure, sound, or movement, by emitting an electrical impulse that can be used to measure an inherent property of a specific material [22]. Sensors are mainly classified into chemical (including electrochemical sensors), biosensors, and electrochemical biosensors. Modern sensors have benefited considerably from improvements in micro-nano technology, which have enabled the production of smaller sensors with increased sensitivity and selectivity and lower production and maintenance costs [22]. As a result, sensors are widely used in healthcare to aid medical diagnosis, health, well-being, and energy production to improve the efficiency of fuel cells, batteries, and solar energy; the security sector; and environmental monitoring.

1.2.1. Chemical sensors

Chemical sensors are devices that convert a chemical property of an analyte into a measurable signal, whose magnitude is proportional to the analyte's concentration [23]. Examples of chemical sensors include gas, catalytic, conduct metric, and electrochemical sensors. Chemical sensors have greater stability and reproducibility when compared to biosensors [24, 25]. When developing an ideal electrochemical sensor for detecting NTs, the following factors should be considered; material chemistry, electrochemical properties, surface properties, and electrode design [26]. There are three electrochemical sensor types: potentiometry, voltammetry, and conductometry [27]. Electrochemical sensors are widely used in pharmacy, industrial,

clinical, and environmental analysis because they can analyse samples without damaging the sample with high sensitivity and specificity [7].

1.2.2. Biosensors

A biosensor is a device that detects a biological or chemical reaction by generating a signal proportional to the concentration of the analyte present in the reaction. [28]. Biosensors have seen wide application across many different research areas such as drug discovery, disease detection, water quality management, food quality monitoring, soil quality monitoring, environmental monitoring, and prosthetic device, due to their exceptional properties that include high sensitivity, specificity, ease of integration with other devices, and portability for utilization at point-of-use [29]. Biosensors were developed by Leland C. Clark, Jr in 1956 for oxygen detection [30].

They consist of an analyte recognition portion, a signal transducer, and a reader interface [31]. The function of the signal transducer in a biosensor is to convert the bio-recognition event into a quantifiable signal through signalization; most signal transducers produce an electrical or optical signal proportional to the concentration of the analyte-bioreceptor interactions. In biosensors, classification is based on the type of recognition molecule and or transducer used. Devices such as electrochemical transducers, optical devices, gravimetric devices, and piezoelectric devices are examples of transducers [29]. Biosensors include optical, magnetic, electrochemical, and acoustic wave biosensors [32].

Nanotechnology has played a huge role in the development of biosensors. Biosensors and other research areas have been greatly improved by the discovery of graphene and graphene oxide. Graphene is a pure form of carbon arranged in a one-atom-thick sheet, which gives it exceptional chemical and physical capabilities. Biosensors made of nanowires, CNTs, graphene, and graphene oxide have increased the detection limit of various analytes beyond previously possible, allowing single-molecule detection [33].

1.3. Nanotechnology

Nanotechnology refers to the study, manipulation, and use of materials with dimensions ranging from 1-100 nm [34]. Nanotechnology has facilitated the development of compact, energy-efficient intelligent sensors. Thus, chemical sensors and biosensors may be mass-produced at a lower cost [35]. In addition, nanotechnology has aided in creating chemical sensors such as nanosensors, nano-systems, nanotherapy,

nanodiagnosis, and nanoprobes [32]. This is due to the exceptional properties of nanomaterial, such as the quantum size effect, the minimum size effect, the surface effect, and the macro-quantum tunnel effect [32, 36]. Nanomaterials such as nanoparticles, nanofilms, nanoflakes, nanotubes, nanofibers, and nanocomposites enable the creation of sensors for use in point-of-care diagnostics, customized medicine, and medical diagnostics [36]. Nanotechnology holds enormous promise in health, electronics, and other sectors [37].

1.3.1. Carbon nanotubes

Carbon nanotubes (CNTs) are hypothetically cylindrically fabricated rolled-up graphene sheets that may be considered as multi-walled carbon nanotubes (MWCNTs) or single-walled carbon nanotubes (SWCNTs) [38]. CNTs, especially MWCNTs, have received a great application as electrochemical sensors. These are due to their unique characteristics: high surface-volume ratio, high modulus of elasticity, high electrical conductivity, and excellent mechanical, structural, and electronic properties. They offer various potential applications in producing supramolecular nano-bio-assemblies and nano-biosensors. Furthermore, using CNTs as a surface modification of electrodes demonstrates exceptional electrical conductivity and resilience to surface corrosion [38-40]. MWCNTs are nanomaterials with a porous structure, great chemical stability, biochemical functionalization, fast electro-catalytic transfer mechanism, large surface area, and high electrical properties [41-43]. These materials could also be easily functionalized by acid treatment. This alters their structural and chemical properties, such as defect sites and oxygen functionalities, improving absorption and electron transfer kinetics [44]. Carbon nanomaterials and metal oxide nanoparticles (MONPs) based nanocomposites have been widely investigated because of enhanced electrical, optical, and magnetic properties because of the synergistic nature of the two nanomaterials. [45, 46]. Moreover, CNTs support the catalytic activity of MONPs [45].

1.3.2. Metal oxide nanoparticles

Nanoparticles (NPs) are tiny particulate materials with less than 100 nm dimensions. NPs can be classified as ceramic, polymeric, carbon-based, lipid-based, semiconductor, and metal nanoparticles based on their morphological, physical, and chemical properties [47]. Relative to their bulk counterparts, NPs possess exceptional physical and chemical attributes such as large surface area, high reactivity, more active absorption sites, and small size [48, 49]. Hence, their adoption is across biomedical, industrial, agricultural, and environmental analysis sectors. Furthermore, NPs have played an important role in developing sensors,

facilitating the production of cheap, portable, selective, fast, and sensitive sensors. The basic function of NPs in the electrochemical sensor is to immobilize biomolecules in electrochemical catalysis reactions, enhance electron transfer, labelling biomolecules, and act as reactants [50].

Metal oxide nanoparticles (MONPs) are made purely of metal precursors, widely used in technological applications such as pigments, semiconductors, food, cosmetics, gas sensors, biomedical fields, superconductors, catalysts, and wastewater management [47]. MONPs are classified into two groups: the common oxides of CuO, NiO, and MnO2, and the platinum group of expensive metal oxides such as RhO_2, PtO_2, IrO_2, and RuO_2 [51]. Due to their nanosize and large surface area, MONPs have been widely used to fabricate chemical and biosensor sensors [51]. Surface area and quantum effects are two important factors contributing to the distinct properties of MONPs [52]. Increased MONPs size results in increased surface area, which negatively affects the optical, electrical, and magnetic properties of the MONPs [53]. These factors can reduce metal oxides' reactivity, strength, and electrical properties [54]. Because of their small size, metal oxides are used in medicine to pass through cell membranes, cellular organs, and in some cases, blood barriers. Furthermore, they can also interact with proteins, and small-sized nanoparticles can be used to enter bacterial cells and dissolve, releasing toxic metal ions [53].

1.4. Problem statement

The physiological and biological roles played by NTs in the human body are greatly understood and documented [1, 55-59]. Altered levels of NTs have been attributed to neurological diseases and disorders such as depression, tryptophan hydroxylase deficiency, tyrosine hydroxylase deficiency, somatization disorder, borderline personality disorder, social phobia, schizotypal personality disorder, and monoamine oxidase deficiency [58, 60, 61]. Since abnormal NTs levels in the body serve as biological indicators for a variety of neurological illnesses and disorders, real-time detection of NTs in living organisms requires a simple, affordable, user-friendly, fast, sensitive, and selective technique of analysis and detection as per the ASSURED criteria developed by the World Health Organisation (WHO) [62]. Furthermore, early identification of abnormal NTs levels in the blood leads to early diagnosis of diseases. It may minimize side effects linked to various neurological illnesses, such as memory loss caused by Parkinson's disease [63]. According to the WHO, neurological diseases kill approximately 12 % of the human population yearly [64]. Their research predicted an increase in neurological-related deaths in developing countries in Africa, North America, and Asia by 2030 compared to developed countries. This was attributed to the poor public healthcare system and planning in the developing world. Often, developing countries lack the infrastructure and financial resources to deal with emerging diseases effectively.

The role played by 5-HT and AA in the human body has been established [65]. For instance, 5-HT helps maintain homeostasis, mood, ejaculatory inclination, muscular activation, gastrointestinal movement, liver rejuvenation, bladder control, neuroendocrine regulation, and melancholy. However, abnormal 5-HT levels in the body have been reported to cause schizophrenia, insomnia, bipolar disorder, fatigue, 5-HT syndrome, headaches, stimulated cerebral activities, depression, blood coagulation, and fibromyalgia [66]. On the other hand, AA is a water-soluble vitamin required for human development. AA has been reported to be involved in the immune system, iron absorption, cholesterol metabolism, and common cold prevention [67, 68]. Unfortunately, excess amounts of AA have also been found to cause gastric irritation, renal problems, and cancer [69]. Low AA levels have been shown to cause a disease called scurvy, which slows down the process of wound recovery, compromising the immune system and resulting in skin complications, gum infections, anaemia, and pneumonia [70, 71]. Scurvy has been alleged to cause respiratory infections [72]. Furthermore, reduced levels of AA in the body are reported to cause urinary oxalate calculus, increase infertility in women and affect embryo development [61, 73]. A study has shown that extended and excessive AA use can cause diarrhoea, nausea, vomiting, headache, and insomnia [74].

1.5. Aim and objectives

1.5.1. Aim

To perform simultaneous electrochemical detection of serotonin and ascorbic acid at multi-walled carbon nanotube-antimony oxide nanoparticle (MWCNT-AONP) nanocomposite modified electrode.

1.5.2. Objectives

The objectives of the study were to:

1. synthesis antimony oxide nanoparticles (AONPs),
2. functionalize raw multi-walled carbon nanotubes (r-MWCNTs) by acid treatment with nitric acid,
3. prepare nanocomposite of multi-walled carbon nanotube- antimony oxide nanoparticle (MWCNT-AONP) with different concentrations of antimony oxide nanoparticles,

4. characterise the synthesized nanomaterials with fourier transformation infrared (FT-IR) spectroscopy, scanning electron microscopy (SEM), transmission electron microscopy (TEM), ultraviolet-visible (UV-vis) spectroscopy, X-ray diffraction (XRD) spectroscopy, and energy-dispersive X-ray (EDX) spectroscopy,

5. study the electrocatalytic properties and electron transport of the synthesized nanomaterials on serotonin and ascorbic acid using cyclic voltammetry, impedance spectroscopy, and square wave voltammetry,

6. study the potential of the multi-walled carbon nanotube- antimony oxide nanoparticle (MWCNT-AONP) nanocomposite towards the detection of ascorbic acid and serotonin in a real-life sample.

CHAPTER 2: Literature review

2.1. Neurotransmitters

NTs are divided into various classes according to their structure and function. The structural classification of NTs includes; amino acids (aspartate, GABA, d-serine, glutamate, and glycine), peptides (oxytocin, endorphin, somatostatin, vasopressin, opioid), monoamines (adrenaline, noradrenaline, serotonin dopamine, and histamine), nitrogen monoxide, adenosine, and acetylcholine (ACh) [4]. Also, NTs can be classified based on their functions in the body as executory, inhibitory, or neuromodulators [4]. The catecholamine NTs are responsible for the feeling of pleasure, awareness, enhanced attention, response, mood, sleep, pain, and appetite [4]. Altering levels and functioning of these NTs result in many different health complications, as summarised in **Table 2.1**.

Table 2. 1. The role of various NTs in the different central nervous system disorders.

Neurotransmitters	Associated disorders
Acetylcholine – causes muscular contraction. Involved in alertness, attention, anger, aggressiveness, sexuality, and thirst.	Alzheimer's disease.
Dopamine - involved in movement and postural control. It also affects mood and plays an essential role in positive reinforcement and dependency.	Muscular stiffness, characteristic of Parkinson's disease.
Glutamate – Aid in the acquisition of knowledge and the retention of information.	Alzheimer's disease diagnosed by memory loss at first.
Norepinephrine - It enhances emotional awareness, sleeping, dreaming, and learning. Additionally, it is linked with increased blood vessel contraction and heart rate.	Manic depression.
Serotonin – regulates body temperature, sleep, mood, appetite, and pain.	Depression, suicidal thoughts, impulsive behavior, and violence are all symptoms of abnormal serotonin levels.
GABA (gamma-aminobutyric acid) - regulates motor control, vision, and brain processes. Additionally, it regulates anxiety.	Some drugs that increase GABA levels in the brain are used to treat epilepsy and lessen tremors in individuals with Huntington's disease.

2.1.1. Serotonin

Serotonin or 5-hydroxytryptamine (5-HT) is one of the most important NTs in the brain [75]. Its chemical structure is represented in **Fig 2.1**, found in a few plants, bacteria, fungi, and animals [76, 77]. 5-HT has an amino group attached by a chain of two carbon atoms to the aromatic group. A Roman scientist, Vittorio Erspamer, discovered it in the 1930s [22]. His discovery led to unprecedented knowledge about the biological and medical functioning of 5-TH in human organs, such as the cardiovascular, central nervous, gastrointestinal, pulmonary, and genitourinary systems [78].

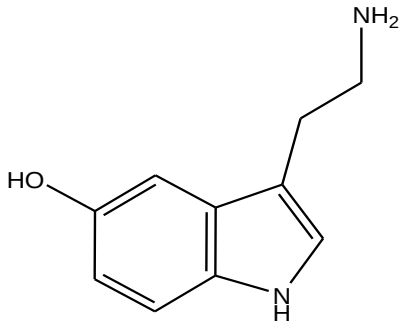

Figure 2. 1. The chemical structure of serotonin.

Due to its importance to the pharmaceutical, clinical, and medical industries, many methods have been explored to determine 5-HT in bodily fluids. These methods include electrochemical [79], voltammetry [80], high-pressure liquid chromatography with fluorometry [65], spectroscopy [81], gas chromatography-mass spectroscopy (GC-MS) [82], capillary electrophoresis [83], and radioimmunoassay [84]. Unfortunately, these methods produced disappointing results due to their inherent disadvantages; they are time-consuming and expensive to perform; and others were not sensitive and selective enough for the application of determining 5-HT due to the availability of interfering biomolecules such as AA, UA, and DA in human blood at high concentrations than 5-HT. On the other hand, electrochemical sensors modified with CNTs, metal oxides nanoparticles; conducting polymers, nanofibers, and graphene have gained a lot of traction for determining 5-HT in the blood, cerebrospinal fluid, urea, and serum samples as summarized in **Table 2.2** [14, 85-89].

Table 2. 2. Electrochemical sensors for 5-HT reported in the literature.

Electrode	Methods	Linear range	Analyte	LOD (µM)	Real sample	R^2	Ref
GCE/MWCNT-NiO	SWV	5.98 x 10^{-3} – 62.8	5-HT	0.118	Human urine	0.9726	[43]
GCE/MWCNT-ZnO	SWV	5.98 x 10^{-3} – 62.8	5-HT	0.129	Human urine	0.9149	[43]
GCE/MWCNT-Fe_3O_4	SWV	5.98 x 10^{-3} – 62.8	5-HT	0.166	Human urine	0.9789	[43]
[1]SPCE-PPy-Fe_3O_4NPsL	SWV	0.007 – 0.1	5-HT	0.021	Banana	0.9878	[90]
[2]SPCE-PPy-Fe_3O_4NPsF	SWV	0.007 – 0.1	5-HT	0.020	Banana	0.9881	[90]
[3]EPPGE	DPV	0.1 – 100	5-HT	0.060	Horse blood	0.9900	[91]
Fe_3O_4–MWCNT–poly(BCG)/GCE	DPV	0.5 – 100	5-HT	0.080	Human serum	0.996	[14]
[4]NiO/CNT/PEDOT	DPV	0.3 – 35	5-HT	0.063	Human serum	0.9988	[21]
SnO_2-SnS_2/GCE	SWV	0.1 – 700	5-HT	0.045	Human blood	0.9960	[71]
COOH-CNTs@ME	FSCV	0.1 – 20	5-HT	0.070	Human blood	-	[92]
$CONH_2$ –CNTs @ME	FSCV	0.1 – 20	5-HT	0.090	Human blood	-	[92]

1. Fe_3O_4NPsL represents iron (III) oxide nanoparticles synthesized from *Callistemon viminalis* leaves modified on screen-printed carbon electrodes.
2. Fe_3O_4NPsF represents iron (III) oxide nanoparticles synthesized from flower extract modified on screen-printed carbon electrodes.
3. Unmodified edge plane pyrolytic graphite electrode
4. NiO/carbon nanotube (CNT)/poly (3, 4-ethylenedioxythiophene) (PEDOT) modified on the glassy carbon electrode

5-HT is derived from tryptophan, an amino acid. Tryptophan is consumed from protein-rich foods and dietary protein sources such as nuts, cheese, and red meat [93]. **Fig 2.2** details the metabolic pathway of 5-HT synthesis from tryptophan. Literature has shown that abnormal levels of tryptophan negatively affect serotonin production and result in the aforementioned neurological diseases and disorders. 5-HT is involved in many different regulatory functions in the human body. For instance, 5-HT regulates body temperature, mood, ejaculation propensity, liver regeneration, muscle contraction, bladder control, intestinal motility, endocrine regulation, and depression. [1, 18, 43, 78, 94]. 5-HT is also involved in regulating platelet aggregation through transglutaminase-dependent covalent attachment to cellular proteins [78].

Altered levels of 5-HT have been observed in patients suffering from celiac and irritable bowel syndrome. Hara *et al*., 2011 found that patients with depressive disorder had about 300 nM lower 5-HT in the blood levels while healthy ones had approximately 1150 nM [95]. In the same light, patients with type-2 diabetes,

chronic kidney diseases, and platelets-poor plasma had 500 nM and 5 – 10 nM individually [96, 97]. Normal levels of 5-HT in a healthy adult person are reported to be at about 500 – 1200 nM [36], about 295 – 687 nM in urine, and about 0.18 – 5.5 nM in saliva [98, 99]. Abnormal levels of tryptophan have been shown to affect 5-HT production negatively and result in neurological diseases and disorders [100]. Due to extremely small concentrations of 5-HT in the body, most methods used to detect 5-HT are expensive, slow, and time-consuming.

However, 5-HT levels can be increased naturally by consuming tryptophan-rich foods such as plantains (30 ± 7.5 µg/g weight), pineapples (17 ± 5.1 µg/g weight), butternuts (398 ± 90 µg/g weight), kiwi fruit (5.80 ± 0.9 µg/g weight), tomatoes (3.75 µg/g weight), bananas (15 ± 2.4 µg/g weight), plums (4.7 ± 0.8 µg/g weight), egg yolk (3.2 ± 0.6 µg/g weight), salmon, and soy products [101]. The consumption of these foods increases urinary 5-hydroxyindoleacetic acid (5-HIAA) excretion while having no impact on platelet 5-HT levels. Therefore, to perform detection of 5-hydroxyindoleacetic acid in urine samples, the stated foods should not be consumed [101]. 5–HT levels can also be increased by maintaining a healthy diet, exercising, mood induction, or taking medical drugs or supplements. Folic acid (Vitamin B9), Vitamin B6, magnesium, zinc, L-thiamine, and probiotics are some vitamins and minerals that can boost 5-HT production. [102].

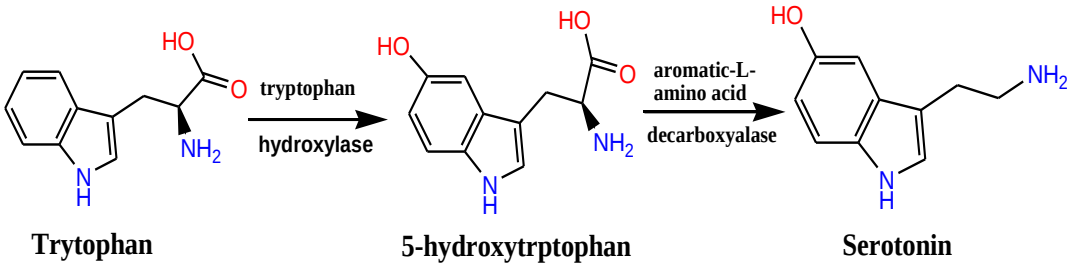

Figure 2. 2. The synthetic metabolic pathway of 5-HT.

2.1.2. Dopamine

Dopamine (3,4-dihydroxyphenethylamine), abbreviated DA, is one of the most important major catecholamine NTs, secreted and realized by adrenal glands and some brain parts [40]. DA is a white powder product with a molecular mass of 153.18 g/mol and a chemical structure shown in **Fig 2.3**. It was first synthesized in 1910 by George Barger and James Ewens in England, but it was discovered as a NT in 1958 by Arvid Carlsson [40, 103]. DA is involved in human metabolism, renal, nervous, and endocrine systems [104]. It helps control the feeling of joy, stress, pleasure, motivation, memory, attention, and body movements

[40]. The DA levels in extracellular and neuronal firing are around 0.11 – 0.03 µM and 0.1 – 1 µM, respectively [105].

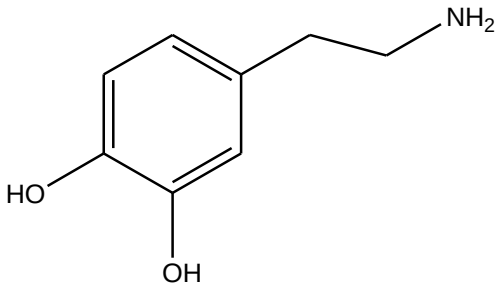

Figure 2. 3. The chemical structure of DA.

It has been shown that abnormal DA levels cause neurological disorders and diseases such as attention deficit hyperactivity disorder (ADHD), anhedonia, depression, Parkinson's disease, and schizophrenia [24, 104, 106-109]. Also, abnormal DA levels have been linked to neurological disorders such as restless leg disease and Tourette's syndrome [104, 109]. DA quantitative analysis is important in many fields such as medicine, pharmaceuticals, clinical and chemical industries. DA is engaged in reproductive organogenesis, ion permeability, antioxidant activity, and the synthesis of alkaloids in plants, and it has a protective function [110].

Different analytical methods such as ELISA, fluorescence, colourimetry, surface plasma resonance, photoelectrochemical sensor, DPV, and HPLC have been used to detect DA [24, 107]. However, these methods produce unsatisfactory results because they are laborious, time-consuming, expensive, and slow [104, 107]. Electrochemical techniques are more favoured by researchers for detecting DA [104, 111-117]. Electrochemical detection of DA remains a challenge. These challenges arise from the low concentration of DA, quick response time of DA, and fast realization and removal of DA from the extracellular space [40]. Since the concentration of DA is very small in the blood, its detection is both difficult and costly. For example, the concentration of UA and AA are reported to be 100 – 1000 times that of DA [104]. The second challenge relates to the presence of DA with interfering biomolecules (AA, UA, and EU) in bodily fluids. The other reason related to the difficulty of detecting DA using electrochemical techniques is the availability of 4-(2-aminoethyl) benzene-1,2-diol in DA, responsible for the functioning of the cardiovascular systems and central nervous system in mammals [118, 119].

From 2009 – 2014, electrodes fabricated with clay, metal-organic frameworks (MOFs), graphene, metal, metal oxides, metal sulphide, CNTs, zeolite, and polymers have been used as DA sensors [120]. DA electrochemical sensors have been used to diagnose Parkinson's and other neurological diseases before the diseases intensified. Electrochemical techniques offer great scope for the detection of DA in bodily fluids. **Table 2.3** summarizes

electrochemical sensors fabricated to determine DA in various real samples. Furthermore, electrochemical techniques such as square wave voltammetry (SWV) [121], cyclic voltammetry (CV) [122], fast-scan cyclic voltammetry (FSCV) [40], amperometry (AMP) [59], etc., offer great scope for detection of DA *in vivo*.

Table 2. 3. Summary of different electrochemical sensors used to determine DA using various methods.

Electrodes	Methods	Linear range	Analyte	LOD (µM)	Real sample	R^2	Ref
Graphene@GCE	SWV	2.5 – 100	DA	0.50	Pharmace-utical	09984	[122]
[1]Polypyrrole-MCM-48@GCE	SWV	2 – 250	DA	2.50	-	0.9996	[121]
Composite modified film electrode	SWV	0.25 – 217	DA	0.05	Blood serum	0.99861	[116]
MCM-41-NH3@GCE	SWV	2×10^{-4} - 1×10^{-1}	DA	1×10^{-4}	Human serum	0.9980	[123]
[2]EµPAN	DPV	0.5 – 120	DA	0.01	Blood & urine	0.9902	[107]
SnO_2/MWNTs/GCE	CV	3 – 200	DA	3.00	–	0.9970	[8]
ZnO/MWNTs/GCE	CV	1 – 300	DA	1.00	–	0.9970	[8]
[3](AuNPs@rGO/pTBA Pd($C_2H_4N2S_2$)$_2$/NF	SWV	0.1 – 200	DA	2.40×10^{-2}	–	0.9970	[11]
MWNT-IE	DPV	0.5 – 10	DA	0.10	Rabbit's brain	0.9996	[39]
EPPGE	DPV	0.2 – 25	DA	0.09	Horse blood	0.9900	[91]

1. Gold electrode modified with polypyrrole–mesoporous silica molecular sieves (MCM-48) Film
2. microfluidic paper-based analytical nanosensor (EµPAN)
3. Pd ($C_2H_4N_2S_2$)$_2$ complex anchored poly 2,2:5,2-tethiophene-3- (pbenzoicacid) (PTBA) layered on AuNPs decorated reduced graphene oxide (AuNPs@rGO)

The amino acid tyrosine is a precursor for synthesizing catecholamine NTs such as DA, norepinephrine, and ephedrine. Stress has been shown to decrease levels of L-tyrosine in animals [124, 125]. While omega 3 supplements have been shown to stimulate the release of DA [103]. The synthesis of DA begins with the amino acid called L-tyrosine, which is converted into L-dopamine by tyrosine hydroxylase. Then L-dopamine is turned into DA by an aromatic L-amino acid decarboxylase, as represented in **Fig 2.4**. DA is a precursor in synthesizing other NTs, including epinephrine and norepinephrine [58]. Drugs such as pramipexole, methylphenidate, and ladostigil have been shown to affect DA levels and result in the following disorders; depression, cocaine additions, Schizophrenia, and antidepressant [125]. Dietary supplements of high and low

DA fruits such as plantains, banana (8 µg/g), avocados (4 - 5 µg/g), oranges, tomatoes, pea, spinach, and apples are recommended [110].

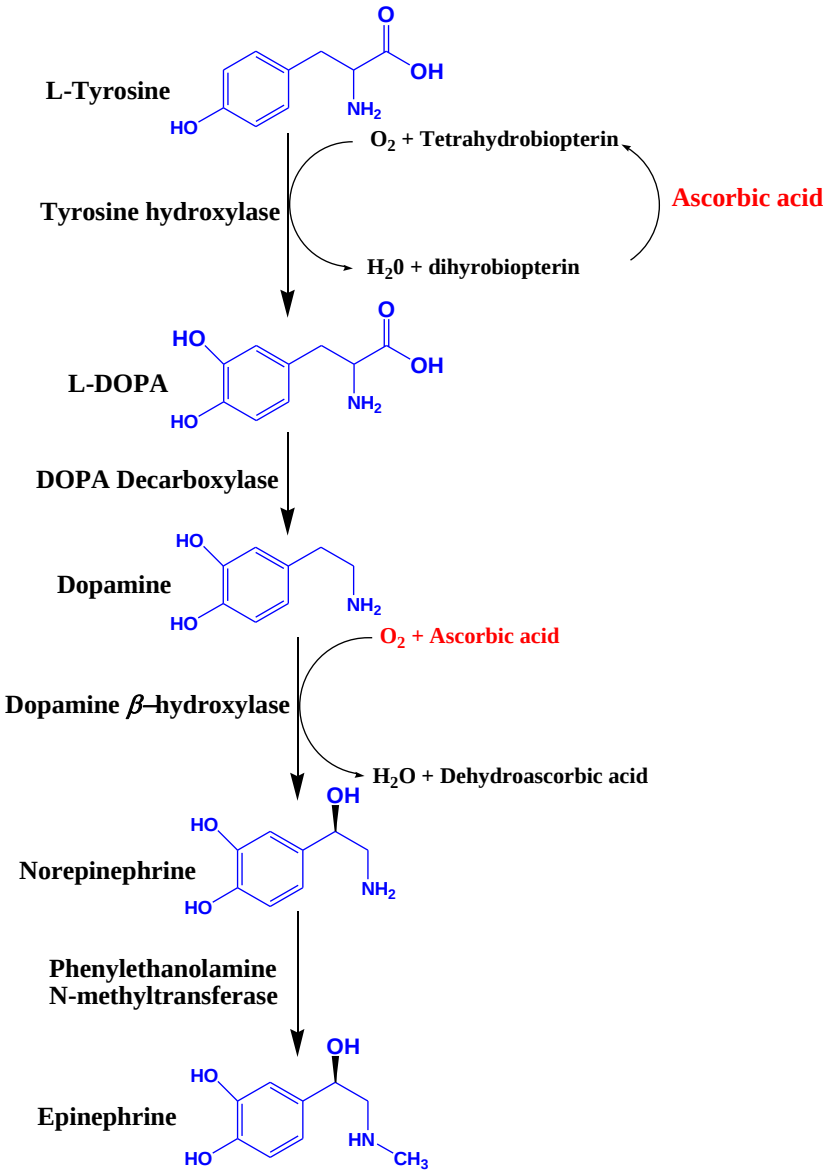

Figure 2. 4. The synthetic pathway of catecholamine neurotransmitters from L-tyrosine.

2.2. Interfering compounds

2.2.1. Ascorbic acid

The chemical structure of L-ascorbic acid (AA) or vitamin C can be seen in **Fig 2.5**. L-ascorbic acid is a water-soluble vitamin found in green vegetables, fruits, and other dietary supplements [126]. It was first discovered

in the 1930s by a Hungarian scientist, Szeged Albert Szent-Györgyi [127]. AA has a molecular mass, melting point, and density of 176.12 g/mol, 190 – 192 ºC, and 1.65 g/cm^3, respectively [126, 127]. The role played by vitamin C in various physiological and biological processes is greatly understood nowadays. Hence, it is used as a nutrient in the pharmaceutical, chemical, cosmetic, and food industries. Vitamin C acts as a water-soluble antioxidant, enzyme cofactor, and neuromodulator, preventing and treating the common cold, infertility, wound healing, and cancers [71, 128-130]. It is also reported to lower blood pressure and cholesterol [130].

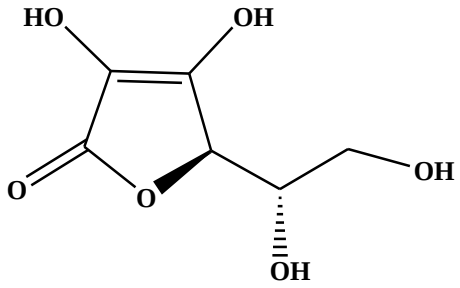

Figure 2. 5. The chemical structure of AA.

The function of vitamin C as an enzyme cofactor has been established. For example, vitamin C plays an important role in synthesising the essential catecholamine NTs, as shown in **Fig 2.6** [5]. AA acts as a cofactor for dopamine beta-hydroxylase, changing DA to norepinephrine, responsible for mood regulation, cognition, mood, interest, and intelligence [61]. Vitamin C is also needed for collagen synthesis to maintain healthy bones, teeth, skin, and cartilage [127]. Studies also show that AA acts as a cofactor for 5-hydroxylase, which is required to convert tryptophan to 5-hydroxytryptophan in 5-HT production.

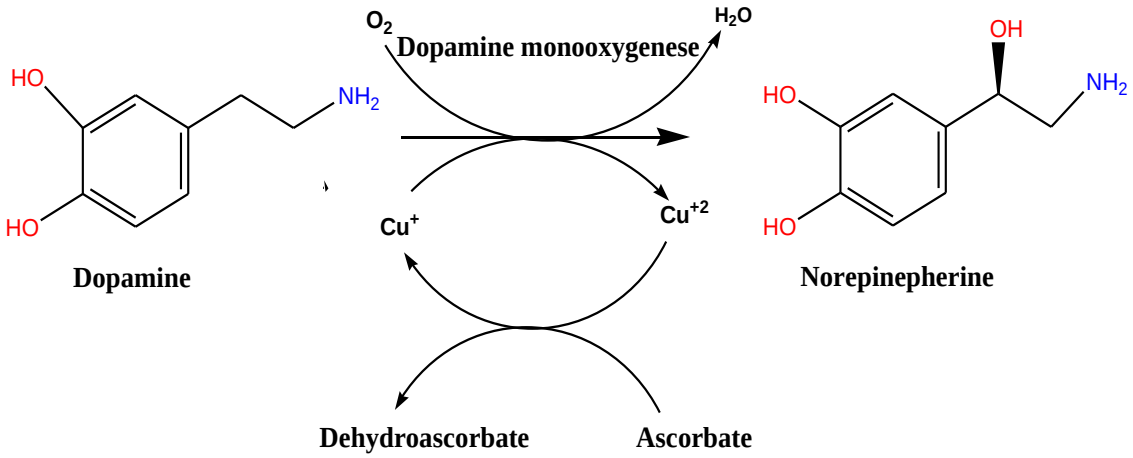

Figure 2. 6. The function of vitamin C in norepinephrine synthesis.

The role played by AA in the immune defence is extensive [70]. It includes improving collagen synthesis and stabilization [131], reducing histamine levels [132], regulating cytokine synthesis [133], enhancing antibody levels and acting as an antioxidant [134], reducing necrosis and facilitating apoptosis [135], enhancing phagocytosis [136], speeds up the wound recovery process [137]. Different analytical techniques have been introduced to determine AA levels in the body and blood. Due to the importance of vitamin C to the food, cosmetic, chemical, and pharmaceutical industries, various analytical methods such as coulometry [138], HPLC with electrochemical colourimetry [139], electrochemical [140], amperometry [141], capillary electrophoresis [100], and gas chromatography [142], and liquid chromatography [143] have been used to determine ascorbic acid. Nonetheless, the analytical methods were less sensitive, expensive, complicated processes requiring trained personnel to use them, longer sample preparation, time-consuming, and required laboratory equipment [94, 144]. Recently, electrochemical techniques have been gaining attention in detecting AA with other biomolecules [145-152]. **Table 2.4** details the different electrochemical sensors used to detect of AA in different samples using modified electrodes

Table 2. 4. Summary of electrochemical sensors used to detect AA using modified electrodes.

Modified electrode	**Method**	**Dynamic range (µM)**	**Analyte**	**LOD (µM)**	**Real sample**	**R^2**	**Ref**
Fe_3O_4NPs/SPCE	SWV	10 – 100	AA	15.7	Oranges	0.9810	[153]
RGO–ZnO/GCE	DPV	50 – 2350	AA	3.18	Urine and plasma	0.9965	[154]
Ni/Ag@rGO-GCE	SWV	4.89 – 90	AA	0.16	-	-	[155]
Sonogel–carbon@ME	SWV	50 – 1000	AA	50	-	0.9958	[156]
[1]PDDA@HCNTs-GCE	DPV	25 – 1045	AA	0.12	Bovine serum	0.9970	[157]
[2]ITO-rGO-AuNPs	LSV	20 – 100	AA	5.63	Fruit juice	0.9997	[158]
[3]N-PCNPs/GCE	DPV	80 – 2000	AA	0.74	Urine	0.9992	[159]

1. Poly(diallyl dimethylammonium) chloride (PDDA) functionalized HCNTs fabricated on glassy carbon nanotubes
2. Reduced graphene oxide and gold nanoparticles modified on indium tin oxide electrode
3. Nitrogen-doped porous carbon nanopolyhedra on the glassy carbon electrode.

Low levels of AA in the body have been shown to cause cardiovascular diseases, Alzheimer's and Parkinson's diseases, and cancer [68, 160]. Furthermore, AA is also involved in the immune system; iron absorption

metabolizes cholesterol in the body. Some studies report that excessive intake of AA is not harmful, but diarrhoea, nausea, vomiting, headache, and insomnia are likely to occur [129]. However, other studies have shown that extended use of AA could cause urinary oxalate calculus, increase infertility in a woman, and affects embryo development [73]. Another study found that high amounts of AA in the blood cause gastric irritation, renal problems, and loss of appetite; AA also acts as a peroxidation in heavy metals such as iron [74]. **Fig 2.7** shows the electro-oxidative mechanism of AA during an electrochemical process at the modified electrode. When pH > pKa, two electrons, and one proton are liberated during the oxidation of AA, while equal numbers of protons and electrons are involved when the pH is lower than the pKa value [161].

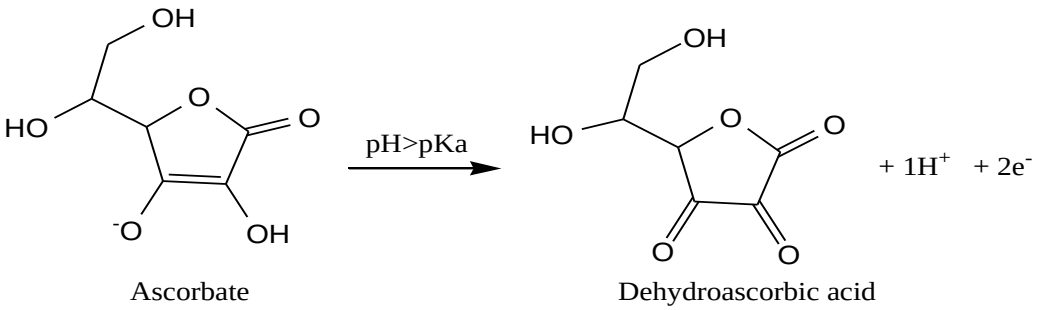

Figure 2. 7. AA mechanism during the electrochemical processes.

Although important for their well-being, humans, guinea pigs, and other species of birds, fishes, and mammals cannot produce AA. These species' inability to produce AA is attributed to their evolution over time. Specifically, the L-gulono-lactone oxidase gene mutation required for catalyzing the final phase of vitamin C synthesis [127, 162]. People obtain their vitamin C supplement from fresh fruits such as oranges, lemons, mangoes, papayas, strawberries, blackberries, and guava, and green vegetables such as tomatoes, carrots, potatoes, cabbage, and spinach [127, 163]. It should be noted that AA in long-lasting foods such as 100 % fruit juice decreases and degrades over time [144]. A daily vitamin C-rich diet averaging 91 mg is recommended for adults to keep healthy and balanced vitamin C levels in the body. A daily vitamin C diet of 110 and 78 mg is recommended [130, 144]. Alcohol abuse, drug abuse, ageing, and the development of diseases such as anorexia and poor diet are among the leading reported causes of reduced AA levels in the body. However, excess AA in the body can cause gastric irritations and renal complications [69]. In electrochemical detection, AA poses a huge challenge because it interferes with the detection of various NTs, thereby reducing the electrode's sensitivity.

2.2.2. Uric acid

Uric acid (UA), scientifically known as 2,6,8-trihydroxypurine, has the chemical structure shown in **Fig 2.8 (a)** and is obtained by consuming a rich purine diet such as meat, dried beans, wine, and liver [164] as depicted in **Fig 2.8 (b)**. UA is a white, odourless, tasteless product of protein synthesis located in the blood and urine with a molar mass of 168.11 g/mol. UA is insoluble in water or ethanol. Carl Wilhelm Scheele discovered UA in the late seventeenth century. UA and AA are widely studied interfering compounds. In healthy adults, levels of UA ranges from 1.5 – 6.0 mg/dL and 2.5 – 7.0 mg/dL for females and males respectively [60]. UA is derived from purines during the metabolism of purine-rich foods. However, purines are synthesized in the body via cell breakdown. A low purine diet reduces serum UA production. The detection of uric UA is of great importance because abnormal UA levels can cause kidney failure, kidney stone development, kidney disorder, and gout condition [50].

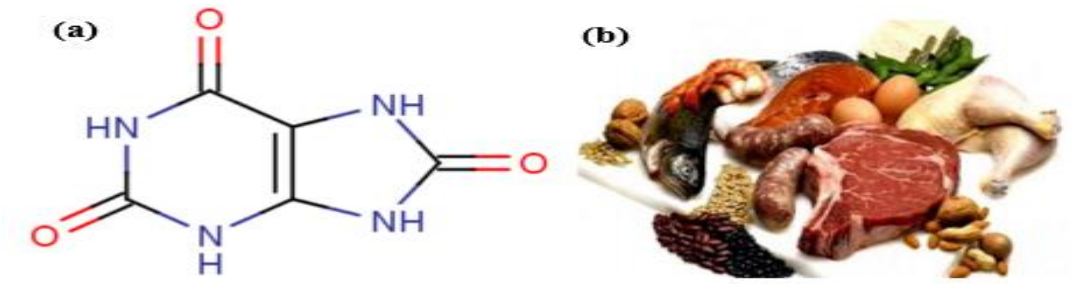

Figure 2. 8. The chemical structure of (a) UA and (b) UA-rich foods.

After consuming a high purines diet, purines undergo multiple chemical reactions to form UA. Then about 15 % of the UA remains in gastrointestinal gout and is used throughout the body. Then the excess 75 % of UA is discarded during urination, although a small amount is lost through stools [58]. Alleviated levels of UA can occur in one of the following ways. Firstly, the body can release more UA than is necessary into the bloodstream, resulting in a condition known as hyperuricemia. Hyperuricemia causes gout conditions, which leaves patients in extreme pain and discomfort [165]. Secondly, since the kidneys are responsible for removing approximately 75 % of the UA from the body, failure of these organs will result in elevated levels of UA, causing health complications. As UA levels fall, so does the amount of UA in the urine. There is no definitive reason why the body produces too much or too little UA. But according to one study, it could be due to increased oxidative stress, such as UA acting as an antioxidant [166]. Thirdly, UA can be increased as a consequence of fasting or weight loss [167], and lastly, levels of UA can be spiked up by administering drugs such as thiazide diuretics [168]. Multiple myelomas, fatty liver, Parkinson's disease, hypertension, metastatic cancer, leukaemia, diabetes, metabolic syndrome, acute inflammatory arthritis, atherosclerosis, Lesche Nyhan syndrome, and the gout condition are all caused by high amounts of UA in the body [165, 166]. As a result, it

is advised to maintain a healthy and balanced diet of high purine content foods and perform aerobic and anaerobic exercises. **Fig 2.9** shows the electro-oxidative mechanism of UA during the electrochemical reaction. This mechanism occurs in the same manner as that of AA in **Fig 2.7**.

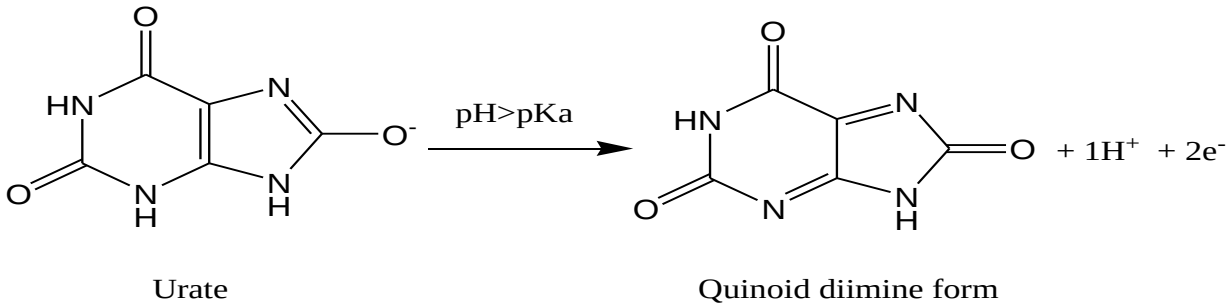

Figure 2. 9. Electro-oxidative mechanism of UA during the electrochemical reaction.

According to the stage at which the kidney stones have developed, patients either have the stones surgically removed or are given medication to treat them. While chronic cases are treated with allopurinol, which inhibits xanthine oxidase and stops hypoxanthine and xanthine from producing UA. The kidney is an important organ in the UA cycle, which helps with UA excretion from the body. Therefore, failure of this organ can cause major health complications. Factors that can affect the kidney are genetic factors, metabolic syndrome, renal impairment, and drugs that negatively affect the kidney. The body produces about 300 – 600 mg/d of purines that are later converted into UA, and a purine diet contributes about 600 mg/d, then it is turned into purine nucleotides. Some purine nucleotides are used as tissue nucleotides, while others are kept as purine bases that contribute to the UA pool. The kidneys excrete approximately 600 mg/d of UA, and 200 mg/d is used in the gut [169].

Different techniques and approaches have been used to find a better sensor for detecting and analysing UA simultaneously with other compounds or individually. These methods include capillary electrophoresis [170], high-pressure liquid chromatography (HPLC) with UV-vis detection [171], HPLC-ECD [172], HPLC-CD [173], ion chromatography [174], fluorescence [175], and surface plasma resonance (SPR) [64]. Electrochemical techniques have become popular among researchers due to their advantages [155, 156, 176-178]. **Table 2.5** shows different electrochemical sensors used to detect UA in different samples using various modified sensor electrodes.

Table 2. 5. The UA electrochemical sensors.

Modified electrode	Method	Dynamic range (µM)	Analyte	LOD (µM)	Real sample	R^2	Ref
Poly(DPA)/SiO_2@Fe_3O_4/ carbon paste	DPV	1.2 – 8.2	UA	0.4	Blood serum and urine	0.9956	[179]
[1](Ni@BC-MIP)-GCE	DPV	0.01 –30	UA	0.008	Urine	0.998	[155]
[2]CL-TiN/GCE	DPV	10 – 300	UA	0.28	–	0.9942	[180]
Sonogel–carbon/ME	SWV	10 – 100	UA	10	–	0.9909	[156]
Prussian blue/poly (4-aminosalicylic acid)/uricase -SPE	AMP	10 – 200	UA	3.0	Urine	0.9974	[178]
ITO-rGO-AuNPs	LSV	20 – 100	UA	2.26	Milk & urine	0.9997	[158]
[3]N-PCNPs/GC	DPV	4 – 50	UA	0.021	Urine	0.9964	[159]

1. Carbon-enwrapped nickel nanoparticles (Ni@BC) were coated with polydopamine (PDA) modified on glassy carbon nanotubes
2. Chrysanthemum-like titanium nitride fabricated on the glassy carbon electrode
3. Nitrogen-doped porous carbon nanopolyhedra on the glassy carbon electrode

2.3. Nanomaterials and their application

Nanomaterials are materials with dimensions ranging from 1–100 nm; such materials include nanoparticles, nanofibers, nanosheets, nanorods, and thin films [181]. These nanomaterials possess outstanding electrical, magnetic, and optical properties [32]. Hence, their wide application in cosmetics, pharmaceutical, bio-imaging, biosensing, bioanalytics, environmental harvesting and remediation, tissue nanotechnology, cosmetics, photonics, energy, data storage, and biomedical fields. Additionally, nanomaterials such as metal oxide nanoparticles and semiconductors nanoparticles have played a leading role in developing electrochemical sensors [182, 183].

Depending on their shape, nanomaterials can be classified as zero-dimensional (0D), one-dimensional (1D), two-dimensional (2D), or three-dimensional (3D). The 0D nanomaterials are nanomaterials that have all dimensions at the nanoscale. Examples include nanoparticles, and 1D nanomaterials have at least one dimension outside the nanoscale; examples include nanorods, nanotubes, and nanowires. 2D nanomaterials have two dimensions outside the nanoscale examples include nanofilms, graphene, nanolayers, and nanocoating. While the 3D nanomaterials have all three dimensions at the microscale, examples include multi-nanolayers, a bundle of nanotubes, and nanowires. Numerous variables affect nanoparticle production, characterization, and use. These include techniques used to synthesize nanoparticles (chemical or biological method), pH, pressure, reaction time, particle shape and size, environment, pore size, proximity, and

preparation costs [181]. In comparison to large particles, nanoparticles display different chemical and physical properties. Nanoparticles have gained a reputation in the electrochemical sensor field due to this reason.

2.3.1. Top-down approach

The top-down or bottom-up approaches can synthesize NPs, as shown in **Figure 2.10**. The top-down approach uses nanolithography-grinding mechanisms to synthesize NPs from bulk material. The top-down approach is advantageous because it does not generate toxic chemicals and is easier to use than the bottom-up approach. The disadvantage of using the top-down approach is that it produces irregularly shaped and poorly sized distributed nanoparticles with low particle surface area. It requires a high amount of energy to synthesize small particles; grinding contaminates the sample. Nonetheless, this method has found application in magnetic, catalytic, and structural studies because of its less complicated nature.

2.3.2. Bottom-up approach

The bottom-up method entails creating nanomaterials from atoms through fabrication. Quantum dots (QDs) or nanoparticles generated from colloidal dispersion are two instances of molecular self-assembly. The bottom-down approach is a more controllable process than the top-down method. Chemical reactions and the environments in which nanoparticles grow can be controlled to control the morphology and size of nanomaterials. This method produces nanoparticles of higher quality and is normally employed in modifying electrochemical sensors. In addition, the bottom-up approach requires a short time to perform compared to the top-down approach. However, the bottom-up techniques produce poor materials than the top-down approach [181].

NPs can be synthesized in one of the three methods. These methods include physical, chemical, and green or biological synthetic methods. The physical method uses electron beam lithographs, arc discharge methods, milling, mechanical grinding, etc., to synthesize nanoparticles. The physical method's advantages include ease of use and controlling the inter-particle spaces. On the other hand, this method requires expensive and complex machines, and the growth size of the nanoparticle cannot be easily controlled and harms the environment [48]. The green synthesis method uses biological agents such as fungi, algae, bacteria, and plants to synthesize nanoparticles, while chemical synthesis utilizes chemicals to synthesise NPs. The advantages of synthesizing nanoparticles following the green synthesis method include being environmentally friendly and cheaper than the chemical synthesis method because it does not use expensive and toxic chemicals. Thus, it can produce

safer by-products and products, produces good yield, and has good reproducibility and scalability. However, the green synthesis method is extremely slow and laborious [48, 181]. The chemical synthesis process is straightforward, tractable, and efficient, with the ability to control the size, composition, and even the morphology of the NPs. The disadvantage is that it uses dangerous and toxic chemicals that harm the environment [181, 184].

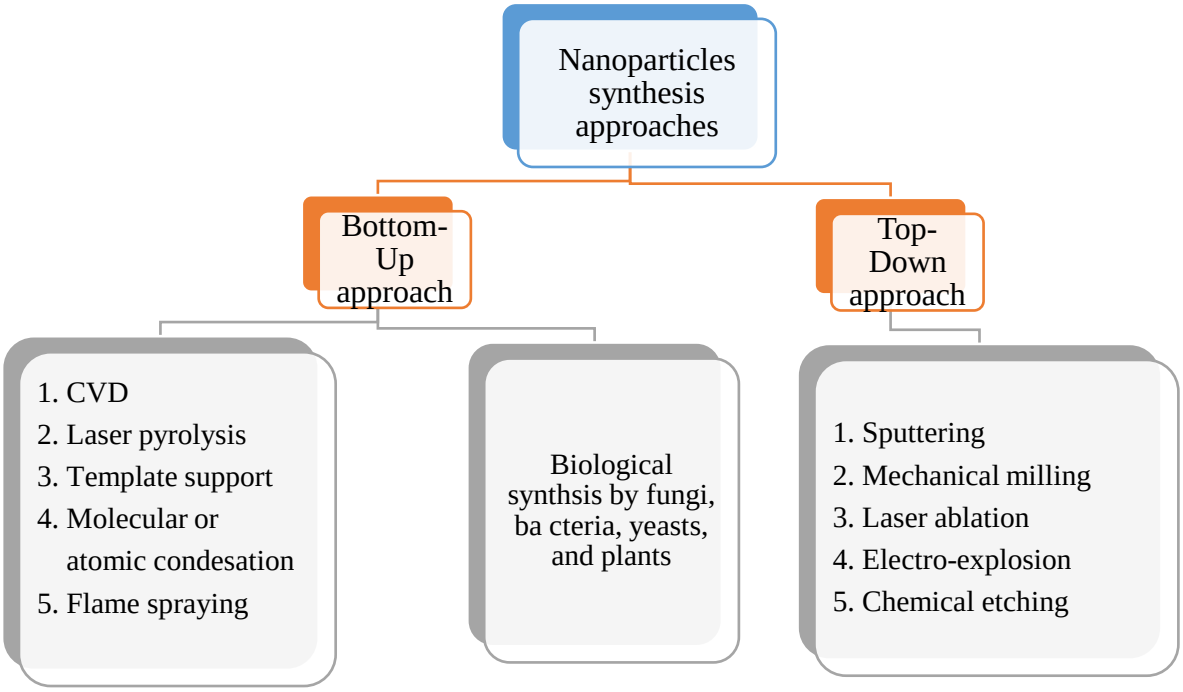

Figure 2. 10. Synthetic methods used in nanotechnology and their typical processes and applications.

2.4. Carbon nanotubes and their applications

CNTs were first discovered in 1991 by Iijima. The extraordinary electrochemical features of CNTs make them suitable for use in Faradaic processes (e.g., the fast electron-transfer kinetics of CNTs, due to the presence of edge plane graphite sites within the walls and at the ends of CNTs [185-187]. The CNTs belong to the family of carbon allotropes that consist of graphite, amorphous carbon, fullerene, diamond, and graphene, as shown in **Fig 2.11** [188]. CNTs are outstanding carbon nanomaterials because of their large surface areas and high chemical and thermal stability, making CNTs an attractive adsorbent for heavy metals.

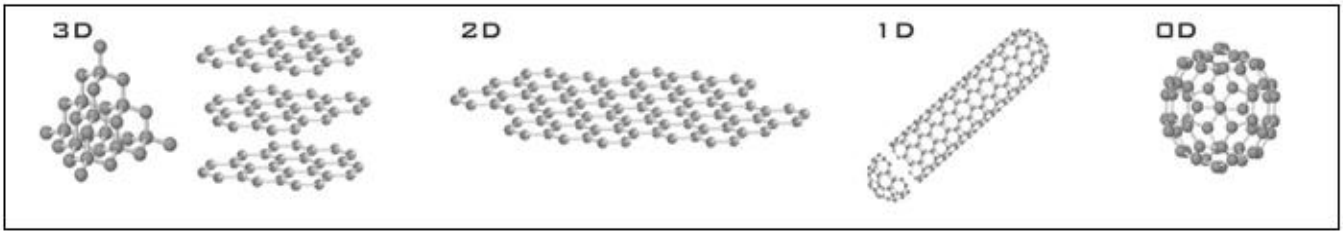

Figure 2. 11. Various allotrope carbon crystal structures. A 3D diamond and graphite, 2D graphene, 1D diamond and graphite, and 0D buck balls left to right. Adopted from Yellampalli *et al*., 2011 [188].

CNTs are classified into three types: SWCNTs, DWCNTs, and MWCNTs, as shown in **Fig 2.12**. SWCNTs are typically made of a single graphite sheet perfectly coiled into a cylindrical tube, whereas MWCNTs are made of an array of such nanotubes. These CNTs are of different thicknesses and possess excellent semiconducting properties [61]. Spectroscopic techniques like Raman spectroscopy are used to determine the class of CNTs. Due to their outstanding structural, mechanical, and electronic nature; there has been a growing use of CNTs in different fields such as the chemical sensor and biosensor field.

Carbon nanotubes have gained a great reputation as electrode modifiers in recent years. CNTs exhibit enhanced electron transfer due to their exceptional electronic nature. Of the three CNTs, MWCNTs have gained a lot of recognition for their excellent properties and thus are widely used compared to SWCNTs. This is because MWCNTs provide a higher current carrying ability. Also, conduction occurs through the outer wall, with a bigger diameter, and lastly, MWCNTs can transfer current in the ampere range, unlike SWCNTs [189]. The MWCNTs decorated with metal oxide nanoparticles have been extensively used to fabricate electrochemical sensors to detect catecholamine neurotransmitters [190].

Figure 2. 12. Various forms of CNTs (a) single-wall CNTs (SWCNTs); (b) double-walled CNTs (DWCNTs); and (c) multi-wall CNTs (MWCNTs). Adopted from Bryning *et al*., 2007 [191].

The three most important synthetic methods for CNTs are arc discharge, laser vaporization, and chemical vapour deposition [10]. The arc method uses high temperatures (> 1700 °C) to synthesize CNTs, whereas, in pulsed laser deposition (PLD), a laser acts on graphite granules containing nickel or cobalt as catalytic materials for CNT production. The chemical vapour deposition method is cost-effective compared to other CNTs production methods. CNTs with high purity and more controlled production can be obtained using the chemical method compared to laser ablation. Therefore, the chemical vapour deposition method is widely used to synthesize carbon nanotubes, which has the advantage of scalability, which can be deposited over a large area, and is easy to collect by providing carbon nanotubes already attached to the substrate [192, 193]. CNTs remain a costly and complex synthesis due to the lack of knowledge about the mechanisms of nanomaterial growth. Due to high production costs, large-scale production of these nanomaterials is not economically viable [10].

In some industries, CNTs are incorporated into other nanomaterials to create nanocomposites. MWCNT/fiber composites exhibit excellent electrical conductivity, water resistance, and fire resistance in the textile industry. [194]. Composites create lightweight and durable aircraft and automobiles in the automotive and aerospace industries. CNTs are also built into sports equipment such as tennis racquets, hockey sticks, bicycle frames, etc., to reduce weight and improve tear resistance, strength, and durability. In the medical industry, CNTs are doped with metals such as nitrogen for efficient drug delivery and are used as imaging agents in other applications [195, 196]. Due to their impressive electrical conductivity, MWCNTs are widely used in biological studies to detect various analytes. Hsiao *et al*., 2017 [197] built an MWCNT/polyethylene detector for analyte detection, and Habibi *et al*. (2010) [198] used MWCNTs to detect AA, DA, and UA all at once. Sims *et al*. (2010) [199] used carbon nanotubes to detect nicotine on a basal plane pyrolytic graphene (BPPG) electrode. Luong *et al*. (2005) proved that they could be used as a biosensor, and Viswanathan *et al*. (2012) confirmed this when they used MWCNT to detect foodborne pathogens [200, 201]. CNTs are widely used for nanofilter production, direct cell growth on surfaces, drug release mechanisms, catalysts, biological fingerprinting, and pharmacological identification [202, 203]. The special properties of MWCNTs and their respective nanocomposite materials make them excellent for engineering applications because of their high thermal, electrical conductivity, strength, chemical stability, aspect ratio, mechanical strength, and reduced weight [204-206]. **Table 2.6** elucidates the applications of MWCNTs over the short, medium, and long term [41].

Table 2. 6. Different applications of MWCNTs in the short, medium, and long term.

Short-term	Mid-term	Long-term
Conducting polymers and composite (electronic & electronic)	Coatings (conductive thin films) and advanced ceramics	Microwave antennas
Sensors & instruments (microscope probe, gas sensors)	Catalysts (petrochemical)	Selding, assembling yarns
Electromagnetic shielding	Textile, caulks, fibers, and fuel cells	Aerospace and medical implants
Sporting (tennis rackets)	Lithium-ion batteries, lamps, semiconducting materials	Drug delivery

2.4.1. Functionalization of CNTs

CNTs are chemically functionalized using an acid treatment method to make CNT nanocomposites. Acid oxidation is one of the best methods for the functionalization of CNTs. This is done to avoid CNT aggregation caused by weak van der Waals interactions between the nanotubes [42]. Strong acids, including nitric acid, sulphuric acid, hydrofluoric acid, and UV zone, normally functionalize CNTs. Strong acids have strong p-type doping on the CNTs; they change sp^2-hybridized CNTs into sp^3-hybridized CNTs, thus decreasing the number of delocalized electrons [207]. **Fig 2.13** illustrates the harsh oxidation process of functionalizing MWCNTs via acid treatment. Due to oxygen functional groups, functionalized CNTs are more electro-active than non-functionalized CNTs. Functionalized MWCNTs additionally increase the composite's dispensability and strength.

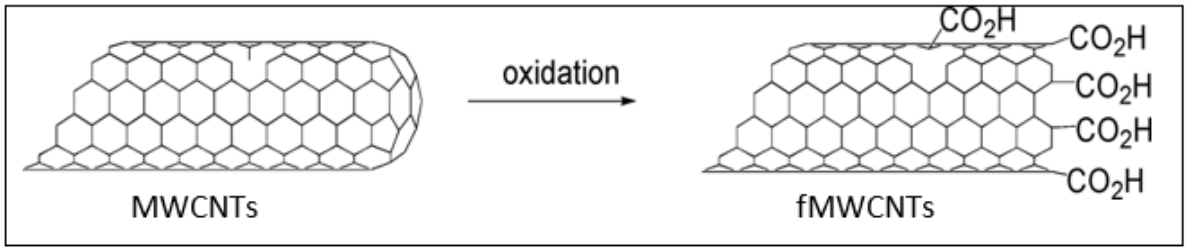

Figure 2. 13. The acid oxidation process of raw MWCNTs. Reused with permission from Prato *et al*., 2008 [208].

2.4. Metal oxide nanoparticles and their applications

Semi-conducting metal oxide nanoparticles (MONPs) are the most widely used nanomaterials for sensor fabrication. The properties that make these nanomaterials an indispensable tool in modern nanotechnology are their nonlinear optical properties, higher ductility at high temperatures than assembled ceramics, cold welding properties, super-paramagnetic behaviour, unique catalytic properties, sensitivity, and selective activity [52].

Metal oxide-based nanomaterials include manganese oxides, nanosized iron oxides, titanium oxides, cerium oxides, zinc oxide, magnesium oxides, aluminium oxides, and zirconium oxides. These nanoparticles play a significant role in many areas of physics, chemistry, and material sciences as a catalyst in the manufacturing industry as well as in nanotechnology to create batteries, magnetic storage media, solar cells, medicine, antennas, rectifiers; optoelectronics, and digital devices such as LEDs, and electrochromic devices [48]. **Fig 2.14** shows the different metal oxide nanoparticles (WO_3NPs, TiO_2NPs, SnO_2NPs, and ZnONPs) and their applications across different fields [49].

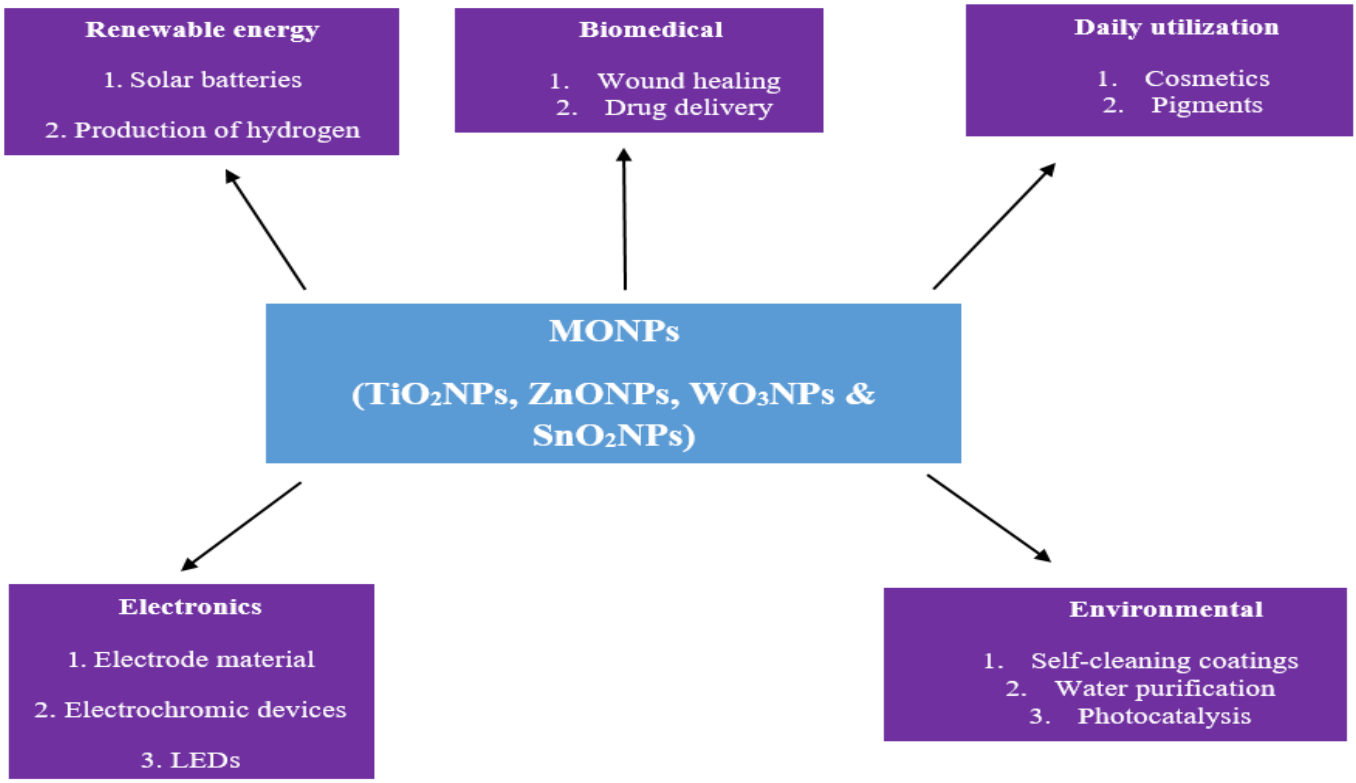

Figure 2. 14. Different uses of TiO_2, ZnO, SnO_2, and WO_3 nanoparticles.

2.4.1. Antimony oxide nanoparticles and their application

Antimony oxide nanoparticle (AONPs) possesses outstanding biocompatibility, high proton conductivity, high surface area, great chemical stability, and mechanical strength [209]. It also facilitates faster electron transfer kinetics and enhanced absorption capacity [210]. AONPs exist in three well-known phases, which are antimony pentoxide (Sb_2O_5), antimony tetroxide (Sb_2O_4), and antimony trioxide (Sb_2O_3). **Fig 2.15** depicts three structures of antimony oxide nanoparticles with senarmontite and valentinite being the most common and well-known. Sb_2O_3 occurs as either a cubic or an orthorhombic polymorph (senarmontite and valentinite respectively), while Sb_2O_4 can be monoclinic (clinocervantite) or orthorhombic (cervantite) [211].

AONPs can be synthesized via the following methods; hydrothermal [212], microemulsion [213], solution-phase reduction, biosynthesis [214], γ-ray radiation oxidation [215], hybrid induction, and laser heating [216], thermal oxidation [217], and vacuum evaporation [210]. AONPs with excellent electrical conductivity, a high melting point of 656°C, and a 1425 °C boiling point are widely adopted across the chemical sensors and semiconductor industries. In the chemical industry, AONPs are widely used as flame retardant synergists for materials such as rubber, paints, textiles, plastics, etc., [218, 219]. It can also be included in alloys and can still be used as catalysts to make moisture sensors. [220], methane gas sensor [221]. Their thermal, electrical, and optical conductivity properties enable their wide application in the production of light-emitting diodes (light-emitting diodes), electronic and optoelectronic devices, including batteries [222], binary glasses [223], solar cells devices [224], anti-friction alloys, and ceramic glaze [210].

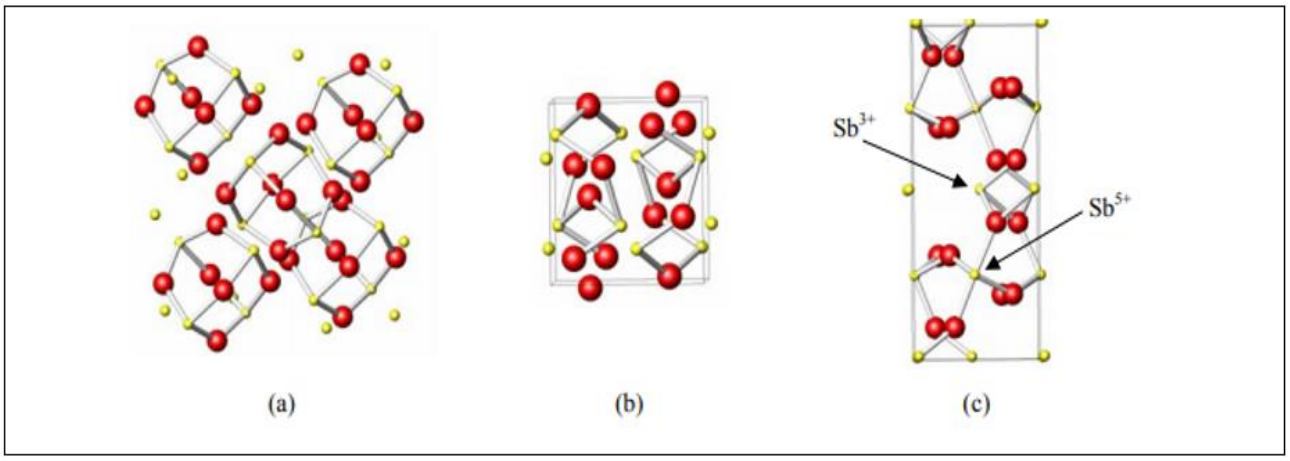

Figure 2. 15. Structures of the antimony oxide nanoparticles; (a) senarmontite, (b) valentinite, and (c) cervantite. Adopted from Orman *et al*., 2005 [211].

AONPs have received considerable attention from the scientific research community and are widely adopted across the technological industry. This is attributed to the exhibition of novel properties by nanostructure when compared to the bulk material. **Table 2.7** contrasts the difference between the bulk antimony oxide and AONPs. With excellent results, the MWCNT-AONP nanocomposite fabricated electrodes have been successfully used to detect various analytes. For instance, Hai *et al*. (2020) fabricated an AONP-MWCNT composite to determine lead (Pb^{2+}) and cadmium (Cd^{2+}) ions in water using SWV. Their sensor showed sensitivity for Cd^{2+} and Pb^{2+} ions at 1.932 µA.L.µg^{-1}, and 2.694 µA.L.µg^{-1} with linearity for Cd^{2+} and Pb^{2+} ions detection ranging from 80 – 150 ppb and 5 – 35 ppb, respectively [225]. In the same light, Masibi *et al*. (2018) created an MWCNT-AONP-PANI composite to determine lindane and endosulfan. For detection of lindane, the modified electrode displayed a limit of detection (LOD) of 2.01 nM and linearity from 0.00 – 18.8 nM (R^2 = 0.9903), and for endosulfan detection, the LOD was 6.8 µM with linearity from 32.3 – 77.6 µM (0.9916) using SWV [226, 227]. In another study, Cidem *et al*. (2019) [228] fabricated GCE with MWCNT-Sb_2O_3 to detect tramadol within a concentration range of 40 – 30000 nM (R^2 = 0.9901) and a LOD value of 9.5 nM using the CV. While, Apinya et al., 2016 [229] developed a sensor using a PANI/MnO_2-AONP nanocomposite to detect ascorbic acid (AA) and acetylsalicylic acid (ASA) in human urine. Using the DPV technique, their sensors demonstrated sensitivity, linear range, and LOD values of 0.9356 nmol L^{-1}, 0.1 – 372.64 nmol L^{-1} (R^2 = 0.9974), and 0.071 nmol L^{-1} in the presence of 0.5 × 10^{-11} mol L^{-1} ASA using DPV method. On the other hand, Düzmen *et al*., (2021) used the SWV technique to determine metaproterenol from biological and pharmaceutical materials using an electrode made of AONP@WO_3-CNTs/GCE. For metaproterenol detection, their electrode has a linear range and LOD of 5.2 × 10^{-8} – 2.7 × 10^{-6} M and 6.6 × 10^{-9} M [230].

Table 2. 7. The contrast between chemical and physical properties of bulk antimony oxide and AONPs.

Properties	**OA – bulk**	**OA nanoparticles**
Particles size	> 100 nm	< 100 nm
Translucent	Maximum loss	Minimum loss
Colourant loading	Higher	Reduced half of bulk
Impact strength	Lower	Higher
Tensile strength	Lower (< 4.05 MPa)	Higher (4.05 – 9.35 MPa)
Absorbability	Weak	Strong
Super-hydrophobic	Unstable (sliding angle > 5˚)	Stable (sliding angle < 5˚)
Refractive index	Lower (< 2)	Higher (> 2)
Abrasive resistance	Lower	Higher
UV-vis absorbance	Lower (< 0.3 a.u of absorbance)	Higher (> 0.3 a.u of absorbance)
Proton conductivity	Lower (< 2.89 x 10^{-3} S/cm)	Higher (2.89 x 10^{-3} S/cm)

2.5. Nanocomposite and their application

A nanocomposite is a composite material with at least one dimension phase at the nanoscale [231]. Nanocomposites combine improved electrocatalytic properties with the advantages of large surfaces to increase electrode selectivity and sensitivity. Recently, the use of electrochemical sensors modified with nanoparticles, conductive polymers, carbon nanostructures, metals, and metal oxide nanoparticles has gained recognition due to the simplicity, high sensitivity, selectivity, and low cost of neurotransmitter detection [5, 6]. Bare electrodes cannot detect NTs such as 5-HT due to their low sensitivity, electrochemical contamination, and the presence of interfering compounds such as UA, EP, DA, and AA [7]. This problem is solved by modifying the electrode surface with a nanocomposite. Numerous studies have used a variety of electrode modifiers, including polymers [8], carbon nanotubes [9], and nanoparticles [7], towards the detection of NTs in bodily fluids. Different studies have used different nanocomposites to modify the bare electrodes with enhanced electrocatalytic and enhanced electron transfer at the modified electrodes [10]. **Table 2.8** compares the advantages and disadvantages of each catalytic material. Since many different materials have exceptional properties, including outstanding electrical, optical, mechanical, and catalytic properties, each material has its shortcomings.

Nevertheless, these shortcomings can be overcome when combined and new products with enhanced properties can be produced. For instance, nanocomposite material has been used to produce durable water pipes, different types of glass, car tires, plastic bags, facemasks, water filters, and many more. **Fig 2.16** shows a typical process used to create a carbon nanotube/ metal oxide (CNT/MO) nanocomposite followed in this study.

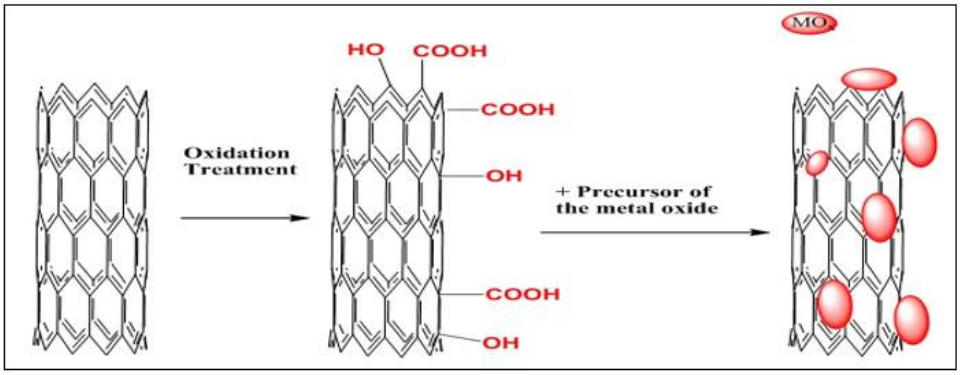

Figure 2. 16. A diagram displays carbon nanotube-metal oxide nanocomposite synthesis. Adopted from Gupta *et al*., 2011 [192].

Types of nanocomposites include ceramic, metal, polymer nanocomposites, and magnetic matrix nanocomposites. Heat-resistant nanocomposites can be used in high-temperature environments due to their

ability to withstand extreme temperatures. Nanocomposite materials in electrochemical sensors have gained tremendous recognition for their ability to improve electrode electrocatalytic and electroanalytic properties to detect analytes in interfering molecules [43, 225, 232]. Nanocomposites significantly increase current response and reduce current drop, making electrochemical sensors more selective, reproducible, reusable, and sensitive [188, 233].

Table 2. 8. Comparison of the advantages and disadvantages of each material. Reused from Sun *et al*., 2018 [234]

Material	*Advantages*	*Disadvantages*
Carbon	Large specific surface area High conductivity Electrochemical stability Cheap price	Low energy density Poor dispersity
Transitional metal oxides or hydroxides	High specific capacitance High conductivity Wide energy density Low cost Easy to prepare	Low conductivity Poor electrochemical stability
Conducting polymers	High specific capacitance Unique solution processability Filming has good flexibility	Low conductivity Poor electrochemical stability
Transitional metal dichalcogenides	Large specific surface area High specific capacitance Good electrochemical stability	Preparation method is immature Physical and chemical properties are easily affected by the environment
Mxenes	Large specific surface area High conductivity Good dispersity Higher area capacitance	Complex production Expensive Low mass capacitance

2.6. Screen-print electrodes and their application

Screen-print electrodes (SPEs) are similar to glassy carbon electrodes (GCE) but of smaller size, often used in electrochemistry to study electrochemical processes. In electrochemistry, SPEs are used to perform research and teach students about electrochemical techniques [235]. Researchers are becoming more interested in SPEs because they are economical to manufacture at a large scale, disposable, responsive, compact, simple to use, adaptable, dependable, enable good reproducibility for analysis, and do not require polishing on the surface of the electrode after use unlike solid electrodes such as GCE [33, 236, 237]. As a result, they are widely used as electrochemical sensors in electrochemistry, environmental, therapeutic, and agricultural-food applications

[37]. Furthermore, the screen-print carbon electrodes (SPCEs) strips can improve the sensitivity and selectivity with slight damage to the electrochemical reactions in an environment of interfering compounds [235]. A regular SPE consists of a three-electrode system, including the working electrode (A/AgCl), reference electrode, and counter or auxiliary electrode, as shown in **Fig 2.17**; for their function, refer to **Section 2.7**.

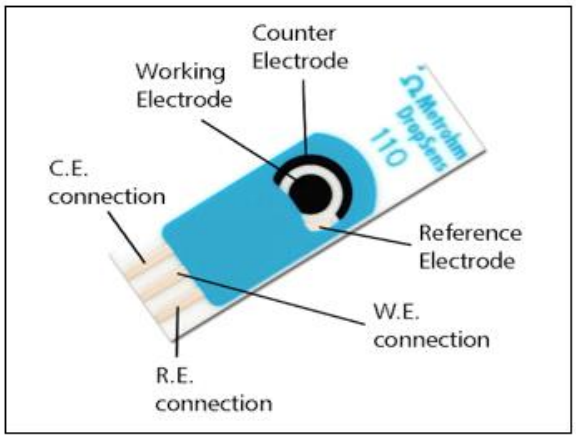

Figure 2. 17. Illustration of the screen-printed carbon electrode with labels. Adopted from Ω Metrohm DropSens Spain site.

SPEs are widely available and can be purchased from different manufacturers in different inks, as shown in **Fig 2.18**. Some of the well-known examples of SPEs are the screen-printed carbon electrode (SPCE), screen-printed gold electrode (SPGE), screen-print-platinum electrode (SPPE), and screen-print transparent electrode (SPTE), etc. SPCEs are widely used because they are cheaper to produce and can absorb various materials, including organic and inorganic solvents, than SPGEs and SPPEs, which are more expensive [238]. Neves *et al*., 2010 performed a comparative study between GCE and SPCE to determine the oxidative quantification of pravastatin [239]. Although their experiment did not show any greater variation regarding the detection limits and accuracy between the GCE and SPCE, their study concluded that SPCE was greatly preferred over GCE because of its higher sensitivity and ease of cleaning the electrode's surface for renewal, which reduces the rate-limiting steps. Different SPEs have been utilized successfully to combat environmental pollution by detecting heavy metals, herbicides, nitrates, phosphates, and phenolic compounds in drinking water [240, 241]. Electrochemical sensors have been used to detect different NTs and their interfering compounds [242].

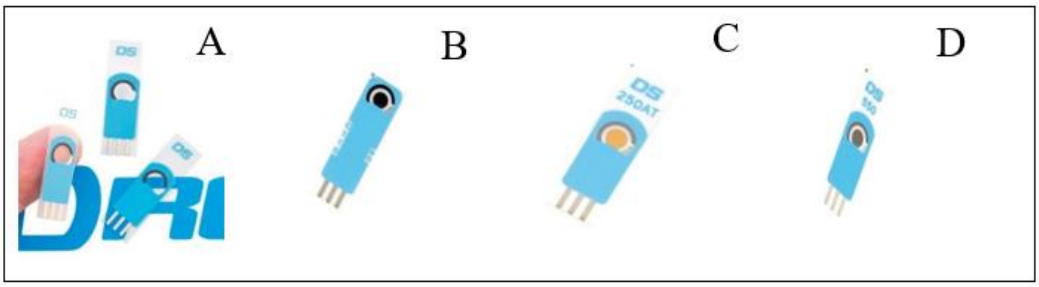

Figure 2. 18. Screen-printed electrodes with different electrode modifiers; (a) SPE-transparent electrode, (b) SPE-carbon electrode, (c) SPE-gold electrode, and (d) SPE-platinum electrode. Taken from Ω Metrohm DropSens Spain site.

2.6.1. Fabrication of screen-printed electrodes

Modification is the process that involves coating the surface of the working electrode with a catalyst such as metal oxide nanoparticles, CNTs, conducting polymers, or even nanocomposite to enhance the electrode's sensitivity. Electrochemical studies usually modify the electrodes to improve electrocatalytic activity due to larger surface area and faster diffusion kinetics [207, 235]. Moreover, modified electrodes allow electro-analysis study and help eliminate access interfering compounds and resist electrode biofouling [235, 243, 244].

There are three main methods for modifying screen-print electrodes (SPEs). These include drop casting, electrodeposition, and ink mixing and printing, as shown in **Fig 2.19.** The drop-casting method involves dropping the catalyst on the surface of the WE and then drying it at room temperature. The drop casting techniques are more widely used than other methods because they are easy and simple. Secondly, the drop-casting methods allow cheaper electrochemical sensors because functionalization is not required. However, the agglomeration of nanoparticles is a major issue when using this method. To overcome this challenge, nanoparticles or electrode modifiers are grown directly on the surface of a conductive carbonous substrate. A drop-casting method is widely adopted when modifying the working electrode because reproducible nano-sized metallic centres are formed [51]. The ink mixing and printing method is the least used method for modification of electrodes because it is expensive and batch reproducibility is not easily obtained.

Modified electrodes are mainly used in research institutions to study energy conversion, electrochemical processes, molecular electronics development, electro-chromatic sensors, storage, and corrosion studies. Modified screen-print electrodes have been used to detect heavy metals, herbicides, pesticides, nitrates, phosphates, glucose levels, and phenolic compounds in drinking water [37, 243-245].

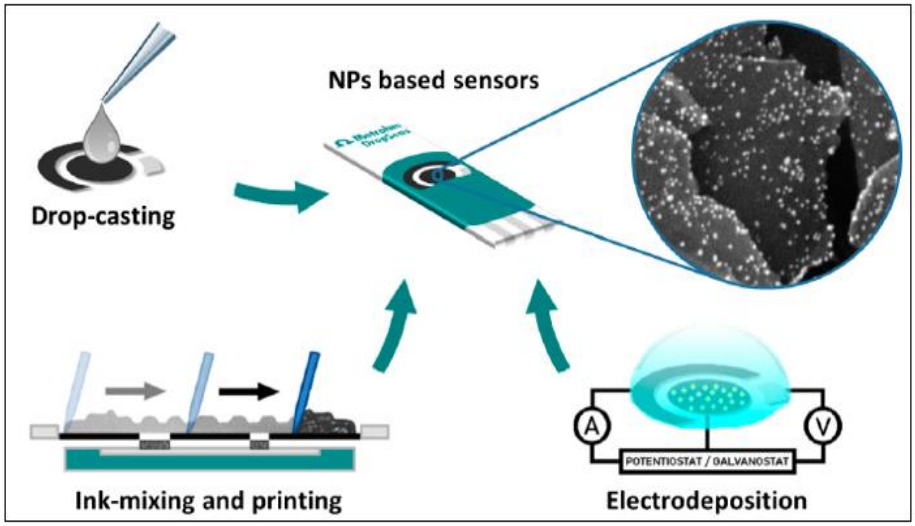

Figure 2. 19. Diagram showing three types of electrode fabrication processes. Adopted from Antuña-Jiménez *et al*. (2020) [51].

2.7. Electrochemical detection and its application

Electrochemical detection is an analytical technique that detects electric currents from a redox reaction in a test compound [246]. Electrochemical methods evaluate reaction concentration, mechanism, reaction kinetics, and physical and chemical properties. Compared to traditional methods, such as HPCL, capillary electrophoresis, and liquid chromatography, electrochemical methods are affordable and offer quick analysis, high sensitivity, and selectivity.

An electrochemical cell comprises three important electrodes, namely the working electrode (WE), the reference electrode (RE), and the auxiliary electrode (AE), as depicted in **Fig 2.20** [129]. The redox reaction takes place at the surface of the WE. The electrode of known potential is the RE (made-up of gold, platinum, and silver as inert materials) used for potential control and to connect the current circuit; the AE is utilized. The processes at the working electrode (WE) can be reversible, irreversible, or quasi-reversible, which can be determined using the cyclic voltammetry approach (**see sub-section 2.9.1**). Electrochemical techniques have been used in different areas, including batteries, fuel cells, and electrochemical sensors. Additionally, electrochemical techniques are utilised in the following areas, clinical, pharmaceutical, chemical, environmental, and medical [247].

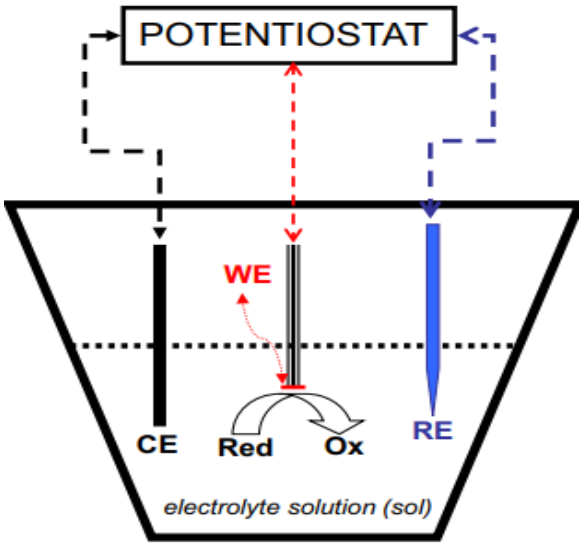

Figure 2. 20. Electrochemical cell set-up. Reused with permission from Mirceski *et al*. (2018) [248].

2.9. Voltammetric techniques

Voltammetric techniques are aspects of electrochemistry, whereby current is measured as a function of the electrode's potential [249, 250]. During the voltammetric process, the potential in the cell is controlled while the current is measured as a time function. Polarimetry was the first voltammetric technique to be discovered and developed in 1922 by Aroslay Heyrovski [251], and he received a Nobel Prize in chemistry for his work in 1959 [252]. Other examples of voltammetric methods include square wave voltammetry (SWV), cyclic voltammetry (CV), chronoamperometry, differential pulse voltammetry (DPV), linear potential sweep voltammetry (LPSV), cyclic voltammetry (CV), staircase voltammetry, chronoamperometry, differential pulse voltammetry (DPV), and so on. Voltammetric methods are extensively used in different fields because they are cheap, sensitive, require no pre-treatment, can achieve detection at extremely small concentrations, are easy to use, offer fast response, and are portable compared to various traditional methods [252]. Voltammetry methods are used throughout the STEM field to perform research; also, they are used in clinical, chemical, pharmaceutical, and a vast array of research institutions [253-255].

2.9.1. Cyclic voltammetry

The cyclic voltammetry (CV) technique measures the current generated in an electrochemical cell when the voltage is greater than predicted by the Nernst equation. In a cyclical phase, the CV is performed by linearly

increasing the voltage at the WE over time. The potential between the WE and RE is measured, as is the current between the WE and CE. The data obtained is then used to generate a current (µA) vs potential (V) plot, as shown in **Fig 2.21 (a & b)** [256]. The solvents used must be soluble in the analyte, stable during the electrochemical experiment, resistant to interfering chemicals, and not react with the analyte [257]. This study utilized DMF (N, N dimethylformamide) as a solvent to inhibit f-MWCNTs agglomeration efficiently, which is important in facilitating electron transfer. The electrolytes reduce the voltage drop so that the obtained potentials correspond with the actual potentials and ensure good electrical conductivity [258]**.**

CV data can be used to calculate the electron transfer coefficient, the number of electrons transported at the electrode, evaluate the reversibility or irreversibility of the reaction, and evaluate the presence or absence of intermediates or adsorption at the surface of the electrode [259, 260]. Additionally, CV techniques have been used to calculate the electron stoichiometry, an analyte's diffusion coefficient, the formal reduction potential, and determine the concentration of an unknown solution using linear plots [261, 262]. CV has been used to measure the concentration in biological samples [263].

For a reversible process, the anodic and cathodic peak potentials must be separated by 59/n mV, the i_{pa}/i_{pc} must equal one, the peak currents must be proportional to the square root of scan rate, and the anodic and cathodic peaks are independent of the scan rate. Lastly, the peak position does not change as a function of voltage scan rate [167]. An irreversible reaction has the following characteristics: the reverse peak is unavailable in the voltammogram. There is a shift of the peak potential with scan rate and the peak currents are lower than those obtained in a reversible reaction. For quasi-reversible reaction, a large anodic and cathodic peak potential is observed in the voltammogram and less than 57/n mV of a reversible reaction [264]

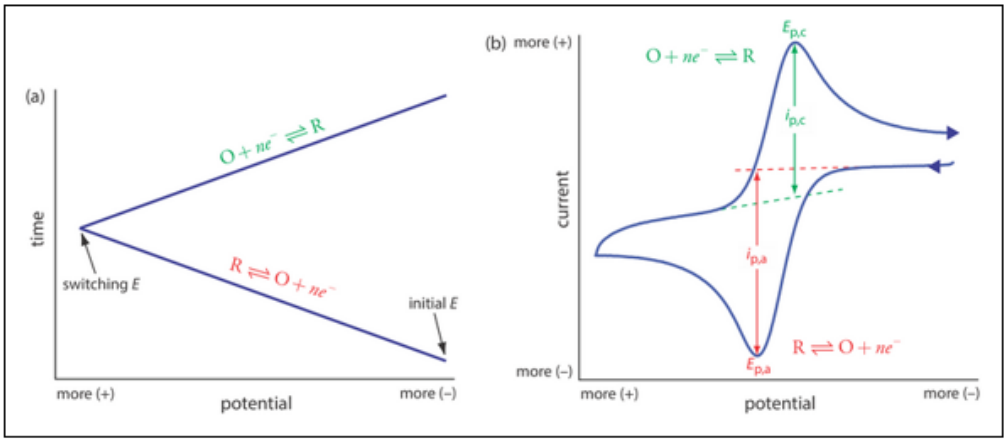

Figure 2. 21. Displays the (a) redox reactions during a cyclic voltammogram and (b) complete cyclic voltammogram with labelings. Reused with permission from Kissinger *et al*., 1983 [265].

The Randles–Ševčík **equation (2.1)** is used to study the correlation between peak current and scan rate. This study investigated the active surface area of each modified and unmodified electrode.

$$i_p = (2.69 \times 10^5) n^{\frac{3}{2}} A D^{\frac{1}{2}} C v^{\frac{1}{2}} n \qquad (2.1)$$

where i_p, A, D, n, C, and v denote the peak current (μA), the active surface area of the electrode (cm^2), the diffusion coefficient (cm^2/s), the number of electrodes transferred, the concentration (mol/cm^3), and the scan rate (V/s) respectively.

The formal reduction potentials for a reversible reaction are calculated using **equation (2.2)**:

$$E^{O'} = \frac{Epa + Epc}{2} \qquad (2.2)$$

The total number of electrons transported during the electro-catalytic process at the electrode can be calculated using **equation (2.3)** for a reversible reaction.

$$\Delta Ep = Epa - Epc \cong \frac{0.059}{n} \qquad (2.3)$$

E_{pa} and E_{pc} represent the peak potential at the anode and the cathodic, respectively, and n represents the number of electrons transferred during a redox process.

2.9.2. Square wave voltammetry

Square wave voltammetry (SWV) is an important technique in electrokinetics and analytical measurements [266]. This technique was developed in 1952 by Kalousek and Barker [266]. The SWV method is widely used and adopted in different research areas because it is more sensitive than the LSV, DPV, and CV techniques. Hence, it is a preferred technique when performing concentration studies in electrochemistry. Furthermore, SWV can detect analysts at picomolar concentrations (10^{-9} M) [266], offers quick analysis, and helps to reduce background signals generated by reduction of oxygen, etc. Compared to non-electrochemical techniques such as chromatographic techniques, SWV is cheaper and time-efficient, sensitive, and selective for the detection

of biomolecules [266, 267]. The SWV technique is obtained by applying the potential to a stationary electrode, combining the square wave and staircase wave potential. The current is measured at the WE while the potential between the WE and the RE is swept linearly over time. The square wave potential from the WE is superimposed on the base staircase with a full square wave cycle display of one step in a staircase waveform. The current is sampled twice during each square wave cycle. The first current is sampled at the end of the forward scan and the other at the end of the reverse scan, resulting in an SWV as shown in **Fig 2.22 (a)**. The change in current vs the base staircase potential is shown in **Fig 2.22 (b)**. The SWV has been used in agriculture, environmental analysis and detecting bacteria in real life samples [247].

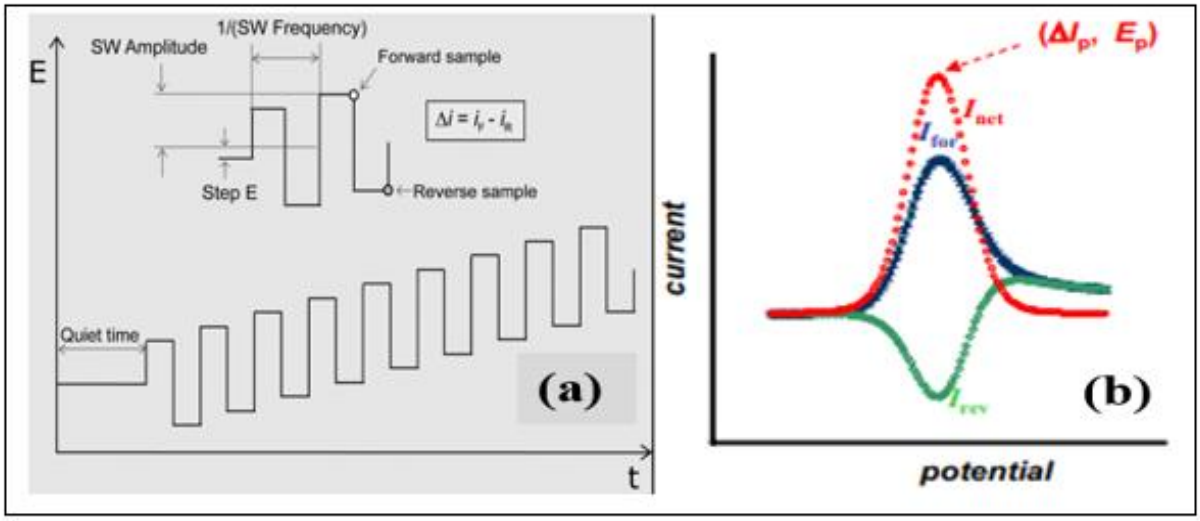

Figure 2. 22. Displays the (a) potential waveform and one potential cycle of a (b) typical square wave voltammogram. Adopted with permission from Dias *et al*., 2017 [268].

2.10. Spectroscopic methods

Some spectroscopic techniques include Raman spectroscopy, photoluminescence, UV-vis, and FT-IR. These techniques use light to analyse and provide quantitative and qualitative information about a sample of interest. Specific light energy is absorbed, reflected, or may excite electrons when light interacts with the material, resulting in light absorption, reflection, or photoluminescence. They are used in various fields, including medicine, clinical research, pharmaceuticals, mining, water treatment, and the food industry. They help investigate nanomaterials' composition, molecular structure, and absorption nature. For example, the surface properties of nanoparticles can be studied using electroluminescence.

2.10.1. Ultraviolet-visible spectroscopy

Ultraviolet-visible (UV-vis) spectroscopy is the process by which external electrons in an atom or molecule absorb radiation energy and transition to higher energy levels. UV-vis is one of the widely used techniques in many different fields such as forensic analysis, medicine, pharmacy, research institutions, beverage, and biotechnology industry because it offers fast analysis, non-invasive, affordable, and simple to use compared to fluorescence techniques [269]. UV-vis light is used to obtain quantitative and qualitative information about unknown samples. As a consequence of different materials absorbing light at different wavelengths, a unique and specific relationship exists between the substance and the UV-vis spectrum, allowing for the identification of unknown compounds, determining sample concentration, calculating the melting point of proteins, and the extinction coefficient of the sample and its molecular structure [270]. UV-vis can be used to study inorganic ions and organic molecules and to estimate the band energy gap of materials using Tauc's plot [271].

2.10.2. Fourier transform infrared spectroscopy

FT-IR spectroscopy is a technique used to determine the infrared spectrum of absorption or emission of a solid or liquid, which can identify unknown compounds based on their chemical structure. The nanomaterials used in this experiment were scanned from 400 to 4000 cm^{-1} regions. FT-IR is used to determine the presence or absence of functional groups in a sample; it can also be used to determine the purity of the prepared samples. An FT-IR spectrum is obtained by passing radiation through the sample, some of the radiation will be absorbed by the sample, and the detector will capture some as transmittance. The detector's data is used to plot absorption vs. transmittance, resulting in a molecular fingerprint of the sample. Samples with varying chemical and physical properties can be qualitatively, and quantitatively analysed because each sample has its unique fingerprint. An intense peak indicates that there is a large amount of nanomaterial present.

2.11. Surface characterization methods

Since nanomaterials are used as catalysts in electrochemical sensors, it is critical to investigate their surface area, which influences their catalytic properties. Properties such as texture and chemical surface are critical when working with catalysts. Some examples of techniques used to characterize the surface of nanomaterials include SEM, XRD, EDX, and TEM.

2.11.1. X-ray diffraction

X-ray diffraction (XRD) is a rapid, non-invasive method used in material science to determine crystallinity and atomic spacing. It was discovered in 1912 by Max von Laue [272]. XRD data can be used to calculate the size of the nanomaterial using Schemer's equation (4.2) and Wallison-Hall plot to determine the dislocation and microstrain on synthesized nanomaterials, particularly nanoparticles [273, 274]. XRD further helps to elucidate the crystallographic orientations of the nanoparticles. The rays generated by the cathodic are filtered to produce monochromatic radiation, which is then concentrated and shot at the sample. When the incident rays interact with the sample, they produce constructive interference only if the conditions satisfy the Bragg's law **equation 2.4** [275]. This law describes the relationship between the wavelength of electromagnetic radiation, the angle of diffraction, and the lattice spacing of crystal samples. Diffracted x-rays are then detected, processed and counted.

$$n\lambda = 2d \sin\theta \qquad (2.4)$$

where n, λ, d, and θ stand for the integer, the wavelength incident of the incident X-ray beam, the distance between atomic layers in a crystal, and the reflected X-ray beam at a certain angle of incidence, respectively.

2.11.2. Transmission electron microscope

The transmission electron microscope is a technique that involves passing electron beams through a specimen to generate an image. Ernst Ruska, a Nobel Prize-winning physicist, was the first to invent the electron microscope between 1932 and 1933. Furthermore, he was also involved in developing commercially viable TEM in 1939. He was recognized and awarded a Noble Prize in 1986 for his invention [276]. TEM provides higher resolutions than a light microscope because of its smaller de Broglie wavelength of electrons. This allows TEM to capture images of small nanomaterials at high resolutions and exposes fine details about the nanomaterial. In TEM, the electrons are emitted by cathode (tungsten filament or lanthanum hexaboride); this emission gun is supplied with voltaic energy of about 100 – 300 kV and provided with sufficient current, the gun emits electrons into the vacuum. After leaving the electron gun, the electrons are sped up through the vacuum by a series of electrostatic plates until they reach their final voltage and enter the other part of the microscope called the condenser lens system. In this system, the upper lens of TEM accurately directs the beam of electrons to the intended location on the sample. TEM has been used in chemical, biological, and physical sciences. It has been successfully applied in material science, medical research, semiconductor research, nanotechnology, and environmental pollution. In electrochemical seniors, TEM is mainly used to

evaluate the nanoparticle size of the various particles and study the internal structure of nanomaterials. Sample preparation in TEM is laborious and requires trained personnel; in contrast, SEM requires little to no sample preparation and is relatively easier to operate [277, 278].

2.11.3. Scanning electron microscope

A scanning electron microscope (SEM) is a microscopic technique that generates a topographical image of a specific material by scanning a focussed electron beam across its surface. The electrons in the electron beam interact with the sample, generating different types of signals used to generate information about the surface topography, composition, and shape [279]. Compared to a light microscope, SEM is more powerful as it can characterize very small materials like the nanofibres layer used in a filtration system. SEM consists of the following parts: electron source, electron column, electron detector devices, sample chamber, and finally, an output source like a computer that will show the image of the scanned surface topography. The resolution obtained in the SEM depends greatly on the following factors: the electron spot's size and the volume amount of the electron beam interacting with the sample. SEM has found a lot of applications in various fields and areas, such as in material science used to perform research, creating nanowires for gas sensing purposes, semiconductors inspection, microchip manufacturing, forensic science, biology (used to study living organisms, for example, bacteria), medical field and arts, where micrographs produced by SEM are utilized to generate digital artwork.

CHAPTER 3: Methods and materials

3.1. Apparatus and reagents

The following chemicals were purchased and used as received from the manufacturers, serotonin (5-HT) hydrochloride powder (98 %), antimony trichloride ($SbCl_3$) (99 %), ascorbic acid (AA) (99 %), hydrochloric acid (HCL) (32 %), sodium hydroxide (NaOH) (98 %), multi-walled carbon nanotubes (MWCNTs) (≥ 98 %), dopamine (DA) hydrochloride powder (98 %), N, N-dimethylformamide (DMF) (99 %), potassium hexacyanoferrate (IV) K_4 [$Fe(CN)_6$] (99 %), potassium hexacyanoferrate (III) K_3 [$Fe(CN)_6$] (99 %), nitric acid (HNO_3) (34 %), and toluene (C_7H_8) (99 %) were obtained from Merck Pty Ltd (Darmstadt, Germany). Sodium phosphate salts Na_2HPO_4 (99 %) and NaH_2PO_4 (99 %) products of LABCHEM and GlassWorld located in Johannesburg, South Africa, were used in the preparation of 0.1 M phosphate buffer solution (PBS) at pH 7. Emplura® Merck (The Chemical Center from Mumbai, India) provided distilled water used during the experiment to prepare chemicals. The electrochemical experiments were performed using the portal Dropsens kit containing Dropview 8400 software disc, screen-printed carbon electrodes (SPCEs) with a diameter of 4 mm (DropSens 110), potentiostat 300 (μstat-i 400s), one cable connector (CABSTAT1), 910 potentiostat mini and power supply cable was supplied by Metrohm from Madrid, Spain.

3.2. Synthesis of antimony oxide nanoparticles

The hydrothermal technique was employed to synthesize antimony oxide nanoparticles (AONPs). To generate a colorless solution, 2 mM antimony trichloride (Sb_2Cl_3) was dissolved in 20 mL toluene with rapid stirring. Then, 20 mL of distilled water was transferred into the solution to generate a lacteous colloid. After 15 min of stirring, 6 M NaOH was introduced to adjust the pH of the solution in the range of 8 - 9. After agitating the mixture for another 20 min, it was transferred into a 100 mL Teflon-lined stainless autoclave and was set at a temperature of 120 ºC for 12 h. The resultant yellow-white product was washed several times with distilled water and ethanol to remove impurities and then dried at 60 ºC in a vacuum for 6 h [280].

3.3. Functionalization of MWCNTs

The nitric acid treatment method was used to functionalize raw multi-walled carbon nanotubes (r-MWCNTs). This was achieved by dissolving approximately 300 mg of r-MWCNTs in 300 mL of 1 M nitric acid. The mixture was then sonicated for 4 h in cold water at 50 ºC. Deionized water was used to wash the mixture until it reached pH 7. The resultant was then allowed to dry in an oven overnight [281].

3.4. Preparation of nanocomposite MWCNT-AONP

Using 2 ml DMF, roughly 2 mg MWCNTs and 6 mg AONPs were suspended and stirred for 2 days at room temperature. The solvent was then eliminated by placing the formed nanocomposite in an oven at 25 ℃ overnight [233].

3.5. Characterization of fabricated catalysts

The following spectroscopic and microscopic techniques were instrumental in characterizing the formed catalysts (f-MWCNTs, AONPs, and AONP-MWCNT). A spectrophotometer of the carry series 300 UV-vis acquired from Agilent technologies in Germany was used to determine the maximum absorption wavelength of each catalyst. The fourier transform infrared (FTIR) spectrophotometry provided by Agilent technologies, cary 600 series, Billerica, MA, USA, was used to identify the presence or absence of functional groups in the formed nanomaterials. The X-ray diffractometer (XRD) sourced from Bruker-AXS, Madison in the USA, was used to determine each nanomaterial's crystallinity and crystal orientation. The scanning electron microscope (SEM) from Tecnai G2 spirit FEI, USA operating at 20 kV, was used to investigate the morphology of each nanomaterial and study the surface of f-MWCNTs. The transform electron microscope (TEM) from Tecnai G2 spirit FEI, USA, in conjunction with the ImageJ software program was used to calculate the average nanoparticle size. Each nanomaterial's elemental composition and weight percentage were investigated using the energy-dispersive x-ray (EDX) analysis.

3.6. Modification of the screen-printed carbon electrodes

The dry cast technique was used to modify the screen-printed carbon electrodes (SPCEs). Each catalyst (AONPs, MWCNT-AONP, and f-MWCNTs) was transferred into 1 mL DMF; following that, each of the catalysts was ultrasonically vibrated at room temperature for 30 min. Using a micropipette, about 20 μL aliquot of each dispersion was dropped on the surface of a bare-SPCE and was dried at room temperature to obtain a modified electrode [282].

3.7. The electro-catalytic experiments

Electrochemical experiments were performed using DropSens connected to a Dropview 8400 software program. Each electrochemical experiment was carried out at room temperature using 0.1 M phosphate-buffered saline (PBS) at pH 7 as the supporting electrolyte. The electrocatalytic experiments were carried out at bare and modified electrodes in 5 mM $K[Fe(CN)_6]^{3-/4-}$, and 0.1 mM (AA and 5-HT) as an analytical probe at a scan rate of 25 mVs^{-1}, using CV technique with potential window ranging from -0.2 – 1.0 V. The parameters selected to be analysed were the formal redox potential (E°'), peak separation (ΔE), and anodic and cathodic peak currents (i_{pa}, i_{pc}).

3.8. Electro-analysis experiments

The electro-analysis experiment was performed at the SPCE@MWCNT-AONP modified using the SWV technique. The operating parameters of the SWV were set as follows; frequency = 10 Hz, Eamp = 0.01 V, Estep = 0.01 V, and potential window ranging from -0.2 – 0.8 V. The fabricated electrode was used to detect varying concentrations of AA ranging from 0.016 – 0.640 μM and 5-HT concentrations from 0.016 – 0.166 μM. The calibration plots of peak currents vs. concentration were constructed from the obtained data. The sensitivity (the slope of the calibration curve) and LOD (the lowest detectable concentration by the electrode) were calculated.

3.9. Interference study

An interference study was carried out at SPCE@AONP-MWCNT using SWV. The electrode selectivity was then determined by varying the concentrations of AA (45 – 190 μM) and 5-HT (35 – 205 μM), respectively, in the presence of 0.5 mM DA as an interfering compound, and the sensitivity, LOD, and LOQ values were calculated using the acquired data.

3.10. Real-sample analysis

The applicability of the designed sensor was accomplished by determining AA and 5-HT in oranges and tomatoes, respectively. The experiments were done in triplicates using SWV method. Fresh tomatoes and oranges were purchased from a local supermarket. A tomato extract solution was obtained using a household electric blender. Then Whatman filter paper was used to obtain a colourless, clear tomato extract solution. To make up to 10 mL of sample, a fixed volume of tomato extract (1 mL) was placed into various volumes of the stock solution. For AA detection in oranges, a similar procedure was followed.

CHAPTER 4: Results and discussions

4.1. Spectroscopic and microscopic analysis

4.1.1. UV-vis spectroscopy

The spectrum in **Fig 4.1(a)** showed an absorption peak for AONPs at 297 nm [282, 283]. Agglomeration and variation in particle size are responsible for a shift in wavelength towards a longer wavelength [284]. The lack of absorption peaks in the 400 − 500 nm wavelength region implies that synthesised the nanoparticles can be used to make non-linear optical sensor devices [283]. No other peaks in the spectrum were due to impurities or structural defects, indicating that the synthesised AONPs were crystalline. To obtain the direct energy band-gap for AONPs, the linear part of (αhν) with respect to (hν) was extrapolated to zero, and it was 3.26 eV, as shown in **Fig 4.1 (c)** [283]. The absorption peak at 297 nm indicates the presence of AONPs in the nanocomposite, and the absorption peaks at 285, 297, and 345 nm were assigned to the π-π * transition of f-MWCNTs in the nanocomposite spectrum (**Fig 4.1 (b))** [233]. The absorption peak of f-MWCNTs overlapped with that of AONPs (297 nm), indicating that the AONPs retained their important conformation and absorbed into f-MWCNTs surface [232].

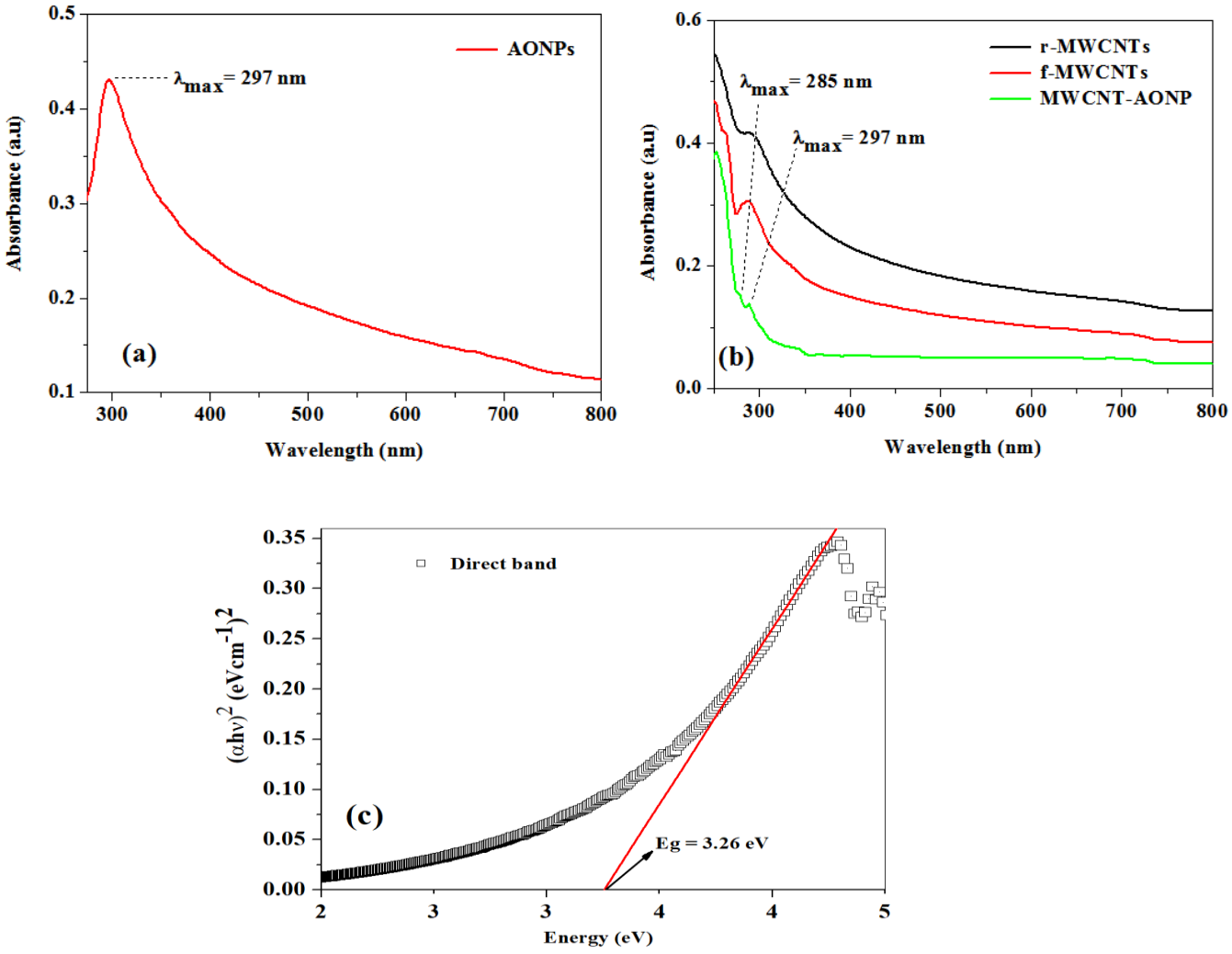

Figure 4. 1. UV-vis spectrum of (a) antimony oxide nanoparticles (AONPs) and (b) raw MWCNTs (r-MWCNT), functionalized MWCNTs (f-MWCNTs), MWCNT-AONP nanocomposite, and (c) band-gap energy of the synthesized AONPs.

4.1.2. FTIR spectroscopy

Fig 4.2 shows the FTIR spectra of (a) f-MWCNTs, r-MWCNTs, and (b) AONPs, AONP-MWCNT nanocomposite. From the spectrum in **Fig 4.2 (a),** the absorption bands of interest were located at 1569, 1742, 2326, 3410, and 3410 cm^{-1} assigned to the vibrational frequency of carboxylate anion (COO−), (C=O) of the (–COOH), (O-H) stretching from the -COOH, (-OH) stretching vibrations of the (-COOH), and free hydroxyl group O-H, respectively [232, 281, 285, 286]. These functionalities make MWCNTs hydrophilic, allowing attachment of nanoparticles at the anchoring sites. The absorption band at 2350 and 3780 cm^{-1} is due to the O–H stretching of the –COOH functional group and aromatic C–H stretching. The nanocomposite spectrum **(Fig 4.2 (b))** showed the absorption bands for AONPs at 630 and 517 cm^{-1} attributed to the stretching and vibration of O-Sb-O and Sb-O bonds, respectively [233, 282]. The FTIR showed traces of toluene functionalities on the surface of the synthesized nanoparticle noted by absorption bands at 1408 cm^{-1} attributed to the vibrational band of C=C stretching benzenoid rings and sp3 C-H vibration at 2999 cm^{-1}. A huge reduction in the signatures appearing at 630, 1008, 1480, and 1569 cm^{-1} absorptions peaks of AONPs when the nanocomposite was formed suggests successful nanocomposite formation as AONPs are absorbed on the surface of f-MWCNTs. The rest of the absorption bands were attributed to the formation of f-MWCNTs in the nanocomposite.

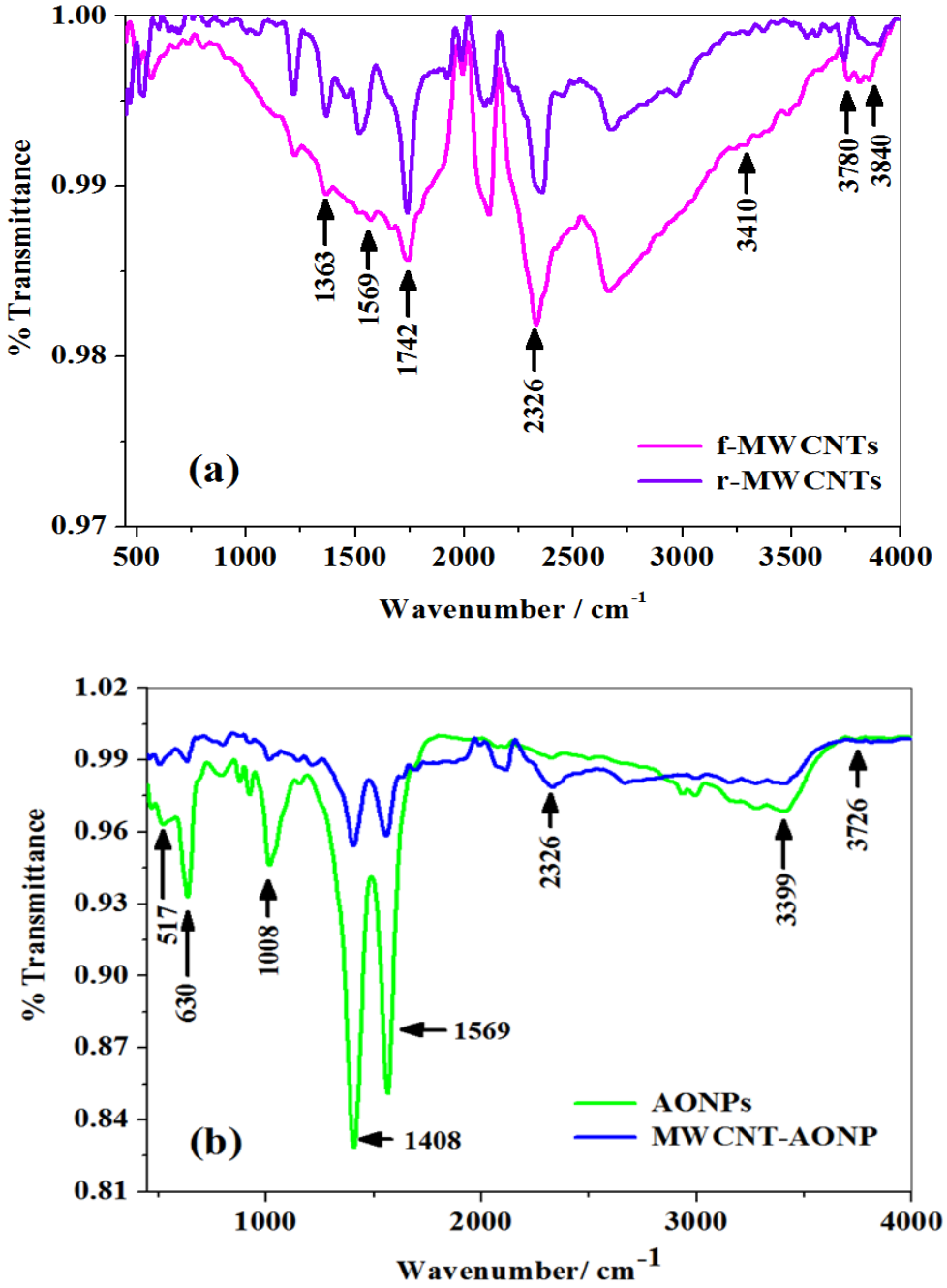

Figure 4. 2. The FTIR analysis of (a) functionalized MWCNTs (f-MWCNTs), raw MWCNTs (r-MWCNTs), and (b) antimony oxide nanoparticles (AONPs), and multi-walled carbon nanotube- antimony oxide (MWCNT-AONP) nanocomposite.

4.1.3. XRD analysis

Fig 4.3 shows the XRD spectra of (a) AONPs, (b) f-MWCNTs, and (c) AONP-MWCNT composite. **Fig 4.3 (a)** shows sharp and strong diffraction peaks, indicating that the formed AONPs are highly crystalline [283].

The diffraction peaks at 2θ = 19.46° (110), 25.48° (111), 27.73° (222), 28.46° (121), 33.02° (002), 32.73° (131), 34.84° (012), 36.54° (200), 39.63° (032), 44.33° (042), 46.02° (231), 47.11° (240), 50.47° (161), 55.78° (170), 58.90° (242), and 60.90° (261) were characteristic of AONPs formation and they had an orthorhombic phase orientation [280]. **Fig 4.3 (b)** shows the XRD image of f-MWCNTs. The f-MWCNTs have amorphous characteristics indicated by the broad diffraction peaks at 2θ = 25.94° (002) and 50.66° (004) [233, 287]. **Fig 4.3 (c)** shows the unique diffraction peaks of all nanomaterials used to synthesize the AONP-MWCNT nanocomposite. The diffraction peaks at 2θ = 19.46° (110), 25.48° (111), 27.73° (222), 28.46° (121), 33.02° (002), 32.73° (131), 34.84° (012), 36.54° (200), 39.63° (032), 44.33° (042), 46.02° (231), 47.11° (240), 50.47° (161), 55.78° (170), 58.90° (242), and 60.90° (261) indicates the presences of AONPs in the nanocomposite, and diffraction peak at 2θ = 25.96 ° (400) represented the availability of f-MWCNTs. Using Scherrer's **equation (4.1)**, the crystalline size of AONPs was calculated to be 30 nm. Since a single particle contains more than one crystalline, slight differences in size were noticed between the TEM and XRD techniques [288] .

$$\tau = \frac{K\lambda}{\beta \cos\theta} \qquad (4.1)$$

Whereby τ, λ; θ and β represents the average size of the crystalline (nm), X-ray wavelength, the Bragg's angle, and the line broadening at half the maximum intensity (FWHM) with a value of 0.9.

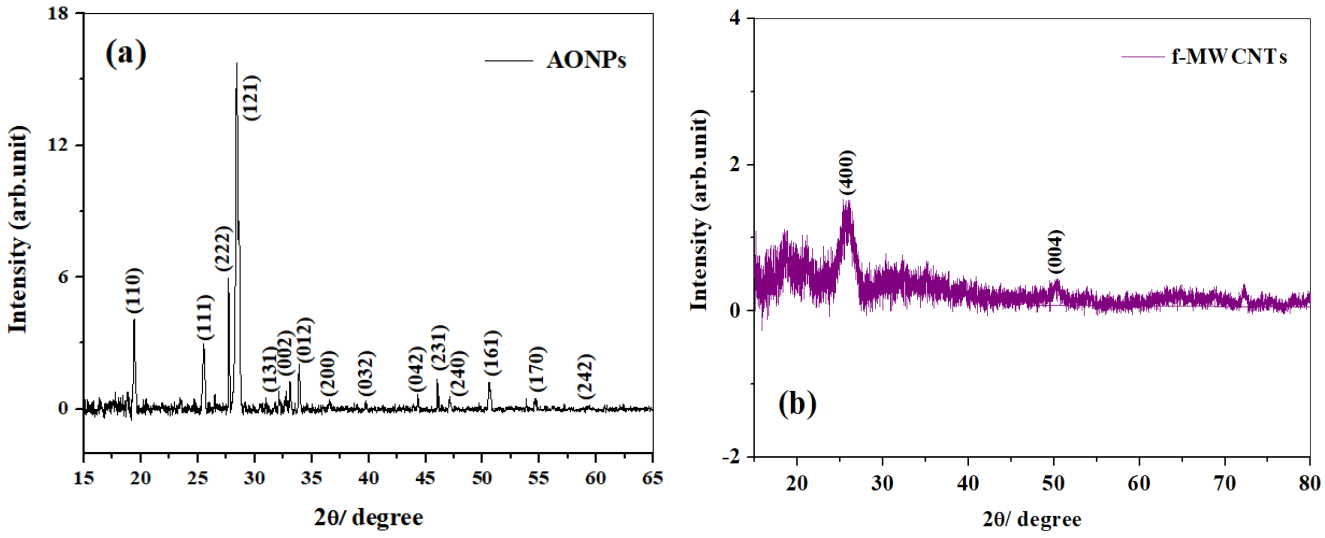

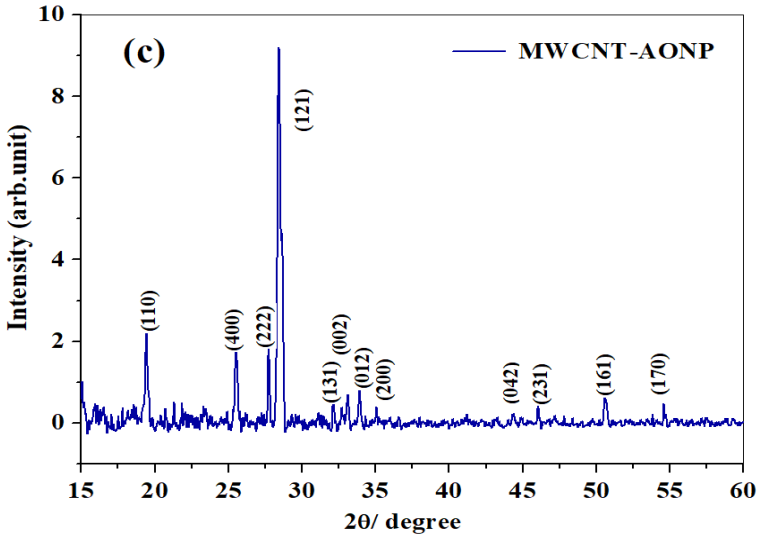

Figure 4. 3. X-ray diffraction of (a) antimony oxide nanoparticles (AONPs), (b) functionalized MWCNTs (f-MWCNTs), and (c) AONP-MWCNT nanocomposite.

4.1.4. EDX characterization

Fig (4.4 & 4.5) shows the EDX plots for AONPs, and AONP-MWCNT nanocomposite, respectively and the inserts represent the weight and atomic percentages of each element in the nanomaterials. The presence of a carbon peak in the AONPs plot could be attributed to the presence of toluene on the surface of the nanoparticles. The fluoride peak in AONP-MWCNT nanocomposite plots could be due to contamination during sample preparation. The prominence of antimony (Sb) and oxygen (O) in **Fig. 4.5** plot indicates that AONPs were successfully formed. While the dominance of antimony (Sb), oxygen (O), and carbon (C) in **Fig 4.6** confirms the formation of MWCNT-AONP nanocomposite. The relative standard deviation for antimony (Sb) in AONPs and MWCNT-AONPs was 2.92 and 0.72.

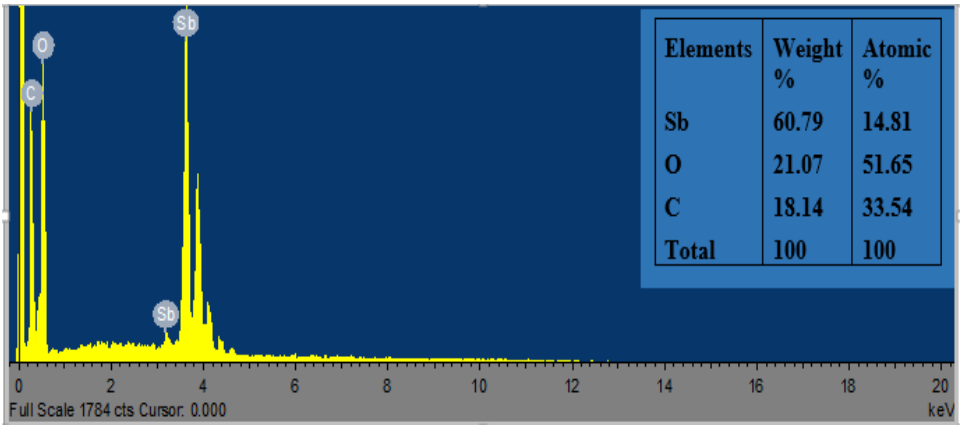

Elements	Weight %	Atomic %
Sb	60.79	14.81
O	21.07	51.65
C	18.14	33.54
Total	100	100

Figure 4. 4. EDX for antimony oxide nanoparticles (AONPs) and the inserts show the elemental composition, weight, and atomic percentage of each element present in the AONPs.

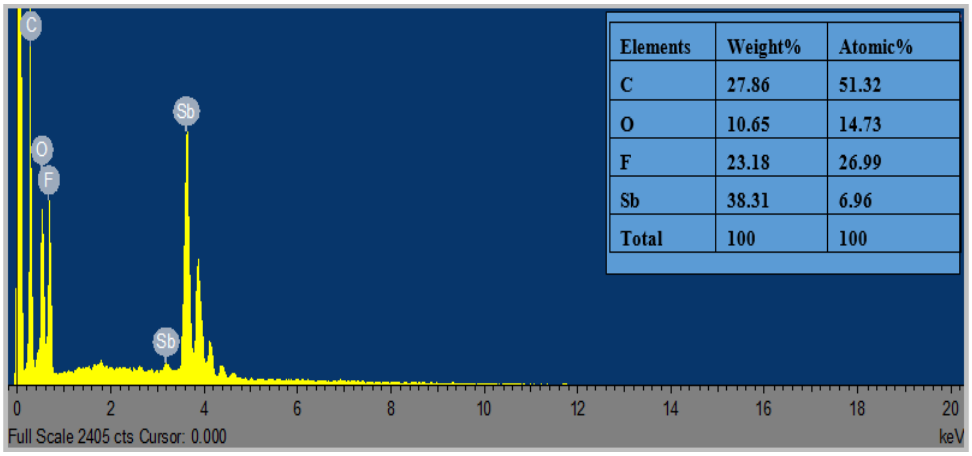

Elements	Weight%	Atomic%
C	27.86	51.32
O	10.65	14.73
F	23.18	26.99
Sb	38.31	6.96
Total	100	100

Figure 4. 5. EDX for MWCNT-AONP nanocomposite and the inserts show the elemental composition, weight, and atomic percentage of each element present in the nanocomposite.

4.1.5. SEM Characterizations

Fig 4.6 (a) indicates that the morphology of the AONPs was rod-like, and **Fig 4.9 (b)** shows loose curly CNTs with no surface degradation or noticeable changes due to acid oxidation [289]. While **Fig 4.6 (c)** shows the SEM images of the nanocomposite material in which AONPs are distributed homogenously on the surface of f-MWCNTs.

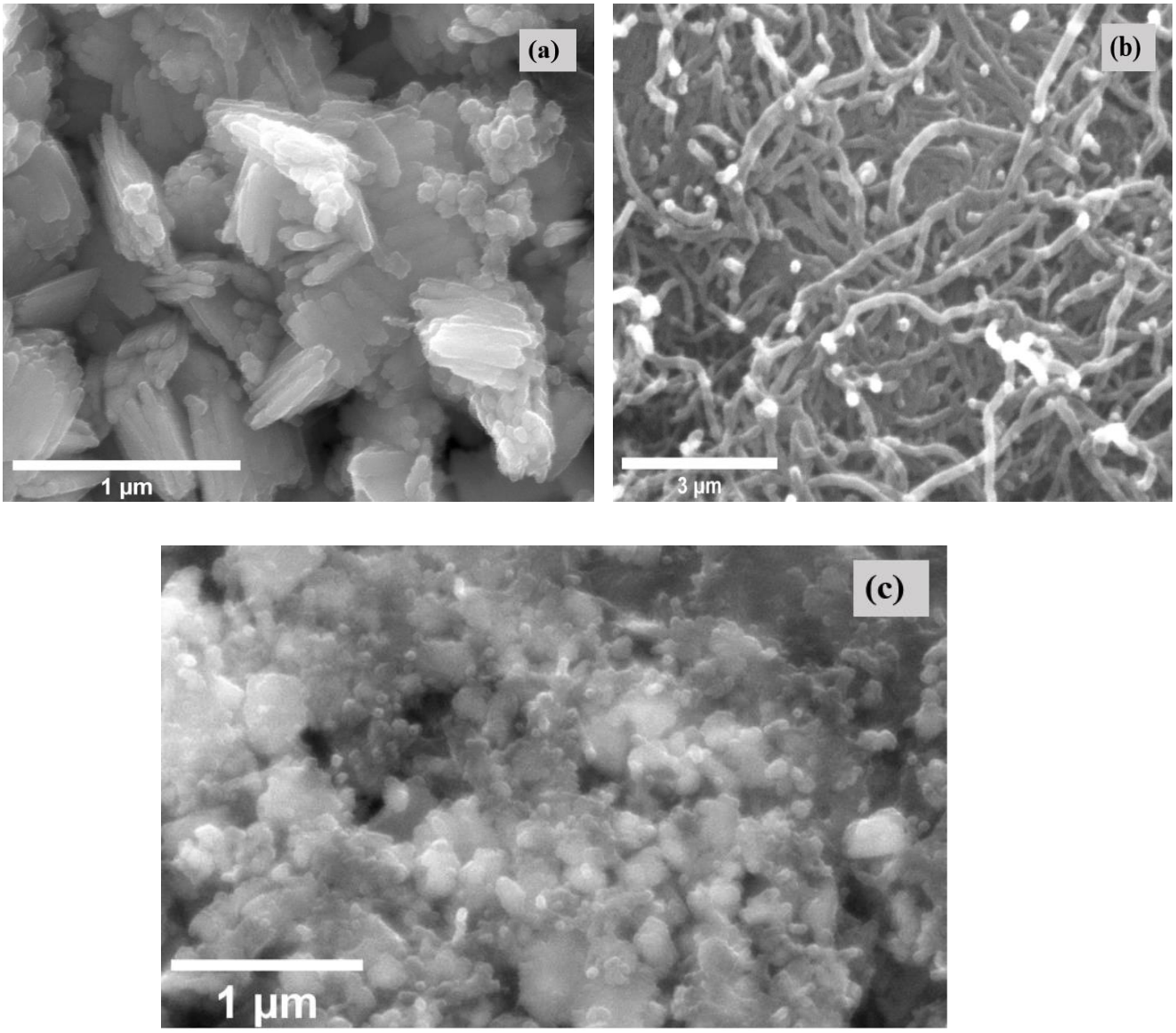

Figure 4. 6. SEM images of the synthesized nanomaterials (a) antimony oxide nanoparticles, (b) functionalized MWCNTs, and (c) AONP-MWCNT nanocomposite.

4.1.6. TEM characterization

Fig 4.7 displays the TEM images of (a) AONPs, and (b) AONP-MWCNT composite, each at 50 nm magnification, and (c) AONPs particle size. The TEM images of AONPs (**Fig 4.7 (a))** were spherical, unevenly distributed, crystalline, and agglomerated due to the ineffective dispensing capability of the solvent. **Fig 4.7 (c)** shows the spiral-like f-MWCNTs and dark spots represent AONPs. **Fig 4.7 (c)** displayed that the mean particle size for AONPs was ≈ 25 nm, and the largest reached 95 nm.

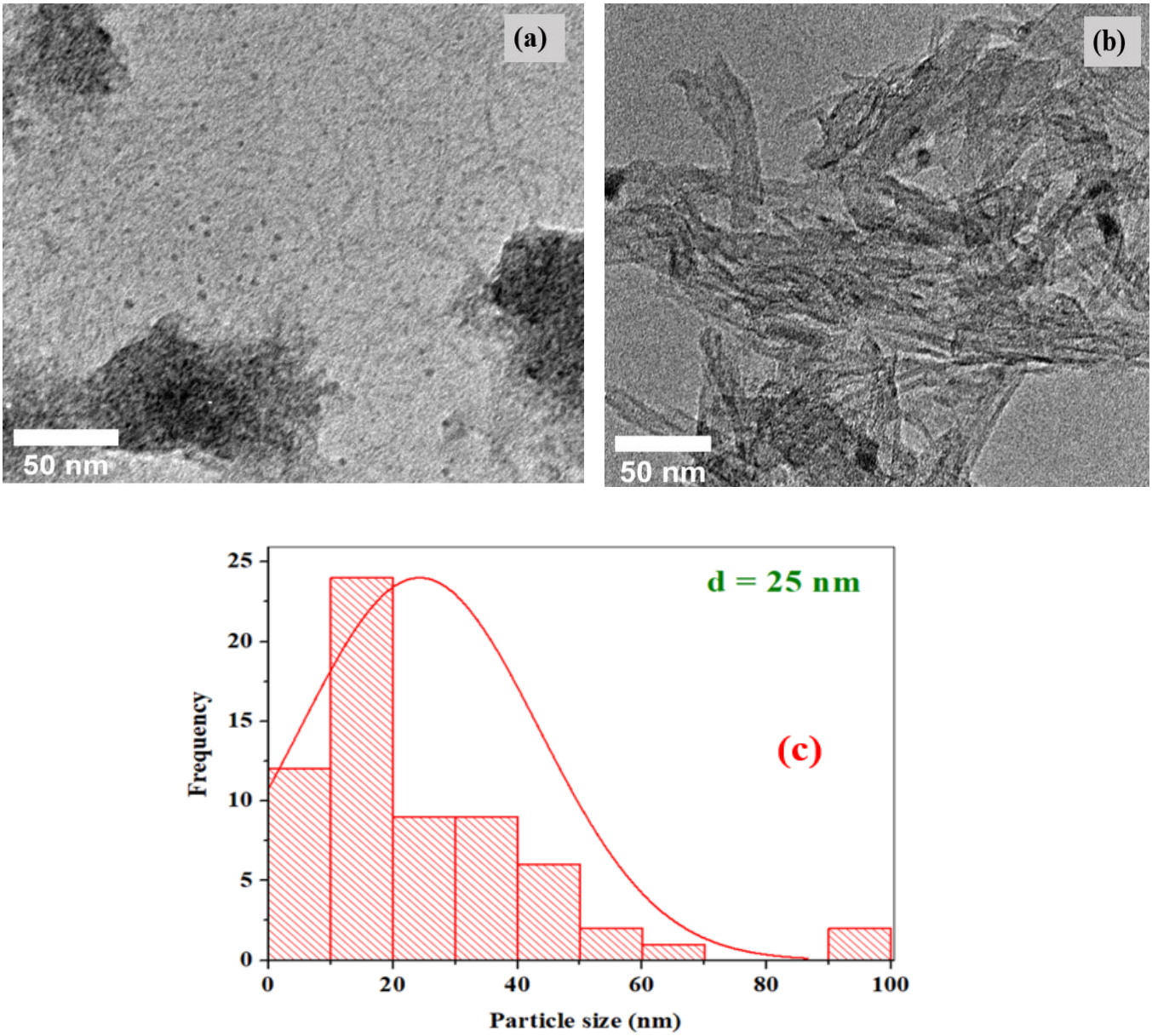

Figure 4. 7. TEM depictions of (a) AONPs, (b) MWCNT-AONP nanocomposite, and (c) average AONPs particle size.

4.2. Comparative study of bare and modified electrodes

The electrochemical properties of bare and CNTs fabricated electrodes were carried out in 5 mM K [Fe (CN) $_6]^{3-/4-}$ in 0.1 M phosphate-buffered saline at pH 7, using cyclic voltammetry at 25 mVs^{-1}. **Fig 4.8** shows the experimental results, and **Table 4.1** summarizes all cyclic parameters obtained at each electrode. The CNTs modified electrodes displayed perfect reversible voltammogram shapes than bare electrodes, indicating easier follow of electrons at the modified electrodes. A slight shift in the SPCE/r-MWCNTs peak potential towards negative potentials indicates a decrease in the over-potential of the redox process at the modified electrode. The peak separation (ΔE) for the SPCE-bare, SPCE/r-MWCNTs, and SPCE/f-MWCNTs was 480, 160, and

150 mV, respectively. All ΔE values were greater than 59 mV for a quick one-electron transfer process. The current response at SPCE/f-MWCNTs was 1.58 and 2.29 times greater than SPCE/r-MWCNTs and SPCE-bare, respectively. This indicates that SPCE/f-MWCNTs can transport electrons much faster than the investigated electrodes and have a greater electroactive surface area due to oxygen functionalities on the surface of the MWCNTs.

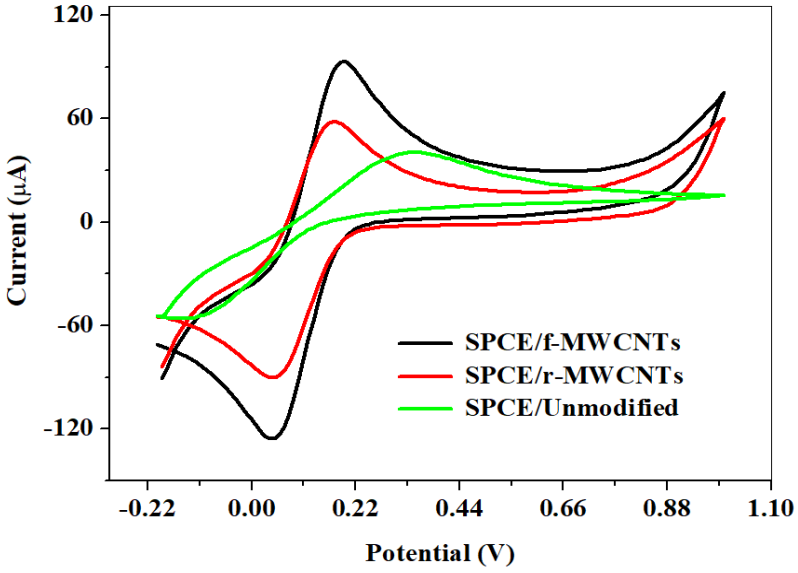

Figure 4. 8. Comparative cyclic voltammogram for SPCE/r-MWCNTs, SPCE/f-MWCNTs, and SPCE/f-MWCNTs.

Table 4. 1. Summary of cyclic voltammetric parameters obtained at bare and CNTs fabricated electrodes.

Electrodes	Ipa(μA)	Ipc(μA)	Ipa/Ipc	Epa(V)	Epc(V)	ΔEp(V)	E^o(V)
SPCE-Bare	40.84	-55.82	-0.73	0.35	-0.13	0.48	0.11
r-MWCNTs	59.14	-90.05	-0.66	0.18	0.02	0.16	0.10
f-MWCNTs	93.37	-125.40	-0.75	0.20	0.04	0.15	0.12

4.3. Optimization study

The optimization study was carried out by varying the concentration of the AONPs while keeping the concentration of f-MWCNTs constant. **Fig 4.9** shows a comparative cyclic voltammogram obtained in **(a)** 0.1 mM 5-HT and **(b)** 5 mM K [Fe (CN) $_6$]$^{3-/4-}$ dissolved in 0.1M supporting buffer at a scan rate of 25 mVs^{-1}. All the voltammograms showed that the 1 f-MWCNTs: 3 AONPs nanocomposite had the highest current response compared to other formed nanocomposites. This suggests greater biocompatibility and faster electron transfer kinetics at 1 f-MWCNTs: 3AONPs modified electrode. Similar results have been reported [225]. Therefore, the 1 f-MWCNTs: 3 AONPs nanocomposite was adopted and used throughout the study.

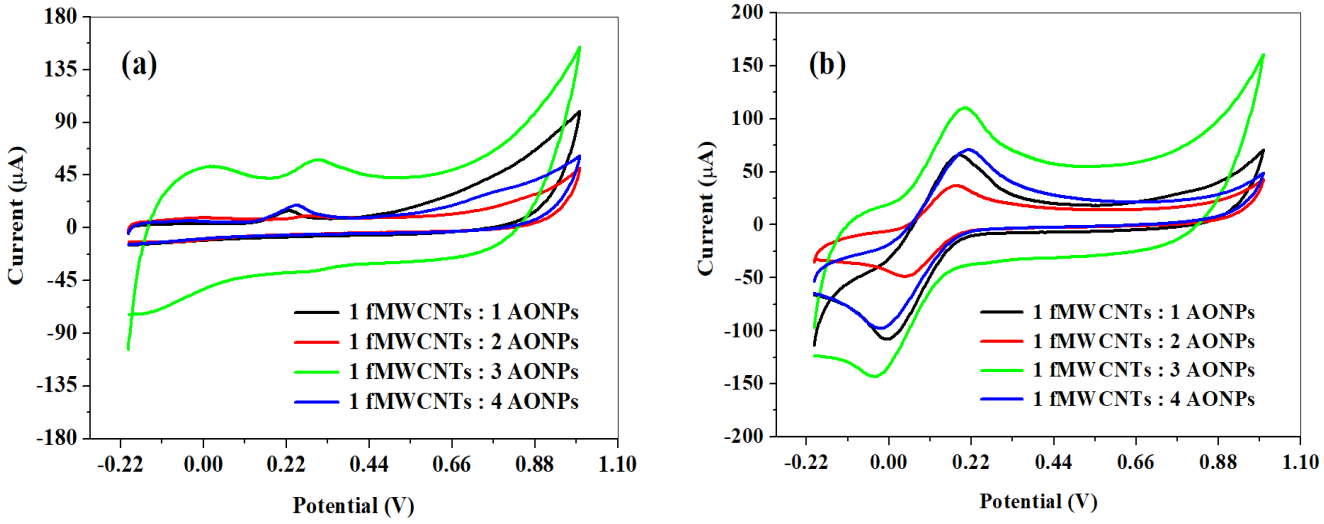

Figure 4. 9. Comparative cyclic voltammogram for the optimization study prepared (a) 0.1 mM 5-HT and (b) 5 mM K [Fe (CN) $_6$]$^{3-/4-}$ dissolved in 0.1 M phosphate-buffered saline at pH 7 utilizing a scan rate of 25 mVs^{-1}.

4.4. pH optimization studies

The pH optimization study was done at SPCE@AONP-MWCNT in 0.1 M phosphate-buffered saline at various pH (pH 3, pH 6, pH 7, and pH 9) containing 0.1 mM 5-HT at 10 and 25 mVs^{-1} scan rates, respectively, using the CV method. This experiment was crucial because most NTs are present in the blood at a physiological pH of 7.40. **Fig 4.10** shows the effects of different pH buffer solutions on the 5-HT peak current. The inserts showed that all scan rates reached the maximum current peak at pH 7 and then decreased. This implies that the SPCE@AONP/MWCNT is stable at pH 7 buffer solution. However, the current peak at 25 mVs^{-1} was almost twice that at a scan rate of 10 mVs^{-1} at same pH. Consequently, the following electrochemical experiments were performed using 0.1 mM 5-HT at pH 7 using a 25 mVs^{-1} scan rate. **Fig 4.10 (b & d)** describes the relationship between Epa vs. pH at scan rates of 10 and 25 mVs^{-1}, respectively. The peak potential shifted towards lower pH values as the pH increased, indicating protons engaged in the reaction. The relationship could be expressed using the linear regression equation: E_{pa} (V) = 0.034 pH + 0.0597

(R^2 = 0.9820) and E_{pa} (V) = 0.032 pH + 0.58 (R^2 = 0.9920), at scan rate of 25 and 10 mVs^{-1}, respectively. The slopes of the dEp / dpH plots were 34 and 32 mV pH^{-1}, which were near to the theoretical Nernst value (59 mV pH^{-1}) for 1H^+ per electron reaction mechanism [43, 290]. Therefore, the reaction mechanism of 5-HT at the proposed sensor electrode occurs as represented in **Scheme 4.1.**

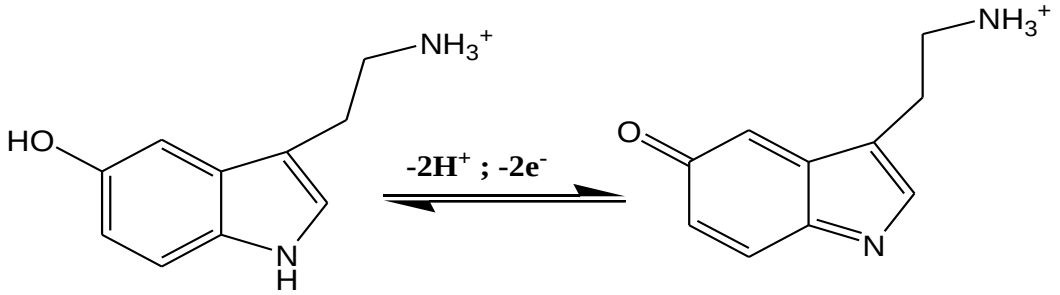

Serotonin (reduced) Serotonin (oxidised)

Scheme 4. 1**.** The proposed redox mechanism for 5-HT.

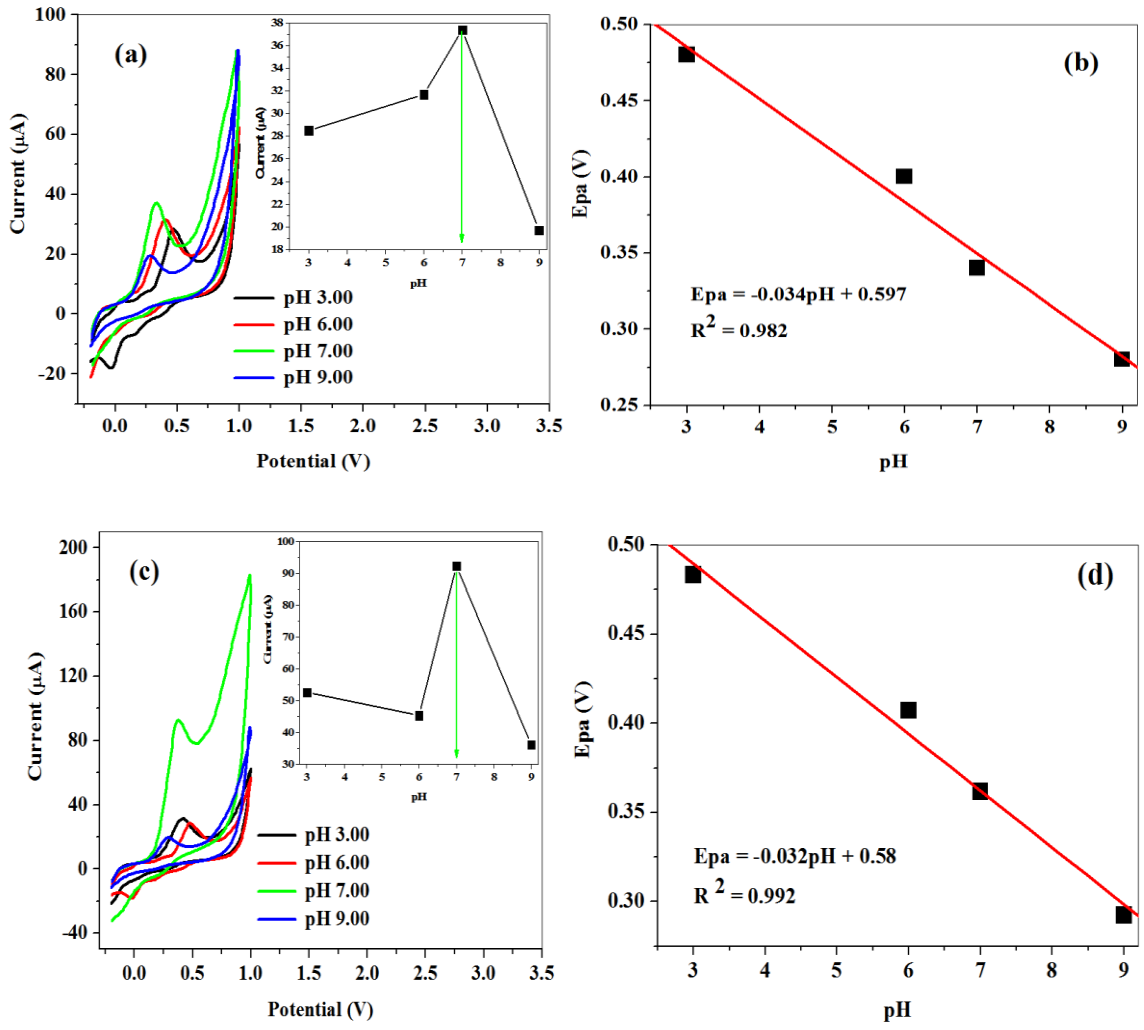

Figure 4. 10. The influence of buffer pH on the peak current of 5-HT in 0.1 M phosphate-buffered saline at pH: 3, 6, 7, and 9 at scan rate (a) 10 and (b) 25 mVs^{-1}. Inset: the relationship between the oxidation current peaks versus the pH (c) and (d) the relationship between the peaks potential versus pH.

4.5. Electrochemical analysis

The schematic diagram showing the electrode fabrication process and electrochemical characterization of each fabricated electrode in 5 mM K $[Fe(CN)_6]^{3-/4-}$ generated in 0.1M phosphate-buffered saline at pH 7 at 25 mVs^{-1} scan rate is represented in **Fig 4.11**.

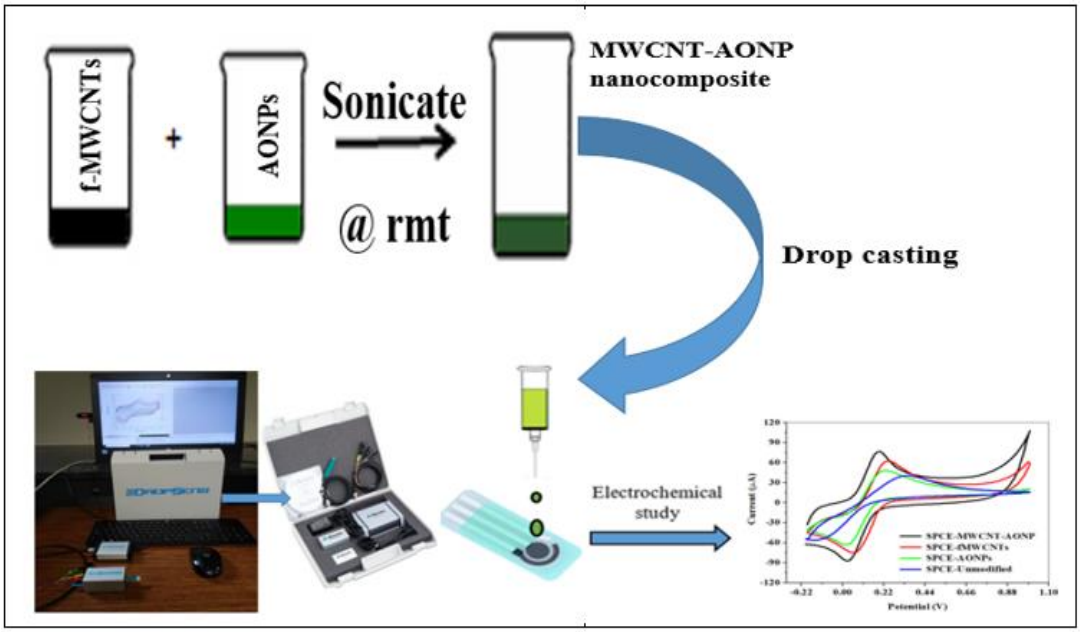

Figure 4. 11. A schematic diagram displaying the modification process of the bare SPCE via the drop-cast method and electrochemical characterization of the modified and bare electrodes. The picture on the bottom left-hand side displays the DropSens tool kit from Metrohm (Madrid, Spain) used to perform electrochemical characterization experiments.

Fig 4.12 (a & b) showed an increase in current response in the following manner, SPCE-bare (Ipa = 40.84 µA ; Epa = 0.35 V), SPCE-AONPs (Ipa = 48.17 µA ; 0.23 V), SPCE/f-MWCNTs (Ipa = 93.37 µA ; Epa = 0.19 V), and SPCE@AONP-MWCNT (Ipa = 99.15 µA; Epa = 0.22 V). The difference in shapes between modified and bare electrodes was attributed to the enhanced electrocatalytic effect of the modification. The current response at the nanocomposite electrode was almost three times that at the bare electrode. From **Table**

4.2, the Ipa/Ipc ratio is closer to one for all electrodes, indicative of a reversible process. The ΔEp value for SPCE@MWCNT-AONP, SPCE/fMWCNTs, SPCE-AONPs, and SPCE-bare, was 0.17, 0.19, 0.21, and 0.48 V, respectively greater than 0.059 V for quick one electron transport processes. This highlights that modified electrodes have better electrocatalytic properties than bare electrodes due to the increased surface-to-volume ratio. The Randles–Ševčík **equation (2.1)** was used to compute the active surface area of each electrode. A larger active surface area indicates increased exposure of electrocatalytic processes to an electroactive site [291]. The active surface area calculated for bare-SPCE, SPCE/AONPs, SPCE/f-MWCNTs, and the nanocomposite electrode was 0.054, 0.123, 0.346, and 0.716 cm^2, respectively. The nanocomposite electrode had an eight times larger active surface area than the SPCE-bare and negligible over-potential than the bare electrode [292]. The experiment showed that the modified electrode, especially the nanocomposite modified electrode, exhibited faster electron transfer kinetics, better redox potentials, and electrode stability than bare electrodes [293]. As a result, the SPCE@AONP-MWCNT nanocomposite electrode was adopted, and further experiments were carried out with it.

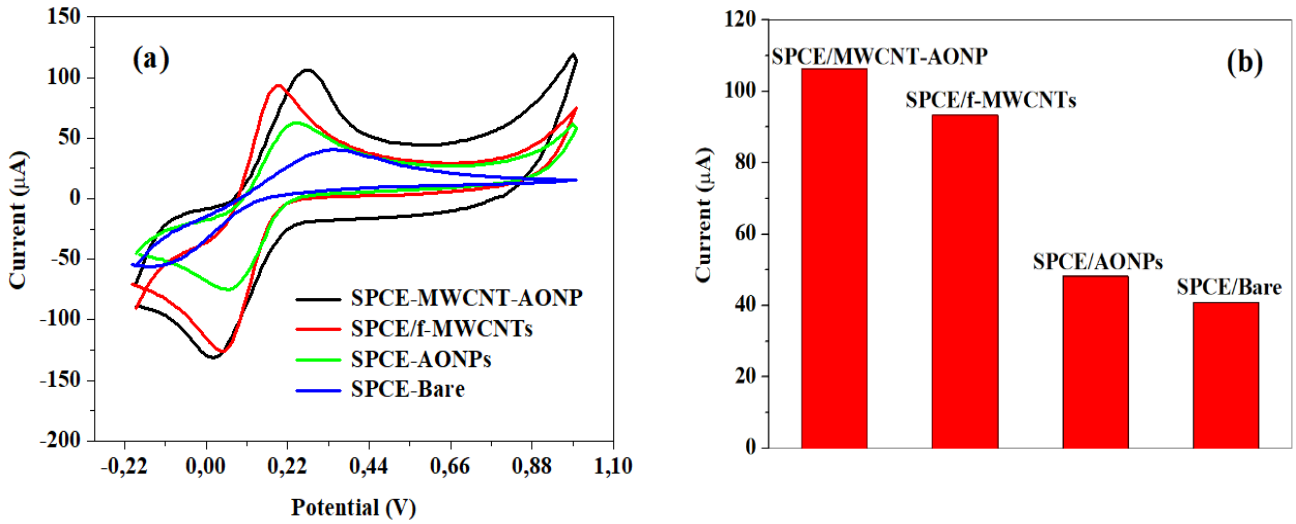

Figure 4. 12. (a) Comparative cyclic voltammogram at the modified and bare electrodes in 5 mM K [Fe (CN) $_6$]$^{3-/4-}$, and (b) comparative current peak between modified and bare electrodes.

Table 4. 2. Summary of cyclic voltammetric parameters obtained at the bare and modified electrodes in 5 mM K [Fe (CN) $_6$]$^{3-/4-}$ generated in 0.1 M supporting buffer at pH 7.

Electrodes	Ipa(µA)	Ipc(µA)	Ipa/Ipc	Epa(V)	Epc(V)	ΔEp(V)	E^o(V)

SPCE-Bare	40.84	-55.82	-0.73	0.35	-0.13	0.48	0.11
SPCE-AONPs	48.17	-64.05	-0.75	0.23	0.02	0.21	0.13
SPCE/f-MWCNTs	93.37	-125.40	-0.75	0.19	0.05	0.14	0.12
SPCE@AONP-MWCNT	106.26	-131.13	-0.81	0.28	0.02	0.26	0.15

The effect of varying the scan rate in 5 mM $[Fe(CN)_6]^{3-/4-}$ prepared in 0.1 M phosphate-buffered saline at pH 7 with a scan rate range from 10 - 300 mVs^{-1} at the nanocomposite modified electrode using CV. The result of the experiment is represented in **Fig 4.13**. From Fig **4.13 (a),** it is evident that as the scan rate increased, the anodic peak potentials shifted towards positive potentials while the cathodic peak potentials shifted towards negative potentials. **Fig 4.13 (b)** shows a linear correlation between scan rate and the cathodic and anodic currents. Also, **Fig 4.13 (b)** suggests an ideal reversible redox reaction [294]. This is supported by almost equal gradient slopes obtained at Ipa = 73.215 µA/ $(mVs^1)^{1/2}$ – 133.50 and Ipc = -73.549 µA/ $(mVs^1)^{1/2}$ + 142.87 each with linear regression value of 0.993, and 0.995 respectively. **Fig 4.13 (b)** almost zero intercepts, demonstrating a diffusion-controlled process with certain amounts of adsorbed reaction intermediates. The plot's linear connection revealed that the nanocomposites were electroactive, conducting, and surface-confined. **Fig 4.13 (c & d)** shows a linear relationship between Ep and scan rate logarithm. **T**he linear relation can be expressed using linear equation**;** Epa = 0.203 log*v* - 0.0857.

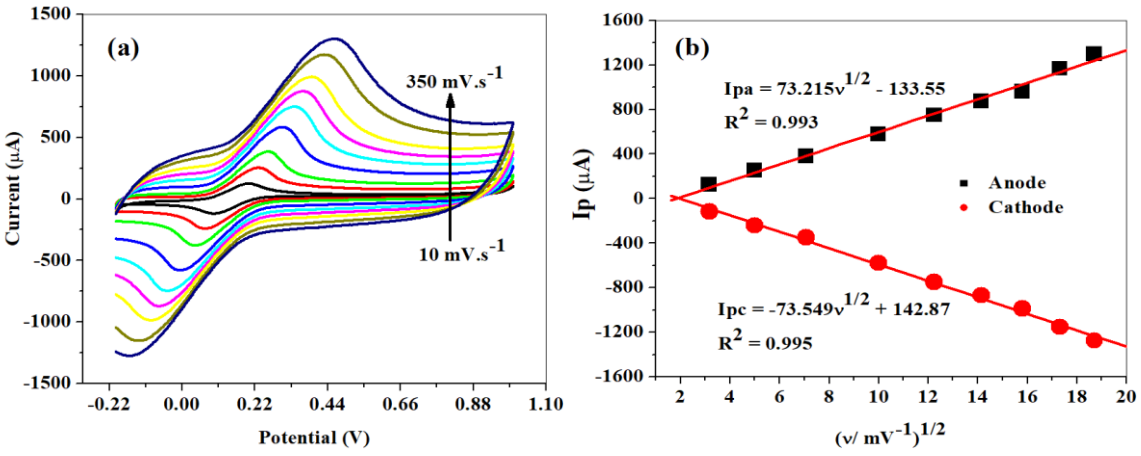

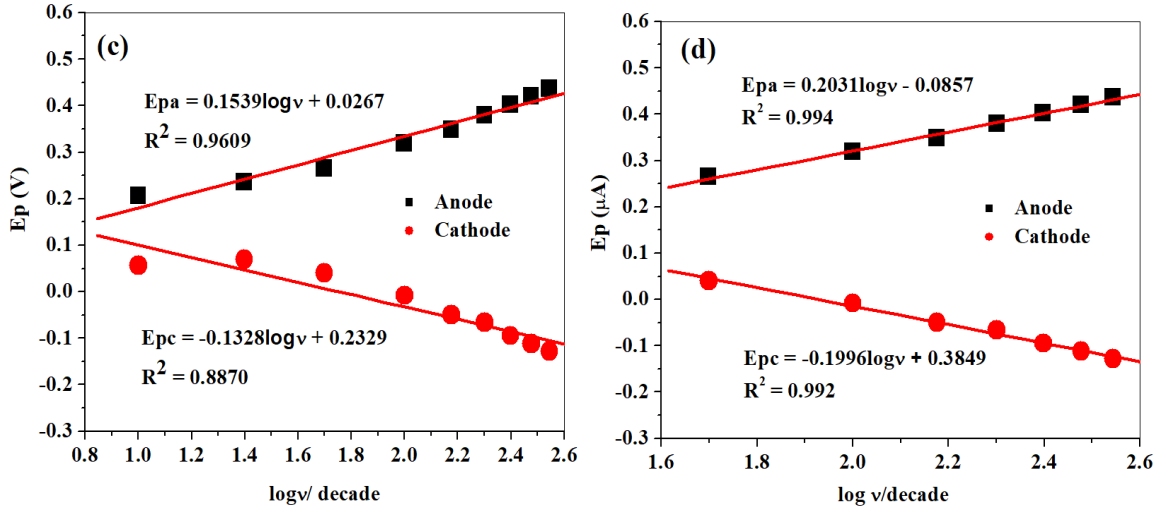

Figure 4. 13. (a) Scan rate study at the proposed sensor (b) linear plots of Ipa/Ipc vs. square root of scan rate, (c and d) linear plots of peak potentials vs. log *v*/decade.

The acquired Tafel value of 406 mVdec^{-1} calculated using **equation (4.2)** exceeded the theoretical value of 118 mVdec^{-1} confirming the involvement of reaction intermediates or adsorption at the electrode. Adsorption could be due to the porous nature of f-MWCNTs [295].

$$Ep = \frac{b}{2}\log v + constant \qquad (4.2)$$

Ep and b constitute the peak potential (V) and gradient slope.

The **equations (4.3 & 4.4)** assigned as the cathodic and anodic peaks by Laviron et al., 1979 [296] were utilized to calculate the electron coefficient (α) of 0.50 and the number of electrons transported (n) of 0.597 approximated to one electron.

$$Slope = \frac{-2.3RT}{\propto nF} \qquad (4.3)$$

$$Slope = \frac{2.3RT}{(1-\propto)nF} \qquad (4.4)$$

The rate constant (k_s) value of 4.63 x10^{-2} cm/s^{-1} was calculated using **equation (4.5)**. The acquired rate constant value was > 0.02 cm/s^{-1} indicating a quick and reversible reaction at the electrode [297].

$$\log ks = \alpha \log(1-\alpha) + (1-\alpha)\log\alpha - \log\frac{RT}{nF\upsilon} - \alpha(1-\alpha)\frac{nFT}{2.3RT} \quad (4.5)$$

While R, T, n, and F represent the gas constant (8.314 $Jmol^{-1}k^{-1}$), the temperature (298K), the number of electrons transferred during a redox process, and the Faraday constant (9600 C / mol), respectively, the term α represents the transfer coefficient, and υ is the scan rate (V/s).

4.6. Electro-oxidation experiments

Fig 4.14 shows the comparative electro-catalytic reactions at the bare and modified electrodes in (a) 0.1 mM 5-HT and (c) 0.1 mM AA generated in 0.1M phosphate-buffered saline at pH 7 at 25 mVs^{-1} scan rate. The voltammograms in **Fig 4.14 (a & c)** indicate that the reactions of 5-HT and AA at the electrodes were irreversible; also, modified electrodes showed enhanced cyclic voltammogram shapes compared to the bare electrodes. **Fig 4.14 (b)** compares the peak currents between the electrodes for 5-HT detection. The peak current reduced in the following pattern, the SPCE@MWCNT-AONP (Ipa = 84.13 µA; Epa = 0.35 V) > SPCE/f-MWCNTs (Ipa = 33.49 µA; Epa = 0.32 V) > SPCE-AONPs (Ipa = 24.40 µA; Epa = 0.27 V) > SPCE-bare (Ipa = 2.89 µA; Epa = 0.50 V). The peak potentials for 5-HT at the nanocomposite electrodes matched others from the literature [19, 43]. The current response at the nanocomposite electrode was 29 times bigger than that at the bare electrode. A decrease in current response for AA was observed in the following manner, SPCE@MWCNT-AONP (Ipa = 60.71 µA; Epa = 0.032 V), SPCE-AONPs (Ipa = 11.36 µA ; Epa = 0.034 V), and SPCE-Bare (Ipa = 14.96 µA; Epa = 0.45 V) as represented in **Fig 4.14 (c & d)**. The Epa value of 0.032 V matched other literature studies [152, 153, 159]. For SPCE/f-MWCNTs, there was no anodic peak current observed, indicating that the SPCE/f-MWCNTs did not interact with the analyte (AA). The current peak at the nanocomposite electrode was 4 times that of the bare–SPCE. The synergy between f-MWCNTs and AONPs in facilitating electron transport at SPCE-modified electrodes cannot be overstated. The conductive properties of the AONPs and f-MWCNTs and the ionic interaction between the AONPs and f-MWCNTs are some of the mechanisms responsible for this considerable electron transport at the SPCE@MWCNT-AONP modified electrodes.

Similarly, the wide surface area provided by the porous f-MWCNT on the electrode allowing free passage of electrolytes and charges between the base electrode and the electroactive species at the electrode surface, is an essential component in the SPCE@MWCNT-AONP electrode's outstanding achievement. Similar findings

for modified electrodes have been described [43, 225, 232]. As a result, the proposed sensor was adopted and investigated further for selectivity, sensitivity, stability, reproducibility, and applicability.

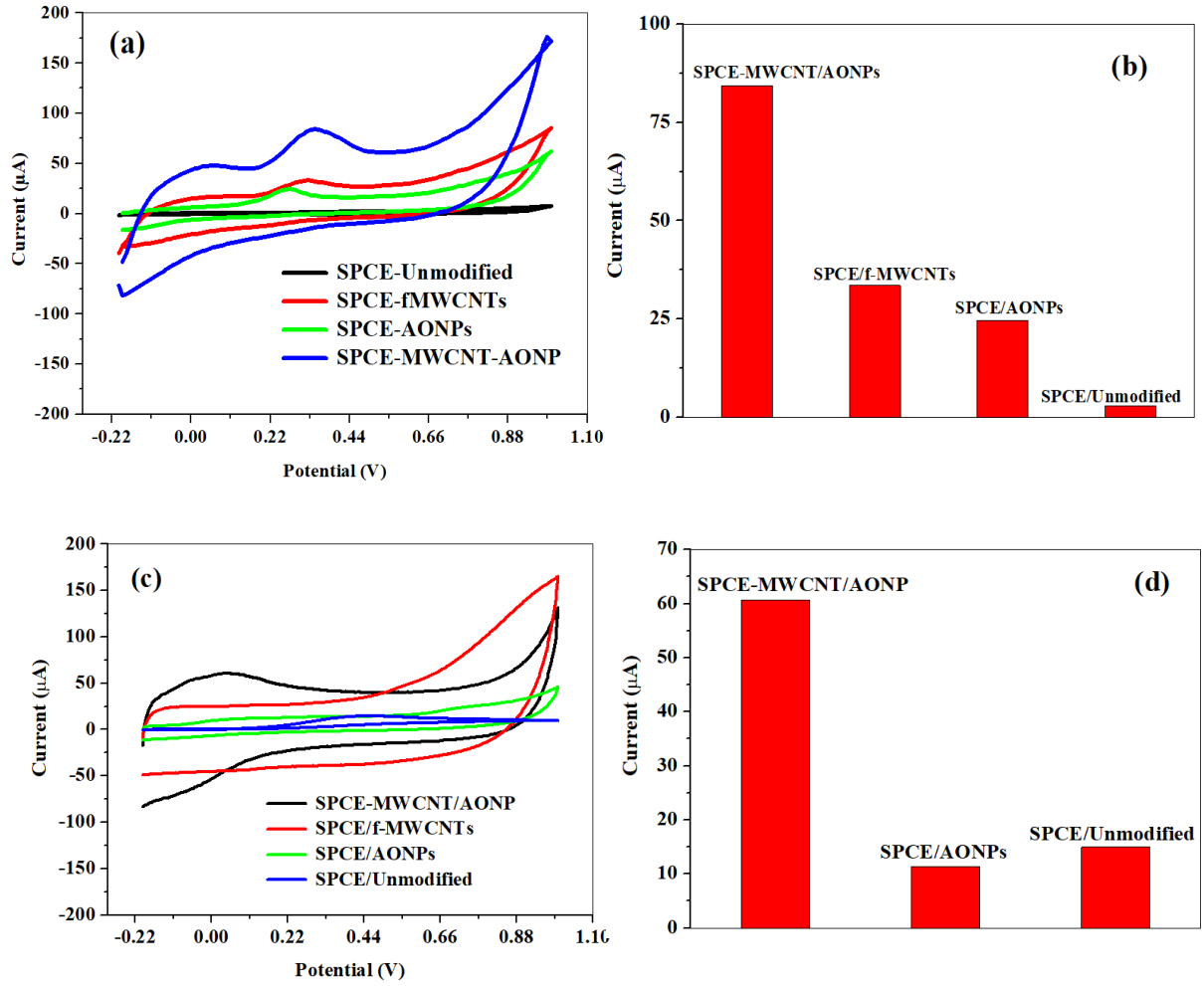

Figure 4. 14. Comparative cyclic voltammogram at the bare and modified electrodes in (a) 0.1 mM 5-HT and (c) 0.1 mM AA prepared in 0.1 M phosphate-buffered saline at pH 7 at a scan rate of 25 mVs^{-1}. (b & d) shows their corresponding current response at various electrodes.

Scan rate studies at the suggested electrode in (a) 5-HT and (c) AA are shown in **Fig 4.15.** Each analyte's voltammogram displayed a shift in anodic peak potential towards high potential values with increasing scan rate. **Fig 4.15 (b & c**) shows linear plots of current (µA) vs square root of scan rate, with a linear expression of Ipa = 40.58 $v^{1/2}$ – 116.79 5-HT (R^2 = 0.988) and Ipa = 44.14 $v^{1/2}$ – 135.55 for 5-HT and AA respectively. The linear relationship indicates that the reactions of 5-HT and AA at the proposed electrodes were diffusion-controlled. The effect of varying scan rates on the current AA and 5-HT was determined at the proposed electrode. The cyclic voltammogram showed a potential peak shift towards higher potentials and increased

current peak with increasing scan rate, as seen in **Fig 4.15 (a & c)**. The linear plots of current with the square root of scan rate are represented in **Fig 4.15 (b & d)** for 5-HT and AA.

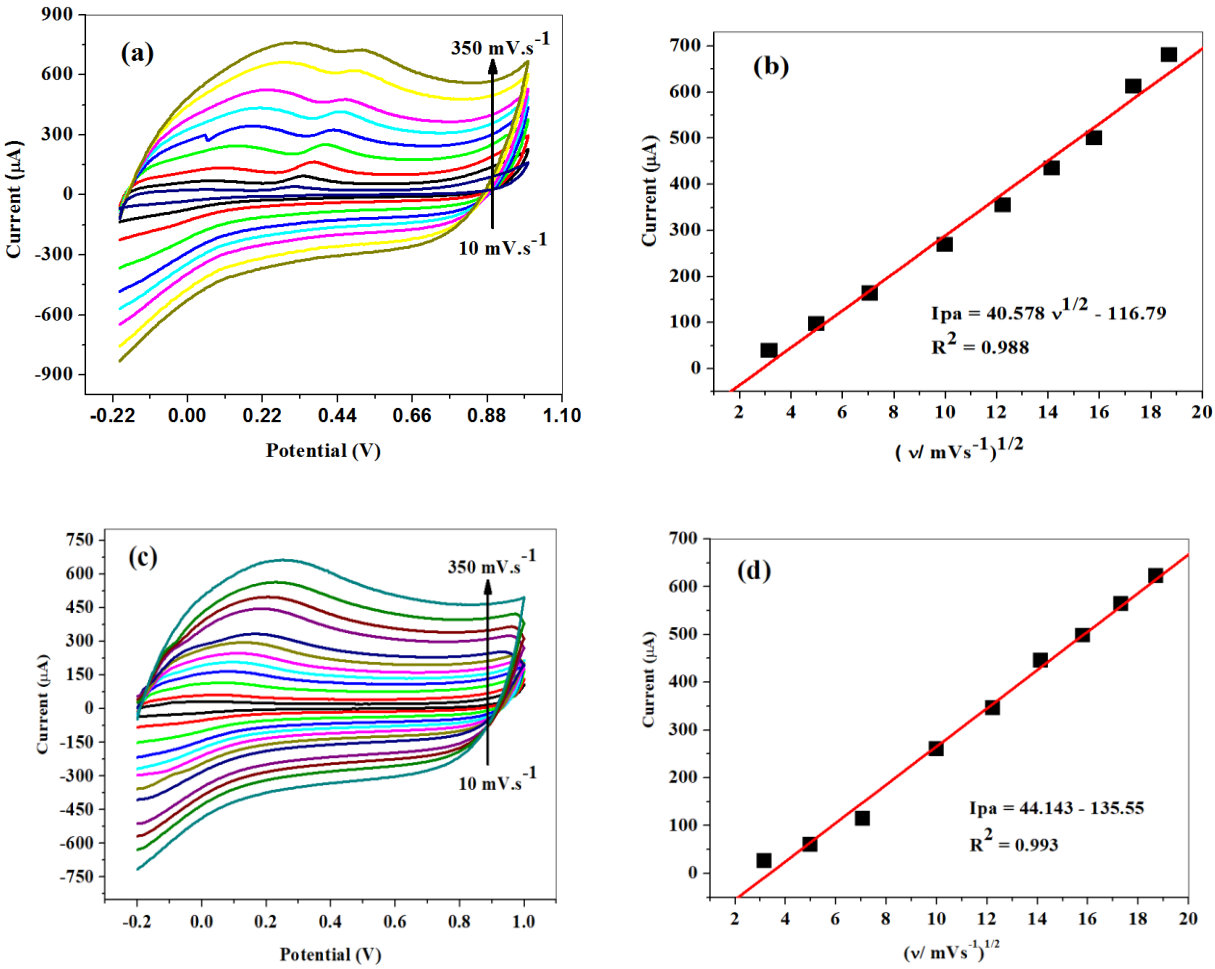

Figure 4. 15. Scan rate cyclic voltammogram at the proposed sensor electrode for (a) 5-HT and (c) AA. Linear plots of current (µA) vs square root of scan rate for (b) 5-HT and (d) AA.

4.7. Selective determination of AA and 5-HT

The cyclic voltammetry technique was used to investigate the selectivity of the proposed electrode by detecting AA and 5-HT simultaneously while varying the scan rate from 10 – 450 mVs^{-1} within the window potential of -0.2 – 1 V. The voltammogram in **Fig 4.16** showed two distinctive peaks at -0.011, and 0.303 V attributed to AA and 5-HT peak potentials at a scan rate of 25 mVs^{-1}. The analyte's peaks did not interfere as the scan rate increased, suggesting that the proposed electrode displayed anti- interference behavior. The linear plots in **Fig 4.16 (b & c)** for AA and 5-HT exhibited a strong linear correlation between scan rate and

current peak, suggesting a diffusion-controlled reaction took place at the surface of the electrode. The relationship between Ipa vs square root of scan rate could be expressed in the following Ipa = 6.615 $v^{1/2}$ – 23.969 (R^2 = 0.991) and Ipa = 5.493 $v^{1/2}$ – 17.893 (R^2 = 0.992) for AA and 5-HT respectively.

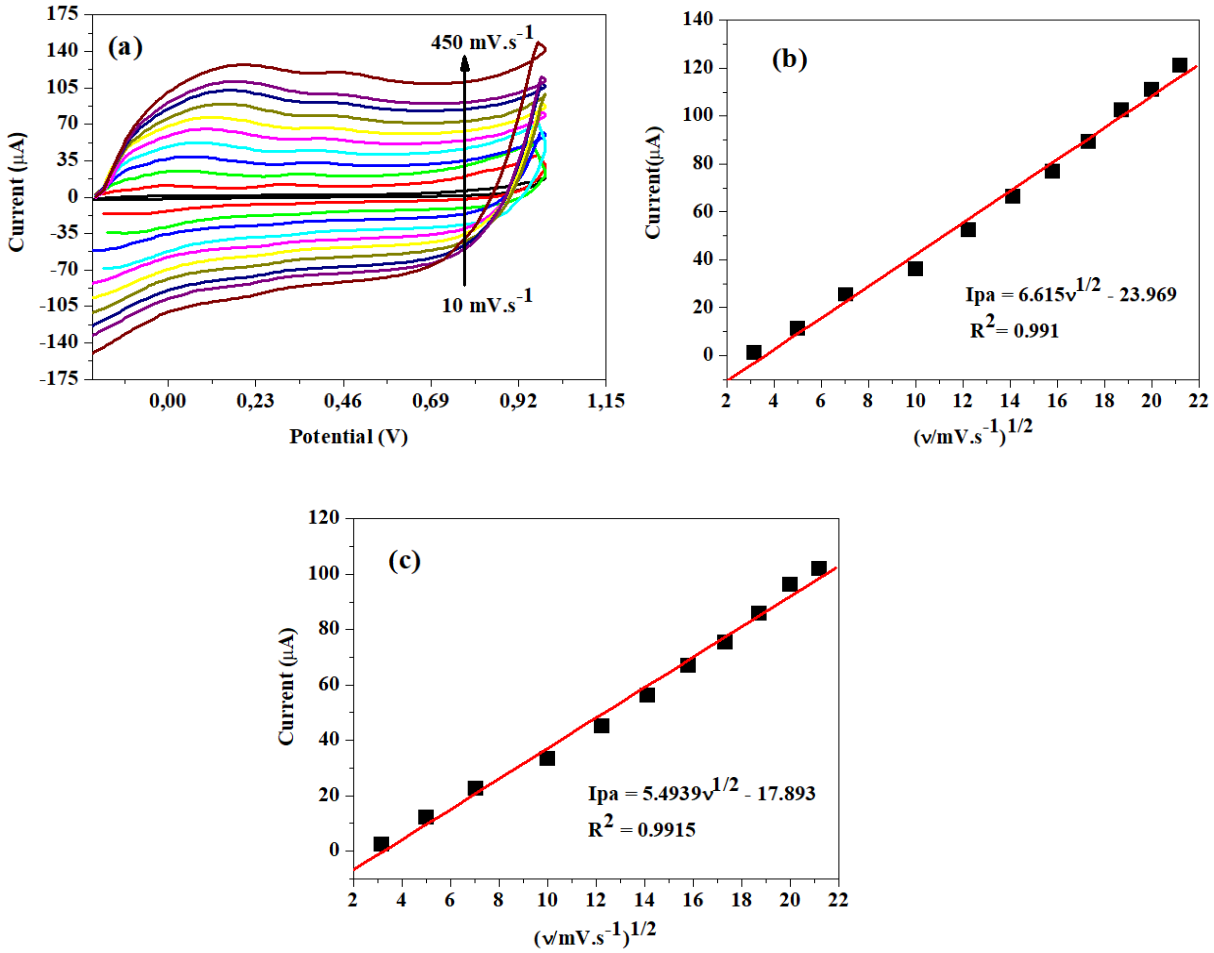

Figure 4. 16. (a) Scan rate study of AA and 5-HT prepared in 0.1 M phosphate-buffered saline from scan rate 10 – 450 mVs^{-1}. Linear plots for (a) AA, and (c) 5-HT.

4.8. Electro-analysis experiments

The sensor electrode's ability to detect 5-HT and AA at the lowest concentrations with high certainty was investigated. The SWV in **Fig 4.17 (b & d)** showed a linear correlation between current peak and concentration for 5-HT and AA, respectively. The peak potential for 5-HT and AA was located at 0.34 and 0.12 V, respectively. For detection of 5-HT, the fabricated electrode showed the sensitivity, LOD, and LOQ values of 0.2863 µA/µM, 24 nM, and 74 nM with a linear range from 1.56 x 10^{-8} – 1.28 x 10^{-7} M (R^2 =

0.9851), and 0.4282 µA/µM, 147 nM, and 446 nM with linearity from 1.60 x 10^{-8} – 6.40 x 10^{-7} M (R^2 = 0.9789) for AA detection. The acquired LOD and LOQ values were calculated using **equations (4.6 & 4.7)**, respectively.

$$\text{LOD} = \frac{3.3 \times SD}{s} \qquad (4.6)$$

$$\text{LOQ} = \frac{10 \times SD}{s} \qquad (4.7)$$

SD represents the standard deviation, and *s* stands for the slope of the calibration plot. The electroanalysis experiment showed that the fabricated sensor is sensitive and can detect analytes (AA and 5-HT) at the smallest concentration with high certainty at 466 and 74 nM for AA and 5-HT, respectively. Compared to other chemical sensor electrodes from the literature, the fabricated sensor electrode performed extremely well, as shown in **Table 4.3**.

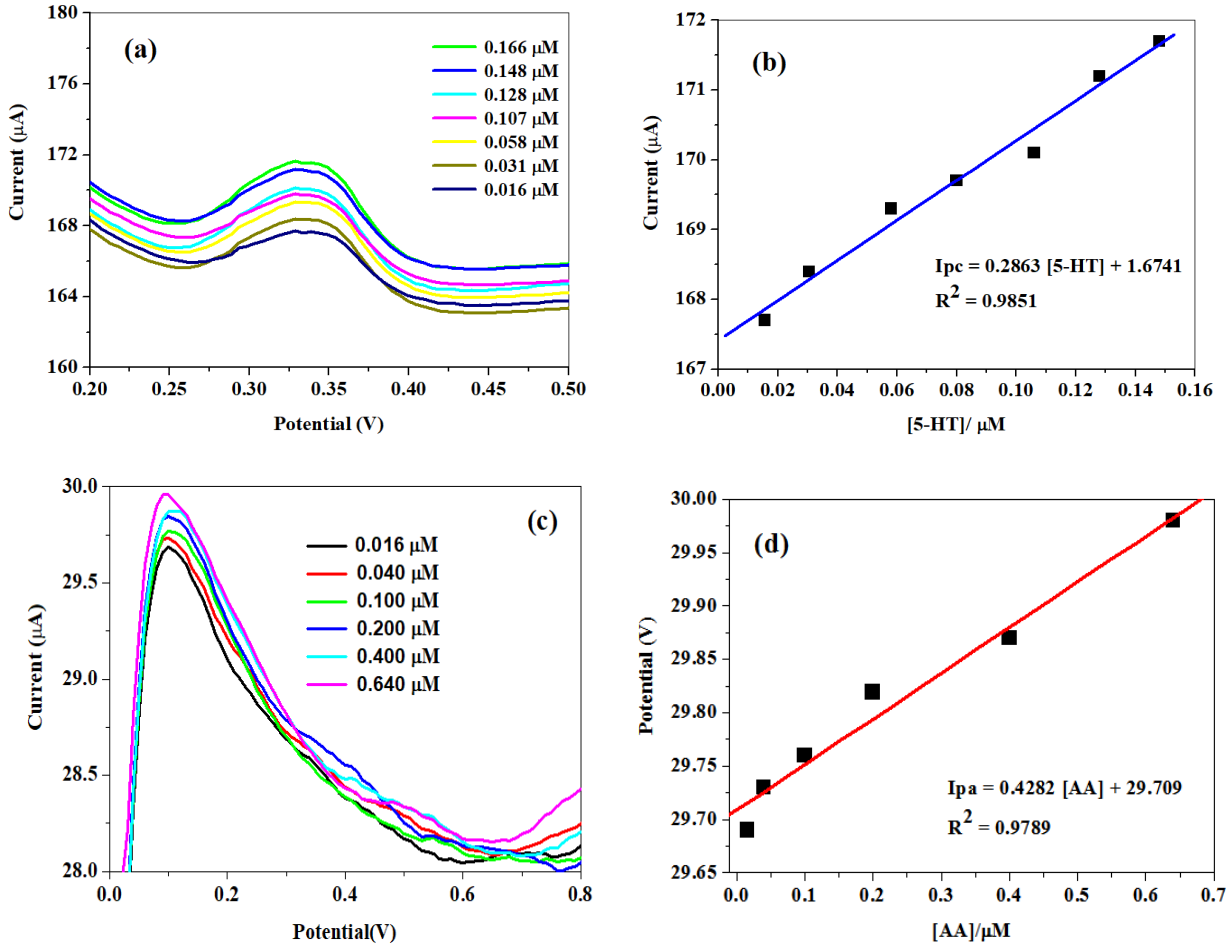

Figure 4. 17. SWV at proposed electrode over the (a) 5-HT (0.016 – 0.166 µM), (c) AA (0.016 – 0.640 µM) prepared in 0.1 M phosphate-buffered saline (pH 7) and (b & d) represents their corresponding linear plots.

Table 4.3. Electrochemical sensors that have been used to detect AA and 5-HT from literature.

Modified electrode	**Method**	**Linearity (µM)**	**Analyte**	**LOD (µM)**	**R^2**	**Ref**
Carbon-sphere@GCE	DPV	40 – 750	5-HT	0.70	0.999	[17]
GCE/MWCNT-NiO	SWV	5.98×10^{-3} – 62.80	5-HT	0.118	0.973	[43]
GCE/MWCNT-ZnO	SWV	5.98×10^{-3} – 62.80	5-HT	0.129	0.915	[43]
GCE/MWCNT-Fe_2O_4	SWV	5.98×10^{-3} – 62.80	5-HT	0.166	0.979	[43]
CNTs@grahite electrode	DPV	1 – 15	5-HT	0.20	0.999	[39]
poly-AzrS/MWCNTs/GCE	DPV	0.5 – 11	5-HT	0.18	0.983	[86]
Ach/GCE	DPV	1 – 30	5-HT	0.50	0.997	[118]
MWCNT-AONP@SPCE	SWV	1.60×10^{-2} – 1.16×10^{-1}	5-HT	0.025	0.985	This work
PVP-GR@GCE	LSV	4 – 1000	AA	0.80	0.989	[298]
Ag/CNT-CPE	DPV	30 – 2000	AA	12.00	0.997	[299]
CoPc–MWNTs/GCE	AMP	10 – 2600	AA	1.00	0.999	[300]
RGO–ZnO/GCE	DPV	50 – 2350	AA	3.71	0.997	[154]
Helical CNTs/GCE	DPV	25 – 1045	AA	0.12	0.997	[157]
CF/ZnO CN@ME	DPV	600 – 1800	AA	156.7	0.992	[301]
Fe_3O_4NPs/SPCE	SWV	10 – 100	AA	15.70	0.981	[153]
MWCNT-AONP@SPCE	SWV	1.60×10^{-1} – 6.40×10^{-1}	AA	0.147	0.979	This work

4.9. Interference studies

The electrode selectivity was determined by varying the concentrations of AA (45 – 190 µM) and 5-HT (35 – 205 µm) in the presence of 0.5 mM DA as an interfering compound. **Fig 4.18 (a & c)** displayed distinctive peaks for each analyte with peak potentials for AA, DA, and 5-HT at -0.05, 0.20, and 0.37 V, respectively, using the SWV. The peak-to-peak separation between DA and AA was 250 mV and 170 mV between 5-HT and DA. However, in **Fig 4.18 (c),** a slight shift in peak potentials (DA and 5-HT) towards high potential values were noticed as the AA concentration increased**.** Still, the peak currents of DA and 5-HT did not increase as AA concentration increased, confirming the proposed electrode selectivity. The electrode sensitivity was tested further by simultaneously detecting AA, 5-HT, and DA at equal concentrations. The experimental results are shown in **Fig 4.19**. The voltammogram showed three distinctive peaks with no interference signal with each other with peak-to-peak separations of more than 100 mV assigned to AA, 5-HT, and DA. This experiment revealed that the fabricated electrode applicability to detect AA and 5-HT simultaneously in the presence of interfering biomolecules suggests the proposed electrode exhibits excellent selectivity and outstanding anti-interference behaviour. The linear plots in **Fig 4.18 (b& d)** for 5-HT and AA were used to determine the linear responses obtained for 5-HT and AA in the 35 – 205 µM (R^2 = 0.9940) and 45 – 190 µM (R^2 = 0.9927) concentration ranges, with detection limits of 24 and 17 µM, respectively.

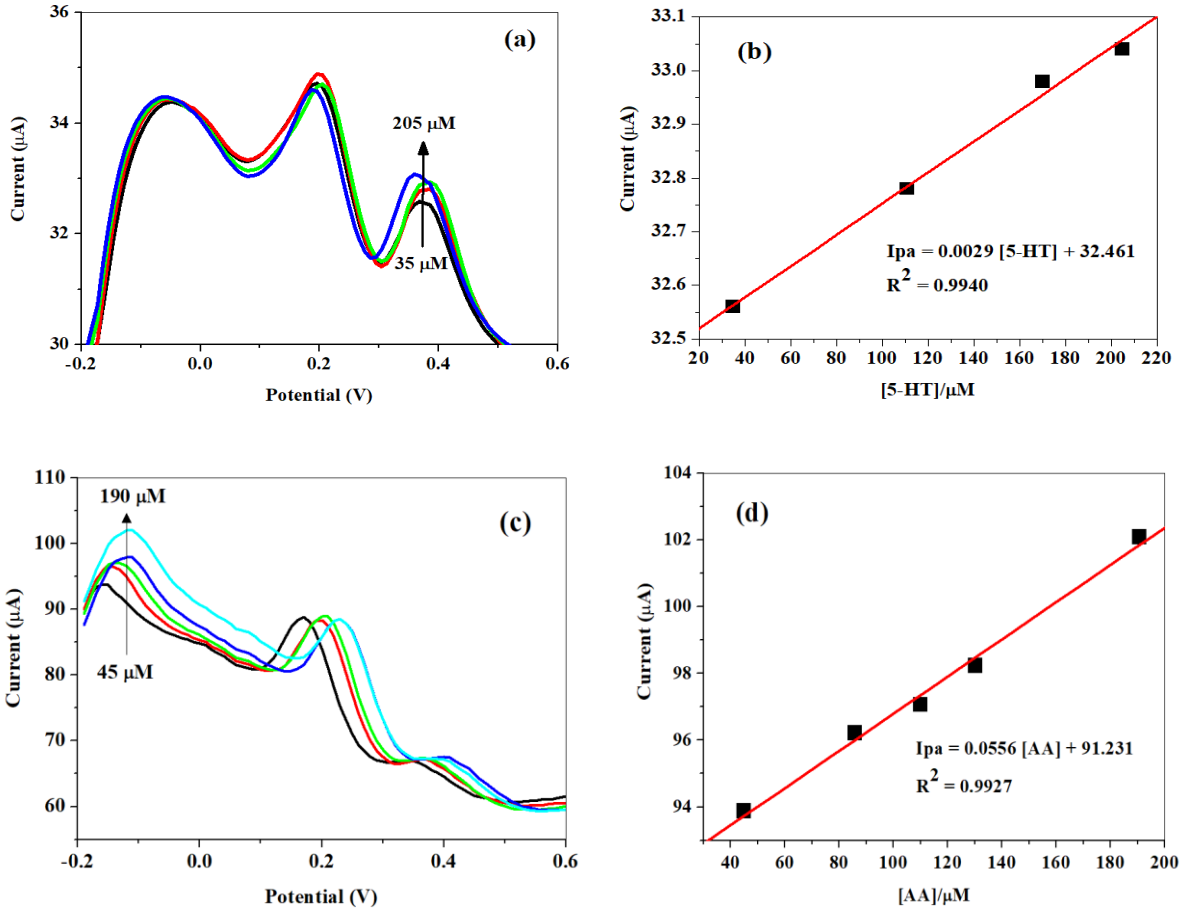

Figure 4. 18. Interference study of (a) 0.5 mM AA, 0.5 mM DA and (35 – 205 µM) 5-HT; (c) 0.5 mM 5-HT and 0.5 mM DA and (45 – 188 µM) AA prepared in 0.1 mM phosphate buffered saline (pH 7) and (b & d) represents the corresponding linear plots of peak currents vs concentration for each analytes.

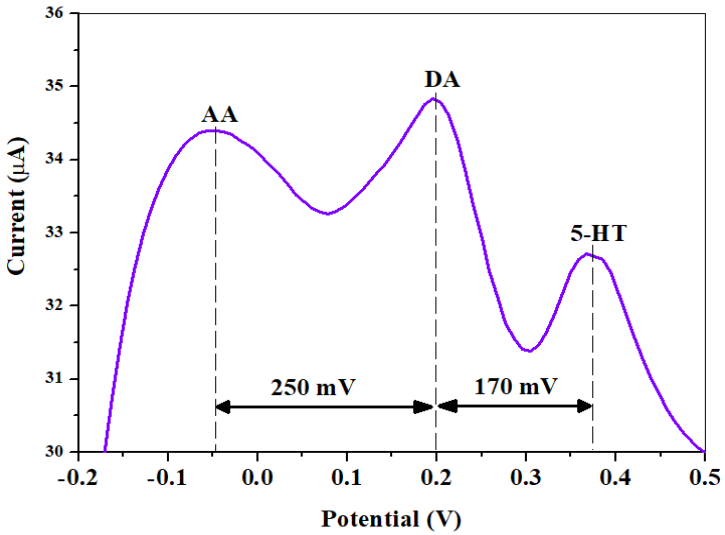

Figure 4. 19. The SWV voltammogram for 5-HT, DA, and AA detected simultaneously at a fixed concentration of 0.1 mM each.

4.10. Reproducibility, stability, and shelve-life experiments

4.10.1. Reproducibility study

The reproducibility of the proposed electrode was carried out to determine the efficiency and reliability of the fabricated electrochemical sensor. The stability of the fabricated sensor was scanned repetitively (20 times) in 5 mM $K[Fe(CN)_6]^{3-/4-}$ prepared in 0.1M phosphate-buffered saline at pH 7 at the scan rate of 25 mVs^{-1} utilizing the CV method as shown in **Fig 4. 20**. It was noticed that the anodic peak current increased by 26.39 %, while the cathodic peak current decreased by 17.71 %. This increase in cathodic peak current could be attributed to the increased electro-active surface area of the probe solution with interactions over time. The repetitive scans indicated that the modified electrode had great stability and did not undergo biofouling during the voltammetry experiment.

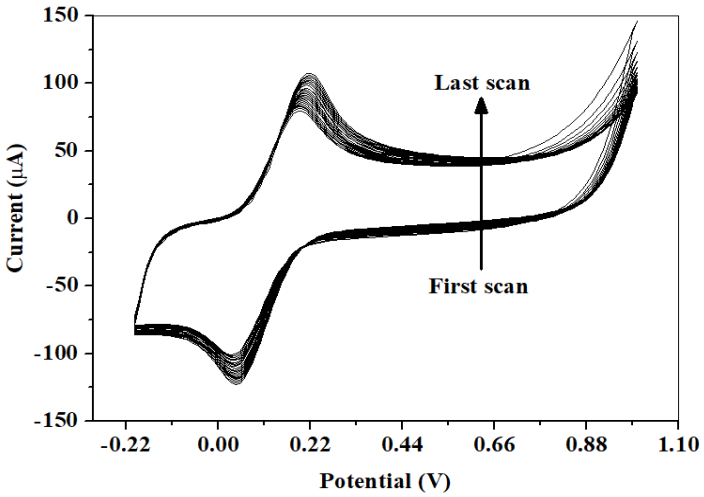

Figure 4. 20. Reproducibility study at the proposed electrode in 5 mM $[Fe(CN)_6]^{3-/4-}$ at the proposed sensor.

4.10.2. Stability studies

Fig 4. 21 shows the stability study at the proposed electrode carried out by scanning the electrode repeatedly (20 scans) in (a) 0.1 mM 5-HT, (b) 0.1 mM AA, and (c) 0.1 mM 5-HT and 0.1 mM AA detected at the same time prepared in 0.1 M phosphate-buffered saline (pH 7) at a 25 mVs^{-1} scan rate using the CV. The anodic peak current for 5-HT and AA decreased by 68 and 53 %, with 35 and 21 % RSD values, respectively. For simultaneous detection of AA and 5-HT, the peak currents decreased by 27 and 33 %, with RSD values of 8 and 10 %, respectively.

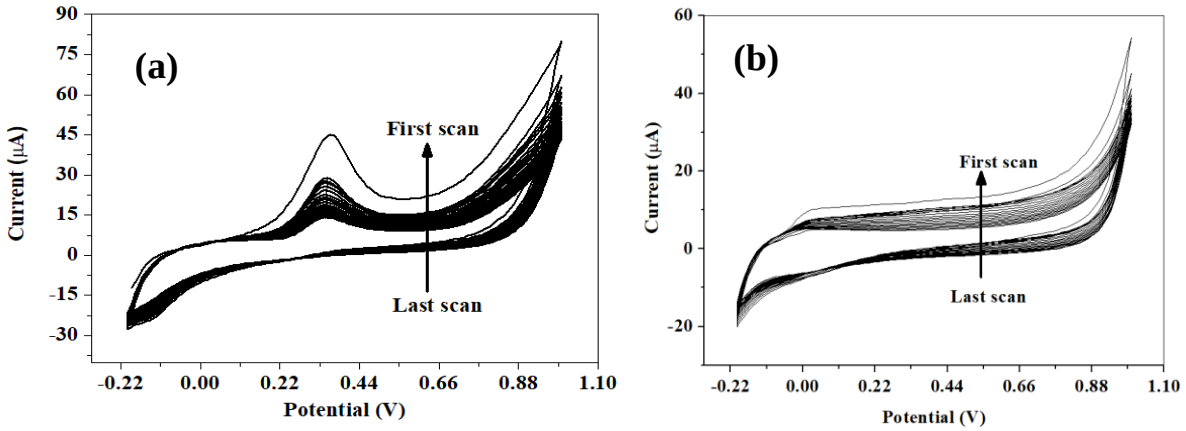

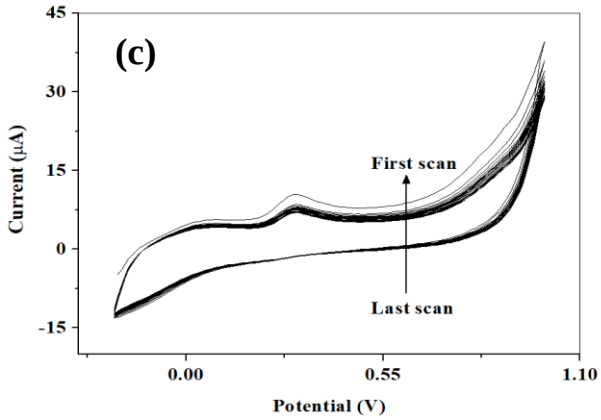

Figure 4. 21. Stability study in (a) 5-HT, (b) AA, and (c) simultaneous detection of 5-HT and AA dissolved in 0.1 M phosphate-buffered saline at pH 7 performed at the proposed electrode.

4.10.3. Shelve life studies

The shelve study was undertaken to determine the longevity of the fabricated sensors. **Fig 4. 22** shows the experimental results in (a) 0.1 mM 5-HT, (b) 0.1 mM AA, and (c) 0.1 mM 5-HT and 0.1 mM AA detected simultaneously made in phosphate-buffered saline at pH 7 at 25 mVs^{-1} carried out using CV method. The fabricated electrode was stored in a dry place when not used. The 5-HT current response dropped by 50 % after 37 days. A drastic drop in AA current response was noticed compared to 5-HT current for the same period. The fabricated electrode reached half of the AA current response after 27 days. For a simultaneous shelve-life study for 5-HT and AA. After 21 days, the 5-HT and AA current responses had reached half their initial value after 21 days and 14 days, respectively. The fabricated electrode displayed a long shelve life for detecting mentioned analytes.

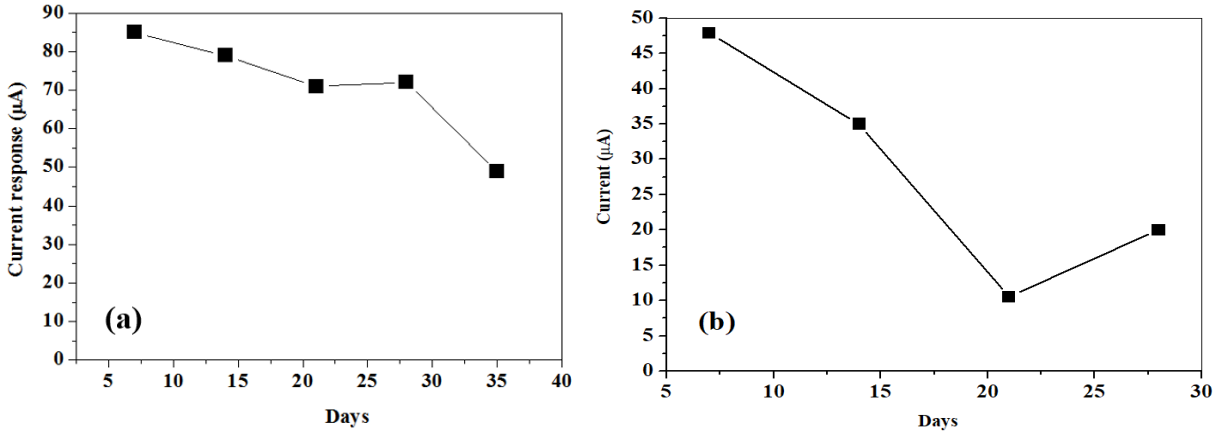

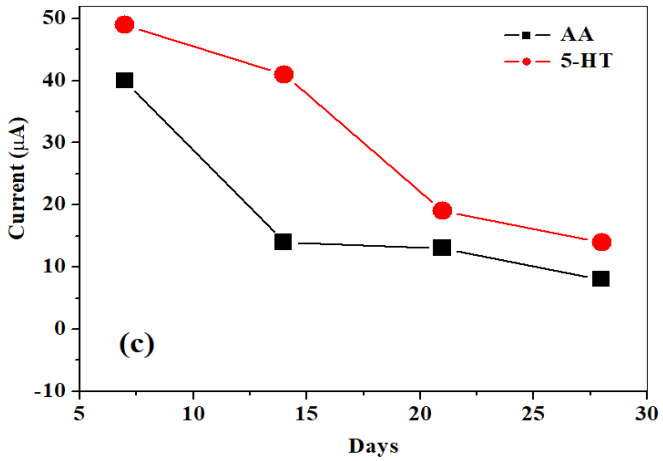

Figure 4. 22. Shelve-life study in (a) 0.1 mM 5-HT, (b) 0.1 mM AA, and (c) simultaneous detection of 5-HT and AA prepared in the supporting buffer solution at the nanocomposite-modified electrode.

4.11. Real-sample analysis

The main objective of this study was to determine the usability of the suggested sensors. **Table 4.3** showed average % recovery of 100.75 % with RSD value of 2.57 % (n = 3) for 5-HT determination in tomatoes. For AA analysis in oranges, the electrode had mean % recoveries of 103.12 % with an RSD value of 3.52 % (n = 3), as shown in **Table 4.4**. The acquired results underpin the usefulness of the fabricated sensor electrode to determine AA and 5-HT in real samples. The resultant percentage recoveries were calculated using **equation (4.9)**.

$$\%\ Recovery = \frac{quantity\ found - quantity\ detected}{quantity\ added} \qquad (4.9)$$

Table 4. 3. Determination of 5-HT in tomatoes

Sample	Added (μM)	Detected(μM)	Recovery (%)	RSD (%)
Tomatoes	400	433.11	108.28	3.20
	600	547.92	91.32	2.60
	900	923.66	102.63	1.90

Average RSD (%) = 2.57; n = 3

Table 4. 4. Determination of AA in oranges.

Sample	Added (µM)	Detected (µM)	Recovery (%)	RSD (%)
Oranges	400	431.03	107.76	5.71
	600	594.69	99.12	3.89
	900	919.52	102.17	0.97

Average RSD (%) = 3.52; n = 3

CHAPTER 5: Conclusion and recommendations

5.1. Conclusion

In conclusion, simultaneous electrochemical detection of AA and 5-HT at the MWCNT-AONP nanocomposite embedded on screen-printed carbon electrodes has been successfully achieved. The FTIR, UV-vis, XRD, EDX, SEM, and TEM techniques positively described the produced nanomaterials. Electrochemical studies were carried out using CV and SWV. The suggested sensor electrode outperformed previous electrodes examined in electron transfer kinetics and electrocatalytic activity for AA and 5-HT detection. For 5-HT detection, the nanocomposite electrode displayed the sensitivity, and limit of detection (LOD) of 0.2863 µA/µM, and 24 nM, with a linear range of 1.56 $x10^{-8}$ – 1.28 x 10^{-7} M, respectively, and 0.4789 µA/µM, and 278 nM in the 1.6$x10^{-8}$ – 6.4$x10^{-7}$ M concentration range for AA detection using SWV. For detection of 5-HT in the presence of interfering biomolecules, the proposed sensors displayed the LOD and concentration range of 24 µM and 35 – 205 µM (R^2 = 0.9940). For AA determination, in the presence of 0.1 mM (5-HT and DA) was 17 µM and 45 – 190 µM (R^2 = 0.9927). The proposed electrode displayed outstanding selectivity and good anti-interference behaviour. Furthermore, the electrode displayed a long shelve-life towards determining AA and 5-HT. The sensor's capacity to detect AA and 5-HT in oranges and tomatoes yielded remarkable recoveries of 99.12 and 91.32 %, respectively, with RSD (%) values of 3.52 and 2.57.

5.2. Recommendations

Although the study's goals and objectives were achieved, the following few recommendations could be made based on the nature of the proposed nanocomposite.

- The stability of the proposed electrode could be enhanced by using electrode stabilizers or binders, and their effect on the electrocatalytic and electroanalytic properties of the electrode should be monitored.
- To further improve the acquired LOD, a three-catalyst system nanocomposite is recommended. For example, conducting polymers such as PANI and poly(pyrrole)s, amongst others, could be utilized in addition to these nanomaterials (AONPs, and fMWCNTs).
- Based on the synergic nature of the two nanomaterials (AONPs, and f-MWCNTs), the fabricated electrode could be used to analyze and detect other analytes such as dopamine, epinephrine, organochloride, glutathione, and other neurotransmitters
- Based on these factors, affordability, rapid analysis, high sensitivity, and a low LOD, the proposed electrode qualifies as a potential candidate as an electrochemical sensor for 5-HT and AA detection in bodily fluids.

- ❖ The careful control of the morphology and size of the MONPs, because it has been found that the shape, size, and uniformity of MONPs improve the electrocatalytic ability.

Research outputs

1. Published and future Articles

1.1. **Motsaathebe, P.C.** and Fayemi, O.E., 2021. Serotonin electrochemical detection in tomatoes at MWCNT-AONP nanocomposite modified electrode. *Materials Research Express*, *8*(11), p.115004.

1.2. **Motsaathebe, P.C.** and Fayemi, O.E., 2021. Ascorbic acid electrochemical determination in oranges using MWCNT-AONP nanocomposite modified electrode (under preparation), targeted journal *Nanomaterials.*

2. Poster presentations

2.1. **Motsaathebe, P.C.** and Fayemi, O.E. Serotonin electrochemical detection in tomatoes at MWCNT-AONP nanocomposite modified electrode. Paper presented at the 10th annual nanoscience young researcher's symposium, University of Witwatersrands, Johannesburg, South Africa, 7th – 8th October 2021. (awarded third position).

2.2. **Motsaathebe, P.C.** and Fayemi, O.E. Ascorbic acid electrochemical determination in oranges using MWCNT-AONP nanocomposite modified electrode. Paper presented at the 2nd commonwealth chemistry poster. Theme: Building networks to address the goals: United Kingdom, 30 September – 1 October 2021.

APPENDICES

Formulas used

$i_p = (2.69 \times 10^5) n^{\frac{3}{2}} A D^{\frac{1}{2}} C v^{\frac{1}{2}}$: Randles–Ševčík equation (2.1)

$E^{\circ\prime} = \frac{E_{Pa} + E_{Pc}}{2}$: $Formal\ reduction\ potential\ equation$ (2.2)

$\Delta E_P = E_{Pa} - E_{Pc} \cong \frac{0.059}{n}$: $Peak\ potential\ separation\ \Delta Ep\ equation$ (2.3)

$n\lambda = 2d\ sin\theta$: $Bragg's\ law$

$D = \frac{K\lambda}{Bcos\theta}$: $Scherrer\ equation$ (4.1)

Ep = $(\frac{b}{2})$ logv + constant : Tafel equation (4.2)

Slope = $\frac{2.3RT}{\alpha nF}$: Cathodic peak equation (4.3)

Slope = $\frac{2.3RT}{(1-\alpha)nF}$: Anodic peak equation (4.4)

LOD = $\frac{3.3 \times SD}{Slope}$: Limit of detection (4.6)

LOQ = $\frac{10 \times SD}{slope}$: Limit of quantification (4.7)

Reference

1. Yang, L. and Beal, M.F., 2011. Determination of neurotransmitter levels in models of Parkinson's disease by HPLC-ECD. In *Neurodegeneration* (pp. 401-415). Humana Press, Totowa, NJ.

2. Dubey, T., Sahu, G., Kumari, S., Yadav, B.S. and Sahu, A.N., 2018. Role of herbal drugs on neurotransmitters for treating various CNS disorders: A review. *IJTK 17*(1), pp. 113-121

3. Tavakolian-Ardakani, Z., Hosu, O., Cristea, C., Mazloum-Ardakani, M. and Marrazza, G., 2019. Latest trends in electrochemical sensors for neurotransmitters: A review. *Sensors*, *19*(9), p.2037.

4. Ayano, G., 2016. Common neurotransmitters: Criteria for neurotransmitters, key locations, classifications and functions. *Advances in Psychology and Neuroscience*, 1(1), pp.1-5.

5. Chauhan, N., Soni, S., Agrawal, P., Balhara, Y.P.S. and Jain, U., 2020. Recent advancement in nanosensors for neurotransmitters detection: Present and future perspective. *Process Biochemistry*, *91*, pp.241-259.

6. Reinhoud, N.J., Brouwer, H.J., Van Heerwaarden, L.M. and Korte-Bouws, G.A., 2013. Analysis of glutamate, GABA, noradrenaline, dopamine, serotonin, and metabolites using microbore UHPLC with electrochemical detection. *ACS chemical neuroscience*, *4*(5), pp.888-894.

7. Motsaathebe, P.C. and Fayemi, O.E., 2021. Serotonin electrochemical detection in tomatoes at MWCNT-AONP nanocomposite modified electrode. *Materials Research Express*, *8*(11), p.115004.

8. Aravind, S.J. and Ramaprabhu, S., 2012. Dopamine biosensor with metal oxide nanoparticles decorated multi-walled carbon nanotubes. *Nanoscience Methods*, *1*(1), pp.102-114.

9. Koyun, O., Gorduk, S., Arvas, M.B. and Sahin, Y., 2018. Electrochemically treated pencil graphite electrodes prepared in one step for the electrochemical determination of paracetamol. *Russian Journal of Electrochemistry*, *54*(11), pp.796-808.

10. Khoshnevisan, K., Honarvarfard, E., Torabi, F., Maleki, H., Baharifar, H., Faridbod, F., Larijani, B. and Khorramizadeh, M.R., 2020. Electrochemical detection of serotonin: a new approach. *Clinica Chimica Acta*, *501*, pp.112-119.

11. Chung, S., Akhtar, M.H., Benboudiaf, A., Park, D.S., and Shim, Y.B., 2020. A Sensor for Serotonin and Dopamine Detection in Cancer Cells Line Based on the Conducting Polymer−Pd Complex Composite. *Electroanalysis*, *32*(3), pp.520-527.

12. Tertiș, M., Cernat, A., Lacatiș, D., Florea, A., Bogdan, D., Suciu, M., Săndulescu, R. and Cristea, C., 2017. Highly selective electrochemical detection of serotonin on polypyrrole and gold nanoparticles-based 3D architecture. *Electrochemistry Communications*, *75*, pp.43-47.

13. Fayemi, O.E., Adekunle, A.S. and Ebenso, E.E., 2017. Electrochemical determination of serotonin in urine samples based on metal oxide nanoparticles/MWCNT on the modified glassy carbon electrode. *Sensing and Bio-Sensing Research*, *13*, pp.17-27.

14. Ran, G., Chen, X. and Xia, Y., 2017. Electrochemical detection of serotonin-based on a poly (bromocresol green) film and Fe_3O_4 nanoparticles in a chitosan matrix. *RSC advances*, *7*(4), pp.1847-1851.

15. Matuschek, L., Göbel, G. and Lisdat, F., 2017. Electrochemical detection of serotonin in the presence of 5-hydroxyindoleacetic acid and ascorbic acid by use of 3D ITO electrodes. *Electrochemistry Communications*, *81*, pp.145-149.

16. Özcan, A., 2016. Selective and sensitive electrochemical sensing of serotonin in human blood serum by means of electrochemically treated pencil graphite electrode. *Anadolu University Journal of Science and Technology A-Applied Sciences and Engineering*, *17*(3), pp.551-562.

17. Zhou, J., Sheng, M., Jiang, X., Wu, G. and Gao, F., 2013. Simultaneous determination of dopamine, serotonin and ascorbic acid at a glassy carbon electrode modified with carbon-spheres. *Sensors*, *13*(10), pp.14029-14040.

18. Wu, K., Fei, J. and Hu, S., 2003. Simultaneous determination of dopamine and serotonin on a glassy carbon electrode coated with a film of carbon nanotubes. *Analytical Biochemistry*, *318*(1), pp.100-106.

19. Uwaya, G.E. and Fayemi, O.E., 2020. Electrochemical detection of serotonin in banana at green mediated PPy/Fe3O4NPs nanocomposites modified electrodes. *Sensing and Bio-Sensing Research*, *28*, p.100338.

20. Tertiș, M., Cernat, A., Lacatiș, D., Florea, A., Bogdan, D., Suciu, M., Săndulescu, R. and Cristea, C., 2017. Highly selective electrochemical detection of serotonin on polypyrrole and gold nanoparticles-based 3D architecture. *Electrochemistry Communications*, *75*, pp.43-47.

21. Sun, D., Li, H., Li, M., Li, C., Dai, H., Sun, D. and Yang, B., 2018. Electrodeposition synthesis of a NiO/CNT/PEDOT composite for simultaneous detection of dopamine, serotonin, and tryptophan. *Sensors and Actuators B: Chemical*, *259*, pp.433-442.

22. Shaw, L. and Dennany, L., 2017. Applications of electrochemical sensors: Forensic drug analysis. *Current Opinion in Electrochemistry*, *3*(1), pp.23-28.

23. Laschi, S. and Mascini, M., 2006. Planar electrochemical sensors for biomedical applications. *Medical engineering & physics*, *28*(10), pp.934-943.

24. Jackowska, K. and Krysinski, P., 2013. New trends in the electrochemical sensing of dopamine. *Analytical and bioanalytical chemistry*, *405*(11), pp.3753-3771.

25. Ohashi, T. and Dai, L., 2006. C60 and carbon nanotube sensors. In *Carbon Nanotechnology* (pp. 525-575). Elsevier.

26. Bockris, J. ed., 2013. *Electrochemistry of cleaner environments*. Springer Science & Business Media.

27. Shetti, N.P., Nayak, D.S., Reddy, K.R. and Aminabhvi, T.M., 2019. Graphene–clay-based hybrid nanostructures for electrochemical sensors and biosensors. In *Graphene-Based Electrochemical Sensors for Biomolecules* (pp. 235-274). Elsevier.

28. Hammond, J.L., Formisano, N., Estrela, P., Carrara, S. and Tkac, J., 2016. Electrochemical biosensors and nanobiosensors. *Essays in biochemistry*, *60*(1), pp.69-80.

29. Yamanaka, K., Vestergaard, M.D.C. and Tamiya, E., 2016. Printable electrochemical biosensors: a focus on screen-printed electrodes and their application. *Sensors*, *16*(10), p.1761.

30. Bai, Y., 2021. Fabrication of Inkjet-Printed Enzyme-Based Biosensors Towards Point-Of-Care Applications.

31. Turner, A.P., 2000. Biosensors--sense and sensitivity. *Science*, *290*(5495), pp.1315-1317.

32. Jianrong, C., Yuqing, M., Nongyue, H., Xiaohua, W. and Sijiao, L., 2004. Nanotechnology and biosensors. *Biotechnology advances*, *22*(7), pp.505-518.

33. Beitollahi, H., Mohammadi, S.Z., Safaei, M. and Tajik, S., 2020. Applications of electrochemical sensors and biosensors based on modified screen-printed electrodes: a review. *Analytical Methods*, *12*(12), pp.1547-1560.

34. Kumar, R. and Singh, S., 2014. A Review on application of Nanoscience for Biosensing. *International Journal of Engineering Research*, *3*(4), pp.279-285.

35. Venugopal, J. and Ramakrishna, S., 2005. Applications of polymer nanofibers in biomedicine and biotechnology. *Applied biochemistry and biotechnology*, *125*(3), pp.147-157.

36. Khoshnevisan, K., Maleki, H., Honarvarfard, E., Baharifar, H., Gholami, M., Faridbod, F., Larijani, B., Majidi, R.F. and Khorramizadeh, M.R., 2019. Nanomaterial based electrochemical sensing of the biomarker serotonin: a comprehensive review. *Microchimica Acta*, *186*(1), p.49.

37. Aflatoonian, M.R., Tajik, S., Aflatoonian, B., Beitollahi, H., Zhang, K., Le, Q.V., Cha, J.H., Jang, H.W., Shokouhimehr, M. and Peng, W., 2020. A Screen-Printed Electrode Modified With Graphene/Co3O4 Nanocomposite for Electrochemical Detection of Tramadol. *Frontiers in Chemistry*, *8*, p.1065.

38. Zestos, A.G., 2018. Carbon nanoelectrodes for the electrochemical detection of neurotransmitters. *International Journal of Electrochemistry*, *2018*.

39. Wang, Z.H., Liang, Q.L., Wang, Y.M. and Luo, G.A., 2003. Carbon nanotube-intercalated graphite electrodes for simultaneous determination of dopamine and serotonin in the presence of ascorbic acid. *Journal of Electroanalytical Chemistry*, *540*, pp.129-134.

40. Eddin, F.B.K. and Fen, Y.W., 2020. Recent advances in electrochemical and optical sensing of dopamine. *Sensors (Basel, Switzerland)*, *20*(4).

41. dineshkumar, s., 2014. *Use of multi-walled carbon nanotubes (MWCNTs) in medium density fiberboard to increase the fire retardancy* (doctoral dissertation, universiti malaysia pahang).

42. Berasid, M.B.M.K., Rinaldi, A., Reiche, S. and Kutty, M.G., 2012. Chemically modified multi-walled carbon nanotubes (MWCNTs) with anchored acidic groups. *Sains Malaysiana*, *41*(5), pp.603-609.

43. Fayemi, O.E., Adekunle, A.S. and Ebenso, E.E., 2017. Electrochemical determination of serotonin in urine samples based on metal oxide nanoparticles/MWCNT on modified glassy carbon electrode. *Sensing and Bio-Sensing Research*, *13*, pp.17-27.

44. McCreery, R.L., 2008. Advanced carbon electrode materials for molecular electrochemistry. *Chemical reviews*, *108*(7), pp.2646-2687.

45. Saleh, T.A., Siddiqui, M.N. and Al-Arfaj, A.A., 2014. Synthesis of multiwalled carbon nanotubes-titania nanomaterial for desulfurization of model fuel. *Journal of Nanomaterials*, *2014*.

46. Li, G., Xia, Y., Tian, Y., Wu, Y., Liu, J., He, Q. and Chen, D., 2019. Recent developments on graphene-based electrochemical sensors toward nitrite. *Journal of the Electrochemical Society*, *166*(12), p.B881.

47. Naseem, T. and Durrani, T., 2021. The role of some important metal oxide nanoparticles for wastewater and antibacterial applications: A review. *Environmental Chemistry and Ecotoxicology*.

48. Chavali, M.S. and Nikolova, M.P., 2019. Metal oxide nanoparticles and their applications in nanotechnology. *SN applied sciences*, *1*(6), pp.1-30.

49. Falcaro, P., Ricco, R., Yazdi, A., Imaz, I., Furukawa, S., Maspoch, D., Ameloot, R., Evans, J.D. and Doonan, C.J., 2016. Application of metal and metal oxide nanoparticles@ MOFs. *Coordination Chemistry Reviews*, *307*, pp.237-254.

50. Luo, S., Fan, J., Liu, W., Zhang, M., Song, Z., Lin, C., Wu, X. and Chu, P.K., 2006. Synthesis and low-temperature photoluminescence properties of SnO2 nanowires and nanobelts. *Nanotechnology*, *17*(6), p.1695.

51. Antuña-Jiménez, D., González-García, M.B., Hernández-Santos, D. and Fanjul-Bolado, P., 2020. Screen-printed electrodes modified with metal nanoparticles for small molecule sensing. *Biosensors*, *10*(2), p.9.

52. Parashar, M., Shukla, V.K. and Singh, R., 2020. Metal oxides nanoparticles via sol–gel method: a review on synthesis, characterization and applications. *Journal of Materials Science: Materials in Electronics*, *31*(5), pp.3729-3749.

53. Murthy, S., Effiong, P. and Fei, C.C., 2020. Metal oxide nanoparticles in biomedical applications. In *Metal Oxide Powder Technologies* (pp. 233-251). Elsevier.

54. Voon, C.H., Foo, K.L., Lim, B.Y., Gopinath, S.C.B. and Al-Douri, Y., 2020. Synthesis and preparation of metal oxide powders. In *Metal Oxide Powder Technologies* (pp. 31-65). Elsevier.

55. Durairaj, S., Sidhureddy, B., Cirone, J. and Chen, A., 2018. Nanomaterials-based electrochemical sensors for in vitro and in vivo analyses of neurotransmitters. *Applied Sciences*, *8*(9), p.1504.

56. Tavakolian-Ardakani, Z., Hosu, O., Cristea, C., Mazloum-Ardakani, M. and Marrazza, G., 2019. Latest trends in electrochemical sensors for neurotransmitters: A review. *Sensors*, *19*(9), p.2037.

57. Zestos, A.G., 2018. Carbon nanoelectrodes for the electrochemical detection of neurotransmitters. *International Journal of Electrochemistry*, *2018*.

58. Swoboda, K.J. and Hyland, K., 2002. Diagnosis and treatment of neurotransmitter-related disorders. *Neurologic clinics*, *20*(4), pp.1143-1161.

59. Si, B. and Song, E., 2018. Recent advances in the detection of neurotransmitters. *Chemosensors*, *6*(1), p.1.

60. Campeau, P.M., Bernard, G. and Clayton, P.T., 2007. Neurotransmitter diseases and related conditions. *Molecular genetics and metabolism*, *92*(3), pp.189-197.

61. Gupta, P., Tiwari, S. and Haria, J., 2014. Relationship between depression and vitamin C status: a study on rural patients from western uttar pradesh in India. *International Journal of Scientific Study*, *1*(4), pp.37-39.

62. Smith, S., Korvink, J.G., Mager, D. and Land, K., 2018. The potential of paper-based diagnostics to meet the ASSURED criteria. *RSC advances*, *8*(59), pp.34012-34034.

63. Cernat, A., Ştefan, G., Tertiş, M., Cristea, C. and Simon, I., 2020. An overview of the detection of serotonin and dopamine with graphene-based sensors. *Bioelectrochemistry*, p.107620.

64. World Health Organization, 2006. Neurological disorders: public health challenges. World Health Organization.

65. Umeda, S., Stagliano, G.W., Borenstein, M.R. and Raffa, R.B., 2005. A reverse-phase HPLC and fluorescence detection method for measurement of 5-hydroxytryptamine (serotonin) in Planaria. *Journal of pharmacological and toxicological methods*, *51*(1), pp.73-76.

66. Hasanzadeh, M., Shadjou, N. and Omidinia, E., 2013. A novel electroanalytical method for simultaneous detection of two neurotransmitter dopamine and serotonin in human serum. *Journal of neuroscience methods*, *219*(1), pp.52-60.

67. de Faria, L.V., Lisboa, T.P., de Farias, D.M., Araujo, F.M., Machado, M.M., de Sousa, R.A., Matos, M.A.C., Muñoz, R.A.A. and Matos, R.C., 2020. Direct analysis of ascorbic acid in food beverage samples by flow injection analysis using reduced graphene oxide sensor. *Food chemistry*, *319*, p.126509.

68. Pisoschi, A.M., Pop, A., Serban, A.I. and Fafaneata, C., 2014. Electrochemical methods for ascorbic acid determination. *Electrochimica Acta*, *121*, pp.443-460.

69. Pisoschi, A.M., Danet, A.F. and Kalinowski, S., 2008. Ascorbic acid determination in commercial fruit juice samples by cyclic voltammetry. *Journal of Automated Methods and Management in Chemistry*, *2008*.

70. Carr, A.C. and Maggini, S., 2017. Vitamin C and immune function. *Nutrients*, *9*(11), p.1211.

71. Lavanya, N. and Sekar, C., 2019. SnO2-SnS2 nanocomposite as electrocatalyst for simultaneous determination of depression biomarkers serotonin and tryptophan. *Journal of Electroanalytical Chemistry*, *840*, pp.1-9.

72. Carr, A.C. and McCall, C., 2017. The role of vitamin C in the treatment of pain: new insights. *Journal of translational medicine*, *15*(1), pp.1-14.

73. Guo, X., Yue, G., Huang, J., Liu, C., Zeng, Q. and Wang, L., 2018. Label-free simultaneous analysis of Fe (III) and ascorbic acid using fluorescence switching of ultrathin graphitic carbon nitride nanosheets. *ACS applied materials & interfaces*, *10*(31), pp.26118-26127.

74. Hodkinson, A., 1977. Oxalic Acid in Biology and Medicine London Academic Press, pp: 207.

75. Whitaker-Azmitia, P.M., 1999. The discovery of serotonin and its role in neuroscience. *Neuropsychopharmacology*, *21*(1), pp.2-8.

76. Tyler Jr, V.E., 1958. Occurrence of serotonin in a hallucinogenic mushroom. *Science*, *128*(3326), pp.718-718.

77. Manahan, S.E., 2002. *Toxicological chemistry and biochemistry*. CRC Press.

78. Berger, M., Gray, J.A. and Roth, B.L., 2009. The expanded biology of serotonin. *Annual review of medicine*, *60*, pp.355-366.

79. Özcan, A., 2016. Selective and sensitive electrochemical sensing of serotonin in human blood serum by means of electrochemically treated pencil graphite electrode. *Anadolu University Journal of Science and Technology A-Applied Sciences and Engineering*, *17*(3), pp.551-562.

80. Zen, J.M., Chen, I.L. and Shih, Y., 1998. Voltammetric determination of serotonin in human blood using a chemically modified electrode. *Analytica chimica acta*, *369*(1-2), pp.103-108.

81. Jin, Q., Shan, L., Yue, J. and Wang, X., 2008. Spectrophotometric determination of total serotonin derivatives in the safflower seeds with Ehrlich's reagent and the underlying colour reaction mechanism. *Food chemistry*, *108*(2), pp.779-783.

82. Berzas Nevado, J.J., Villaseñor Llerena, M.J., Guiberteau Cabanillas, C., Rodríguez Robledo, V. and Buitrago, S., 2006. Sensitive capillary GC-MS-SIM determination of selective serotonin reuptake inhibitors: Reliability evaluation by validation and robustness study. *Journal of separation science*, *29*(1), pp.103-113.

83. Peterson, Z.D., Lee, M.L. and Graves, S.W., 2004. Determination of serotonin and its precursors in human plasma by capillary electrophoresis–electrospray ionization–time-of-flight mass spectrometry. *Journal of Chromatography B*, *810*(1), pp.101-110.

84. Engbaek, F. and Voldby, B., 1982. Radioimmunoassay of serotonin (5-hydroxytryptamine) in cerebrospinal fluid, plasma, and serum. *Clinical chemistry*, *28*(4), pp.624-628.

85. Sarada, B.V., Rao, T.N., Tryk, D.A. and Fujishima, A., 1999. Electrochemical detection of serotonin using conductive diamond electrodes. *Chemistry Letters*, *28*(11), pp.1213-1214.

86. Reddaiah, K., Rao, K.S.V.K. and Reddy, T.M., 2018. Electrochemical detection of serotonin in human serum sample and simultaneous resolution in presence of epinephrine. *Anal. Bioanal. Electrochem*, *10*, pp.175-191.

87. Maughan, N., Nguyen, L.M. and Gamagedara, S., 2015. Microfluidic separation and electrochemical detection of serotonin using a portable lab-on-a-chip device. *Anal. Bioanal. Electrochem*, *7*(1), pp.1-11.

88. Matt, S.B., Shivanna, M., Manjunath, S., Siddalinganahalli, M. and Siddalingappa, D.M., 2020. Electrochemical Detection of Serotonin Using t-ZrO_2 Nanoparticles Modified Carbon Paste Electrode. *Journal of The Electrochemical Society*, *167*(15), p.155512.

89. Al-Graiti, W., Foroughi, J., Liu, Y. and Chen, J., 2019. Hybrid graphene/conducting polymer strip sensors for sensitive and selective electrochemical detection of serotonin. *ACS omega*, *4*(26), pp.22169-22177.

90. Uwaya, G.E. and Fayemi, O.E., 2020. Electrochemical detection of serotonin in banana at green mediated PPy/Fe3O4NPs nanocomposites modified electrodes. *Sensing and Bio-Sensing Research*, *28*, p.100338.

91. Kachoosangi, R.T. and Compton, R.G., 2007. A simple electroanalytical methodology for the simultaneous determination of dopamine, serotonin and ascorbic acid using an unmodified edge plane pyrolytic graphite electrode. *Analytical and bioanalytical chemistry*, *387*(8), pp.2793-2800.

92. Jacobs, C.B., Vickrey, T.L. and Venton, B.J., 2011. Functional groups modulate the sensitivity and electron transfer kinetics of neurochemicals at carbon nanotube modified microelectrodes. *Analyst*, *136*(17), pp.3557-3565.

93. Strasser, B., Gostner, J.M. and Fuchs, D., 2016. Mood, food, and cognition: role of tryptophan and serotonin. *Current Opinion in Clinical Nutrition & Metabolic Care*, *19*(1), pp.55-61.

94. Habibi, B., Jahanbakhshi, M. and Pournaghi-Azar, M.H., 2011. Differential pulse voltammetric simultaneous determination of acetaminophen and ascorbic acid using single-walled carbon nanotube-modified carbon–ceramic electrode. *Analytical Biochemistry*, *411*(2), pp.167-175.

95. Hara, K., Hirowatari, Y., Shimura, Y. and Takahashi, H., 2011. Serotonin levels in platelet-poor plasma and whole blood in people with type 2 diabetes with chronic kidney disease. *Diabetes research and clinical practice*, *94*(2), pp.167-171.

96. Watts, S.W., Morrison, S.F., Davis, R.P. and Barman, S.M., 2012. Serotonin and blood pressure regulation. *Pharmacological reviews*, *64*(2), pp.359-388.

97. Sa, M., Ying, L., Tang, A.G., Xiao, L.D. and Ren, Y.P., 2012. Simultaneous determination of tyrosine, tryptophan and 5-hydroxytryptamine in serum of MDD patients by high performance liquid chromatography with fluorescence detection. *Clinica Chimica Acta*, *413*(11-12), pp.973-977.

98. Adumitrăchioaie, A., Tertiș, M., Suciu, M., Graur, F. and Cristea, C., 2019. A novel immunosensing platform for serotonin detection in complex real samples based on graphene oxide and chitosan. *Electrochimica Acta*, *311*, pp.50-61.

99. Szeitz, A. and Bandiera, S.M., 2018. Analysis and measurement of serotonin. *Biomedical Chromatography*, *32*(1), p.e4135.

100. Versari, A., Mattioli, A., Parpinello, G.P. and Galassi, S., 2004. Rapid analysis of ascorbic and isoascorbic acids in fruit juice by capillary electrophoresis. *Food control*, *15*(5), pp.355-358.

101. Feldman, J.M. and Lee, E.M., 1985. Serotonin content of foods: effect on urinary excretion of 5-hydroxyindoleacetic acid. *The American journal of clinical nutrition*, *42*(4), pp.639-643.

102. Johnson, B., 2019. Serotonin Brain Food Review: A natural mood boosting nootropic?. *Safety*, *10*, p.10.

103. Blum, K., Chen, A.L., Giordano, J., Borsten, J., Chen, T.J., Hauser, M., Simpatico, T., Femino, J., Braverman, E.R. and Barh, D., 2012. The addictive brain: all roads lead to dopamine. *Journal of psychoactive drugs*, *44*(2), pp.134-143.

104. Kim, D.S., Kang, E.S., Baek, S., Choo, S.S., Chung, Y.H., Lee, D., Min, J. and Kim, T.H., 2018. Electrochemical detection of dopamine using periodic cylindrical gold nanoelectrode arrays. *Scientific reports*, *8*(1), pp.1-10.

105. Jacobs, C.B., Peairs, M.J. and Venton, B.J., 2010. Carbon nanotube based electrochemical sensors for biomolecules. *Analytica chimica acta*, *662*(2), pp.105-127.

106. Yang, C., Denno, M.E., Pyakurel, P. and Venton, B.J., 2015. Recent trends in carbon nanomaterial-based electrochemical sensors for biomolecules: A review. *Analytica chimica acta*, *887*, pp.17-37.

107. Manbohi, A. and Ahmadi, S.H., 2019. Sensitive and selective detection of dopamine using electrochemical microfluidic paper-based analytical nanosensor. *Sensing and Bio-Sensing Research*, *23*, p.100270.

108. Schulz-Schaeffer, W.J., 2015. Is cell death primary or secondary in the pathophysiology of idiopathic Parkinson's disease? *Biomolecules*, *5*(3), pp.1467-1479.

109. Petzinger, G.M., Holschneider, D.P., Fisher, B.E., McEwen, S., Kintz, N., Halliday, M., Toy, W., Walsh, J.W., Beeler, J. and Jakowec, M.W., 2015. The effects of exercise on dopamine neurotransmission in Parkinson's disease: targeting neuroplasticity to modulate basal ganglia circuitry. *Brain plasticity*, *1*(1), pp.29-39.

110. Briguglio, M., Dell'Osso, B., Panzica, G., Malgaroli, A., Banfi, G., Zanaboni Dina, C., Galentino, R. and Porta, M., 2018. Dietary neurotransmitters: a narrative review on current knowledge. *Nutrients*, *10*(5), p.591.

111. Mallesha, M., Manjunatha, R., Nethravathi, C., Suresh, G.S., Rajamathi, M., Melo, J.S. and Venkatesha, T.V., 2011. Functionalized-graphene modified graphite electrode for the selective determination of dopamine in presence of uric acid and ascorbic acid. *Bioelectrochemistry*, *81*(2), pp.104-108.

112. Peik-See, T., Pandikumar, A., Nay-Ming, H., Hong-Ngee, L. and Sulaiman, Y., 2014. Simultaneous electrochemical detection of dopamine and ascorbic acid using an iron oxide/reduced graphene oxide modified glassy carbon electrode. *Sensors*, *14*(8), pp.15227-15243.

113. Keerthi, M., Boopathy, G., Chen, S.M., Chen, T.W. and Lou, B.S., 2019. A core-shell molybdenum nanoparticles entrapped f-MWCNT s hybrid nanostructured material based non-enzymatic biosensor for electrochemical detection of dopamine neurotransmitter in biological samples. *Scientific reports*, *9*(1), pp.1-12.

114. Ouellette, M., Mathault, J., Niyonambaza, S.D., Miled, A. and Boisselier, E., 2019. Electrochemical Detection of Dopamine Based on Functionalized Electrodes. *Coatings*, *9*(8), p.496.

115. Shankar, S.S., Shereema, R.M., Prabhu, G.R.D., Rao, T.P. and Swamy, K.B., 2015. Electrochemical detection of dopamine in presence of serotonin and ascorbic acid at tetraoctyl ammonium bromide modified carbon paste electrode: a voltammetric study. *J Biosens Bioelectron*, *6*(2), p.1.

116. Zhang, L., Ning, L., Li, S., Pang, H., Zhang, Z., Ma, H. and Yan, H., 2016. Selective electrochemical detection of dopamine in the presence of uric acid and ascorbic acid based on a composite film modified electrode. *RSC advances*, *6*(71), pp.66468-66476.

117. Kundys-Siedlecka, M., Bączyńska, E. and Jönsson-Niedziółka, M., 2019. Electrochemical detection of dopamine and serotonin in the presence of interferences in a rotating droplet system. *Analytical chemistry*, *91*(16), pp.10908-10913.

118. Jin, G.P., Lin, X.Q. and Gong, J.M., 2004. Novel choline and acetylcholine modified glassy carbon electrodes for simultaneous determination of dopamine, serotonin and ascorbic acid. *Journal of Electroanalytical Chemistry*, *569*(1), pp.135-142.

119. Kachoosangi, R.T. and Compton, R.G., 2007. A simple electroanalytical methodology for the simultaneous determination of dopamine, serotonin and ascorbic acid using an unmodified edge plane pyrolytic graphite electrode. *Analytical and bioanalytical chemistry*, *387*(8), pp.2793-2800.

120. Pandikumar, A., How, G.T.S., See, T.P., Omar, F.S., Jayabal, S., Kamali, K.Z., Yusoff, N., Jamil, A., Ramaraj, R., John, S.A. and Lim, H.N., 2014. Graphene and its nanocomposite material based electrochemical sensor platform for dopamine. *Rsc Advances*, *4*(108), pp.63296-63323.

121. Zablocka, I., Wysocka-Zolopa, M. and Winkler, K., 2019. Electrochemical detection of dopamine at a gold electrode modified with a polypyrrole–mesoporous silica molecular sieves (MCM-48) film. *International journal of molecular sciences*, *20*(1), p.111.

122. Ma, X., Chao, M. and Wang, Z., 2012. Electrochemical detection of dopamine in the presence of epinephrine, uric acid and ascorbic acid using a graphene-modified electrode. *Analytical Methods*, *4*(6), pp.1687-1692.

123. Hasanzadeh, M., Shadjou, N. and Omidinia, E., 2013. A novel electroanalytical method for simultaneous detection of two neurotransmitter dopamine and serotonin in human serum. *Journal of neuroscience methods*, *219*(1), pp.52-60.

124. Young, S.N., 2007. L-Tyrosine to alleviate the effects of stress?. *Journal of Psychiatry and Neuroscience*, *32*(3), p.224.

125. Juarez Olguin, H., Calderon Guzman, D., Hernandez Garcia, E. and Barragan Mejia, G., 2016. The role of dopamine and its dysfunction as a consequence of oxidative stress. *Oxidative medicine and cellular longevity*, *2016*.

126. Fadhel, D.H., 2012. Spectrophotometric determination of ascorbic acid in aqueous solutions. *Al-Nahrain Journal of Science*, *15*(3), pp.88-94.

127. Elgailani, I.E.H., Elkareem, M.A.M.G., Noh, E., Adam, O. and Alghamdi, A., 2017. Comparison of two methods for the determination of vitamin C (ascorbic acid) in some fruits. *American Journal of Chemistry*, *2*(1), pp.1-7.

128. Ghanbari, K. and Bonyadi, S., 2018. An electrochemical sensor based on reduced graphene oxide decorated with polypyrrole nanofibers and zinc oxide–copper oxide p–n junction heterostructures for the simultaneous voltammetric determination of ascorbic acid, dopamine, paracetamol, and tryptophan. *New Journal of Chemistry*, *42*(11), pp.8512-8523.

129. Rice, M.E., 2000. Ascorbate regulation and its neuroprotective role in the brain. *Trends in neurosciences*, *23*(5), pp.209-216.

130. Majidi, M.I.H.A. and Al-Gubury, H., 2016. Determination of vitamin C (ascorbic acid) contents in various fruit and vegetable by UV-spectrophotometry and titration methods. *Journal of Chemical and Pharmaceutical Sciences*, *9*(4), pp.2972-2974.

131. Tajima, S. and Pinnell, S.R., 1996. Ascorbic acid preferentially enhances type I and III collagen gene transcription in human skin fibroblasts. *Journal of dermatological science*, *11*(3), pp.250-253.

132. Johnston, C.S. and Huang, S., 1991. Effect of ascorbic acid nutriture on blood histamine and neutrophil chemotaxis in guinea pigs. *The Journal of nutrition*, *121*(1), pp.126-130.

133. Mohammed, B.M., Fisher, B.J., Kraskauskas, D., Farkas, D., Brophy, D.F. and Natarajan, R., 2013. Vitamin C: a novel regulator of neutrophil extracellular trap formation. *Nutrients*, *5*(8), pp.3131-3150.

134. Stankova, L.I.B.U.S.E., Gerhardt, N.B., Nagel, L.A.R.R.Y. and Bigley, R.H., 1975. Ascorbate and phagocyte function. *Infection and Immunity*, *12*(2), pp.252-256.

135. Sharma, P., Raghavan, S.A., Saini, R. and Dikshit, M., 2004. Ascorbate-mediated enhancement of reactive oxygen species generation from polymorphonuclear leukocytes: modulatory effect of nitric oxide. *Journal of leukocyte biology*, *75*(6), pp.1070-1078.

136. Ganguly, R., Durieux, M.F. and Waldman, R.H., 1976. Macrophage function in vitamin C-deficient guinea pigs. *The American journal of clinical nutrition*, *29*(7), pp.762-765.

137. Desneves, K.J., Todorovic, B.E., Cassar, A. and Crowe, T.C., 2005. Treatment with supplementary arginine, vitamin C and zinc in patients with pressure ulcers: a randomised controlled trial. *Clinical nutrition*, *24*(6), pp.979-987.

138. Kyaw, A., 1978. A simple colorimetric method for ascorbic acid determination in blood plasma. *Clinica chimica acta*, *86*(2), pp.153-157.

139. Washko, P.W., Hartzell, W.O. and Levine, M., 1989. Ascorbic acid analysis using high-performance liquid chromatography with coulometric electrochemical detection. *Analytical biochemistry*, *181*(2), pp.276-282.

140. Badea, M., Florescu, M., Veregut, V., Chelmea, L., Corcan, O., Floroian, L., Restani, P., Marty, J.L. and Moga, M., 2015. Optimization of electrochemical detection of L-ascorbic acid from plant food supplements using screen-printed transducers.

141. de Faria, L.V., Lisboa, T.P., de Farias, D.M., Araujo, F.M., Machado, M.M., de Sousa, R.A., Matos, M.A.C., Muñoz, R.A.A. and Matos, R.C., 2020. Direct analysis of ascorbic acid in food beverage samples by flow injection analysis using reduced graphene oxide sensor. *Food chemistry*, *319*, p.126509.

142. Silva, F.O., 2005. Total ascorbic acid determination in fresh squeezed orange juice by gas chromatography. *Food Control*, *16*(1), pp.55-58.

143. Oliveira, E.J. and Watson, D.G., 2001. Chromatographic techniques for the determination of putative dietary anticancer compounds in biological fluids. *Journal of Chromatography B: Biomedical Sciences and Applications*, *764*(1-2), pp.3-25.

144. López-Pastor, J.A., Martínez-Sánchez, A., Aznar-Poveda, J., García-Sánchez, A.J., García-Haro, J. and Aguayo, E., 2020. Quick and Cost-Effective Estimation of Vitamin C in Multifruit Juices Using Voltammetric Methods. *Sensors*, *20*(3), p.676.

145. Zhang, X., Zhang, Y.C. and Ma, L.X., 2016. One-pot facile fabrication of graphene-zinc oxide composite and its enhanced sensitivity for simultaneous electrochemical detection of ascorbic acid, dopamine and uric acid. *Sensors and Actuators B: Chemical*, *227*, pp.488-496.

146. Sun, C.L., Lee, H.H., Yang, J.M. and Wu, C.C., 2011. The simultaneous electrochemical detection of ascorbic acid, dopamine, and uric acid using graphene/size-selected Pt nanocomposites. *Biosensors and Bioelectronics*, *26*(8), pp.3450-3455.

147. Das, T.R. and Sharma, P.K., 2020. Hydrothermal-assisted green synthesis of Ni/Ag@ rGO nanocomposite using Punica granatum juice and electrochemical detection of ascorbic acid. *Microchemical Journal*, *156*, p.104850.

148. Gai, P., Zhang, H., Zhang, Y., Liu, W., Zhu, G., Zhang, X. and Chen, J., 2013. Simultaneous electrochemical detection of ascorbic acid, dopamine and uric acid based on nitrogen doped porous carbon nanopolyhedra. *Journal of Materials Chemistry B*, *1*(21), pp.2742-2749.

149. Park, S.G., Park, J.E., Cho, E.I., Hwang, J.H. and Ohsaka, T., 2006. Electrochemical detection of ascorbic acid and serotonin at a boron-doped diamond electrode modified with poly (N, N-dimethylaniline). *Research on chemical intermediates*, *32*(5), pp.595-601.

150. Ibarlucea, B., Roig, A.P., Belyaev, D., Baraban, L. and Cuniberti, G., 2020. Electrochemical detection of ascorbic acid in artificial sweat using a flexible alginate/CuO-modified electrode. *Microchimica Acta*, *187*(9), pp.1-11.

151. Silvestrini Fernandes, D. and do Carmo, D.R., 2021. Silsesquioxane modified with PAMAM Dendrimer and a Bimetallic Complex for Electrochemical detection of Ascorbic Acid. *Electroanalysis*, *33*(2), pp.365-374.

152. Aryal, K.P. and Jeong, H.K., 2020. Electrochemical detection of ascorbic acid with chemically functionalized carbon nanofiber/β-cyclodextrin composite. *Chemical Physics Letters*, *757*, p.137881.

153. Uwaya, G.E. and Fayemi, O.E., 2021. Electrochemical Detection of Ascorbic acid in Orange on Iron (III) Oxide Nanoparticles Modified Screen Printed Carbon Electrode. *Journal of Cluster Science*, pp.1-9.

154. Zhang, X., Zhang, Y.C. and Ma, L.X., 2016. One-pot facile fabrication of graphene-zinc oxide composite and its enhanced sensitivity for simultaneous electrochemical detection of ascorbic acid, dopamine and uric acid. *Sensors and Actuators B: Chemical*, *227*, pp.488-496.

155. Wang, Y., Liu, X., Lu, Z., Liu, T., Zhao, L., Ding, F., Zou, P., Wang, X., Zhao, Q. and Rao, H., 2019. Molecularly imprinted polydopamine modified with nickel nanoparticles wrapped with carbon: fabrication, characterization and electrochemical detection of uric acid. *Microchimica Acta*, *186*(7), pp.1-9.

156. Choukairi, M., Bouchta, D., Bounab, L., Elkhamlichi, R., Chaouket, F., Raissouni, I. and Rodriguez, I.N., 2015. Electrochemical detection of uric acid and ascorbic acid: application in serum. *Journal of Electroanalytical Chemistry*, *758*, pp.117-124.

157. Zhang, B., Huang, D., Xu, X., Alemu, G., Zhang, Y., Zhan, F., Shen, Y. and Wang, M., 2013. Simultaneous electrochemical determination of ascorbic acid, dopamine and uric acid with helical carbon nanotubes. *Electrochimica Acta*, *91*, pp.261-266.

158. Mazzara, F., Patella, B., Aiello, G., O'Riordan, A., Torino, C., Vilasi, A. and Inguanta, R., 2021. Electrochemical detection of uric acid and ascorbic acid using r-GO/NPs based sensors. *Electrochimica Acta*, *388*, p.138652.

159. Gai, P., Zhang, H., Zhang, Y., Liu, W., Zhu, G., Zhang, X. and Chen, J., 2013. Simultaneous electrochemical detection of ascorbic acid, dopamine and uric acid based on nitrogen doped porous carbon nanopolyhedra. *Journal of Materials Chemistry B*, *1*(21), pp.2742-2749.

160. Manjunatha, J.G., Swamy, B.K., Deraman, M. and Mamatha, G.P., 2013. Simultaneous determination of ascorbic acid, dopamine and uric acid at poly (aniline blue) modified carbon paste electrode: A cyclic voltammetric study. *Int J Pharm Pharm Sci*, *5*(2), pp.355-362.

161. Motshakeri, M., Travas-Sejdic, J., Phillips, A.R. and Kilmartin, P.A., 2018. Rapid electroanalysis of uric acid and ascorbic acid using a poly (3,4-ethylenedioxythiophene)-modified sensor with application to milk. *Electrochimica Acta*, *265*, pp.184-193.

162. Drouin, G., Godin, J.R. and Pagé, B., 2011. The genetics of vitamin C loss in vertebrates. *Current genomics*, *12*(5), pp.371-378.

163. Vissers, M.C., Carr, A.C., Pullar, J.M. and Bozonet, S.M., 2013. The bioavailability of vitamin C from kiwifruit. *Advances in food and nutrition research*, *68*, pp.125-147.

164. Yarman, A., Kurbanoglu, S. and Scheller, F.W., 2020. Noninvasive biosensors for diagnostic biomarkers. *Commercial Biosensors and Their Applications: Clinical, Food, and Beyond*, p.167.

165. Hashmi, S., 2014. Comprehensive materials processing. *Newnes*, pp 297 - 331

166. Singh, R.S., Singh, T. and Singh, A.K., 2019. Enzymes as diagnostic tools. In *Advances in enzyme technology* (pp. 225-271). Elsevier.

167. Howard, A.N., 1981. The historical development, efficacy and safety of very-low-calorie diets. *International journal of obesity*, *5*(3), pp.195-208.

168. Sica, D.A., 2004. Diuretic-related side effects: development and treatment. *The Journal of Clinical Hypertension*, *6*(9), pp.532-540.

169. Rees, F., Hui, M. and Doherty, M., 2014. Optimizing current treatment of gout. *Nature Reviews Rheumatology*, *10*(5), pp.271-283.

170. Pormsila, W., Krähenbühl, S. and Hauser, P.C., 2009. Capillary electrophoresis with contactless conductivity detection for uric acid determination in biological fluids. *Analytica chimica acta*, *636*(2), pp.224-228.

171. Kanďár, R., Drábková, P. and Hampl, R., 2011. The determination of ascorbic acid and uric acid in human seminal plasma using an HPLC with UV detection. *Journal of Chromatography B*, *879*(26), pp.2834-2839.

172. Li, X. and Franke, A.A., 2009. Fast HPLC–ECD analysis of ascorbic acid, dehydroascorbic acid and uric acid. *Journal of Chromatography B*, *877*(10), pp.853-856.

173. Inoue, K., Namiki, T., Iwasaki, Y., Yoshimura, Y. and Nakazawa, H., 2003. Determination of uric acid in human saliva by high-performance liquid chromatography with amperometric electrochemical detection. *Journal of Chromatography B*, *785*(1), pp.57-63.

174. Zhao, F.Y., Wang, Z.H., Wang, H., Zhao, R. and Ding, M.Y., 2011. Determination of uric acid in human urine by ion chromatography with conductivity detector. *Chinese Chemical Letters*, *22*(3), pp.342-345.

175. Xin, X., Zhang, M., Zhao, J., Han, C., Liu, X., Xiao, Z., Zhang, L., Xu, B., Guo, W., Wang, R. and Sun, D., 2017. Fluorescence turn-on detection of uric acid by a water-stable metal–organic nanotube with high selectivity and sensitivity. *Journal of Materials Chemistry C*, *5*(3), pp.601-606.

176. Zhang, L., Feng, J., Chou, K.C., Su, L. and Hou, X., 2017. Simultaneously electrochemical detection of uric acid and ascorbic acid using glassy carbon electrode modified with chrysanthemum-like titanium nitride. *Journal of Electroanalytical Chemistry*, *803*, pp.11-18.

177. Tukimin, N., Abdullah, J. and Sulaiman, Y., 2018. Electrochemical detection of uric acid, dopamine and ascorbic acid. *Journal of The Electrochemical Society*, *165*(7), p.B258.

178. da Cruz, F.S., de Souza Paula, F., Franco, D.L., dos Santos, W.T.P. and Ferreira, L.F., 2017. Electrochemical detection of uric acid using graphite screen-printed electrodes modified with Prussian blue/poly (4-aminosalicylic acid)/Uricase. *Journal of Electroanalytical Chemistry*, *806*, pp.172-179.

179. Reddy, Y.V.M., Sravani, B., Agarwal, S., Gupta, V.K. and Madhavi, G., 2018. Electrochemical sensor for detection of uric acid in the presence of ascorbic acid and dopamine using the poly (DPA)/SiO_2@ Fe_3O_4 modified carbon paste electrode. *Journal of Electroanalytical Chemistry*, *820*, pp.168-175.

180. Zhang, L., Feng, J., Chou, K.C., Su, L. and Hou, X., 2017. Simultaneously electrochemical detection of uric acid and ascorbic acid using glassy carbon electrode modified with chrysanthemum-like titanium nitride. *Journal of Electroanalytical Chemistry*, *803*, pp.11-18.

181. Patra, J.K. and Baek, K.H., 2014. Green nanobiotechnology: factors affecting synthesis and characterization techniques. *Journal of Nanomaterials*, *2014*.

182. Chopra, N., Gavalas, V.G., Bachas, L.G., Hinds, B.J. and Bachas, L.G., 2007. Functional one-dimensional nanomaterials: applications in nanoscale biosensors. *Analytical Letters*, *40*(11), pp.2067-2096.

183. Pérez-López, B. and Merkoçi, A., 2011. Nanomaterials based biosensors for food analysis applications. *Trends in Food Science & Technology*, *22*(11), pp.625-639.

184. Wu, W., He, Q. and Jiang, C., 2008. Magnetic iron oxide nanoparticles: synthesis and surface functionalization strategies. *Nanoscale research letters*, *3*(11), pp.397-415.

185. Eatemadi, A., Daraee, H., Karimkhanloo, H., Kouhi, M., Zarghami, N., Akbarzadeh, A., Abasi, M., Hanifehpour, Y. and Joo, S.W., 2014. Carbon nanotubes: properties, synthesis, purification, and medical applications. *Nanoscale research letters*, *9*(1), pp.1-13.

186. Iijima, S., 1991. Helical microtubules of graphitic carbon. *nature*, *354*(6348), pp.56-58.

187. Nováková, L., Solichová, D. and Solich, P., 2009. Hydrophilic interaction liquid chromatography–charged aerosol detection as a straightforward solution for simultaneous analysis of ascorbic acid and dehydroascorbic acid. *Journal of Chromatography A*, *1216*(21), pp.4574-4581.

188. Yellampalli, S. ed., 2011. *Carbon Nanotubes: Polymer Nanocomposites*. BoD–Books on Demand.

189. Dhall, S., Vaidya, G. and Jaggi, N., 2014. Joining of broken multiwalled carbon nanotubes using an electron beam-induced deposition (EBID) technique. *Journal of electronic materials*, *43*(9), pp.3283-3289.

190. Mphuthi, N.G., Adekunle, A.S., Fayemi, O.E., Olasunkanmi, L.O. and Ebenso, E.E., 2017. Phthalocyanine doped metal oxide nanoparticles on multiwalled carbon nanotubes platform for the detection of dopamine. *Scientific reports*, *7*(1), pp.1-23.

191. Bryning, M.B., 2007. *Carbon nanotube networks in epoxy composites and aerogels*. University of Pennsylvania.

192. Gupta, V. and Saleh, T.A., 2011. Syntheses of carbon nanotube-metal oxides composites; adsorption and photo-degradation. *Carbon Nanotubes-From Research to Applications*, *17*, pp.295-312.

193. Colomer, J.F., Stephan, C., Lefrant, S., Van Tendeloo, G., Willems, I., Konya, Z., Fonseca, A., Laurent, C. and Nagy, J.B., 2000. Large-scale synthesis of single-wall carbon nanotubes by catalytic chemical vapor deposition (CCVD) method. *Chemical Physics Letters*, *317*(1-2), pp.83-89.

194. Vigolo, B., Mamane, V., Valsaque, F., Le, T.H., Thabit, J., Ghanbaja, J., Aranda, L., Fort, Y. and McRae, E., 2009. Evidence of sidewall covalent functionalization of single-walled carbon nanotubes and its advantages for composite processing. *Carbon*, *47*(2), pp.411-419.

195. Hilder, T.A. and Hill, J.M., 2008. Carbon nanotubes as drug delivery nanocapsules. *Current Applied Physics*, *8*(3-4), pp.258-261.

196. Liu, Z., Tabakman, S., Welsher, K. and Dai, H., 2009. Carbon nanotubes in biology and medicine: in vitro and in vivo detection, imaging and drug delivery. *Nano research*, *2*(2), pp.85-120.

197. Hsiao, A.E., Tsai, S.Y., Hsu, M.W. and Chang, S.J., 2012. Decoration of multi-walled carbon nanotubes by polymer wrapping and its application in MWCNT/polyethylene composites. *Nanoscale research letters*, *7*(1), pp.1-5.

198. Habibi, B. and Pournaghi-Azar, M.H., 2010. Simultaneous determination of ascorbic acid, dopamine and uric acid by use of a MWCNT modified carbon-ceramic electrode and differential pulse voltammetry. *Electrochimica Acta*, *55*(19), pp.5492-5498.

199. Sims, M.J., Rees, N.V., Dickinson, E.J. and Compton, R.G., 2010. Effects of thin-layer diffusion in the electrochemical detection of nicotine on basal plane pyrolytic graphite (BPPG) electrodes modified with layers of multi-walled carbon nanotubes (MWCNT-BPPG). *Sensors and Actuators B: Chemical*, *144*(1), pp.153-158.

200. Luong, J.H., Hrapovic, S. and Wang, D., 2005. Multiwall carbon nanotube (MWCNT) based electrochemical biosensors for mediatorless detection of putrescine. *Electroanalysis: An International Journal Devoted to Fundamental and Practical Aspects of Electroanalysis*, *17*(1), pp.47-53.

201. Viswanathan, S., Rani, C. and Ho, J.A.A., 2012. Electrochemical immunosensor for multiplexed detection of food-borne pathogens using nanocrystal bioconjugates and MWCNT screen-printed electrode. *Talanta*, *94*, pp.315-319.

202. Balasubramanian, K. and Burghard, M., 2005. Chemically functionalized carbon nanotubes. *small*, *1*(2), pp.180-192.

203. Bhaskar, A., Deepa, M. and Narasinga Rao, T., 2013. MoO2/multiwalled carbon nanotubes (MWCNT) hybrid for use as a Li-ion battery anode. *ACS applied materials & interfaces*, *5*(7), pp.2555-2566.

204. Guo, J., Liu, Y., Prada-Silvy, R., Tan, Y., Azad, S., Krause, B., Pötschke, P. and Grady, B.P., 2014. Aspect ratio effects of multi-walled carbon nanotubes on electrical, mechanical, and thermal properties of polycarbonate/MWCNT composites. *Journal of Polymer Science Part B: Polymer Physics*, *52*(1), pp.73-83.

205. Saafi, M., Andrew, K., Tang, P.L., McGhon, D., Taylor, S., Rahman, M., Yang, S. and Zhou, X., 2013. Multifunctional properties of carbon nanotube/fly ash geopolymeric nanocomposites. *Construction and Building Materials*, *49*, pp.46-55.

206. Dombovari, A., Halonen, N., Sapi, A., Szabo, M., Toth, G., Mäklin, J., Kordas, K., Juuti, J., Jantunen, H., Kukovecz, A. and Konya, Z., 2010. Moderate anisotropy in the electrical conductivity of bulk MWCNT/epoxy composites. *Carbon*, *48*(7), pp.1918-1925.

207. Tóháti, H.M., Pekker, Á., Pataki, B.Á., Szekrényes, Z. and Kamarás, K., 2014. Bundle versus network conductivity of carbon nanotubes separated by type. *The European Physical Journal B*, *87*(6), pp.1-6.

208. Prato, M., Kostarelos, K. and Bianco, A., 2008. Functionalized carbon nanotubes in drug design and discovery. *Accounts of chemical research*, *41*(1), pp.60-68.

209. Viter, R. and Iatsunskyi, I., 2019. Metal oxide nanostructures in sensing. In *Nanomaterials Design for Sensing Applications* (pp. 41-91). Elsevier.

210. Chin, H.S., Cheong, K.Y. and Razak, K.A., 2010. Review on oxides of antimony nanoparticles: synthesis, properties, and applications. *Journal of materials science*, *45*(22), pp.5993-6008.

211. Orman, R.G., 2005. *Phase transitions in antimony oxides and related glasses* (Doctoral dissertation, University of Warwick).

212. Edelstein, A.S. and Cammaratra, R.C. eds., 1998. *Nanomaterials: synthesis, properties and applications*. CRC press.

213. Zhang, Z., Guo, L. and Wang, W., 2001. Synthesis and characterization of antimony oxide nanoparticles. *Journal of materials Research*, *16*(3), pp.803-805.

214. Jha, A.K., Prasad, K. and Prasad, K., 2009. A green low-cost biosynthesis of Sb2O3 nanoparticles. *Biochemical engineering journal*, *43*(3), pp.303-306.

215. Liu, Y., Zhang, Y., Zhang, M., Zhang, W., Qian, Y., Yang, L., Wang, C. and Chen, Z., 1997. Preparation of nanocrystalline antimony oxide powders by use of γ-ray radiation—oxidization route. *Materials Science and Engineering: B*, *49*(1), pp.42-45.

216. Xie, C., Hu, J., Wu, R. and Xia, H., 1999. Structure transition comparison between the amorphous nanosize particles and coarse-grained polycrystalline of cobalt. *Nanostructured Materials*, *11*(8), pp.1061-1066.

217. Xu, C.H., Shi, S.Q., Surya, C. and Woo, C.H., 2007. Synthesis of antimony oxide nano-particles by vapor transport and condensation. *Journal of materials science*, *42*(23), pp.9855-9858.

218. Karak, N. and Maiti, S., 1998. Antimony polymers. III. Flame retardant behavior of chloroprene and natural rubber vulcanizates with antimony polymer. *Journal of applied polymer science*, *68*(6), pp.927-935.

219. Mostashari, S. and Baie, S., 2008. Thermogravimetry studies of cotton fabric's flame-retardancy by means of synergism of lithium bromide and antimony trioxide. *Journal of thermal analysis and calorimetry*, *94*(1), pp.97-101.

220. Miura, N., Mizuno, H. and Yamazoe, N., 1988. Humidity sensor using antimony phosphate operative at a medium temperature of 150–250° C. *Japanese journal of applied physics*, *27*(5A), p.L931.

221. Badawy, W.A. and El-Taher, E.A., 1988. Preparation and electrochemical behaviour of some metal oxide films. *Thin Solid Films*, *158*(2), pp.277-284.

222. Sahoo, N.K. and Apparao, K.V.S.R., 1996. Process-parameter optimization of Sb 2 O 3 films in the ultraviolet and visible region for interferometric applications. *Applied Physics A*, *63*(2), pp.195-202.

223. El-Diasty, F., Abdel Wahab, F.A. and Abdel-Baki, M., 2006. Optical band gap studies on lithium aluminium silicate glasses doped with Cr 3+ ions. *Journal of applied physics*, *100*(9), p.093511.

224. Tigau, N., Ciupina, V. and Prodan, G., 2005. The effect of substrate temperature on the optical properties of polycrystalline Sb2O3 thin films. *Journal of crystal growth*, *277*(1-4), pp.529-535.

225. Le Hai, T., Hung, L.C., Phuong, T.T.B., Ha, B.T.T., Nguyen, B.S., Hai, T.D. and Nguyen, V.H., 2020. Multiwall carbon nanotube modified by antimony oxide (Sb2O3/MWCNTs) paste electrode for the simultaneous electrochemical detection of cadmium and lead ions. *Microchemical Journal*, *153*, p.104456.

226. Masibi, K.K., Fayemi, O.E., Adekunle, A.S., Sherif, E.S.M. and Ebenso, E.E., 2018. Electrocatalysis of lindane using antimony oxide nanoparticles based-SWCNT/PANI nanocomposites. *Frontiers in chemistry*, *6*, p.423.

227. Masibi, K.K., Fayemi, O.E., Adekunle, A.S., Al-Mohaimeed, A.M., Fahim, A.M., Mamba, B.B. and Ebenso, E.E., 2021. Electrochemical detection of endosulfan using an AONP-PANI-SWCNT modified glassy carbon electrode. *Materials*, *14*(4), p.723.

228. Çidem, E., Teker, T. and Aslanoglu, M., 2019. A sensitive determination of tramadol using a voltammetric platform based on antimony oxide nanoparticles. *Microchemical Journal*, *147*, pp.879-885.

229. Puangjan, A., Chaiyasith, S., Wichitpanya, S., Daengduang, S. and Puttota, S., 2016. Electrochemical sensor based on PANI/MnO2-Sb2O3 nanocomposite for selective simultaneous voltammetric determination of ascorbic acid and acetylsalicylic acid. *Journal of Electroanalytical Chemistry*, *782*, pp.192-201.

230. Düzmen, Ş. and Aslanoglu, M., 2021. An electrochemical platform of bimetallic oxide (Sb2O3@ WO3) nanoparticles and carbon nanotubes for the sensitive determination of metaproterenol in pharmaceuticals and biological samples. *Measurement*, *173*, p.108572.

231. Kadhim, B.B., Salim, F.M. and Muhsen, H.O., Thermal Properties of Carbon Nano Tubes Reinforced Epoxy Resin Nano Composites.

232. Uwaya, G.E. and Fayemi, O.E., 2021. Electrochemical detection of choline at f-MWCNT/Fe_3O_4 nanocomposite modified glassy carbon electrode. *Materials Research Express*, *8*(5), p.055403.

233. Masibi, K.K., Fayemi, O.E., Adekunle, A.S., Sherif, E.S.M. and Ebenso, E.E., 2018. Electrocatalysis of lindane using antimony oxide nanoparticles based-SWCNT/PANI nanocomposites. *Frontiers in chemistry*, *6*, p.423.

234. Sun, J., Cui, B., Chu, F., Yun, C., He, M., Li, L. and Song, Y., 2018. Printable nanomaterials for the fabrication of high-performance supercapacitors. *Nanomaterials*, *8*(7), p.528.

235. Redepenning, J.G., 1987. Chemically modified electrodes: a general overview. *TrAC Trends in Analytical Chemistry*, *6*(1), pp.18-22.

236. Taleat, Z., Khoshroo, A. and Mazloum-Ardakani, M., 2014. Screen-printed electrodes for biosensing: a review (2008–2013). *Microchimica Acta*, *181*(9-10), pp.865-891.

237. Rodríguez-Méndez, M.L., Gay, M., Apetrei, C. and De Saja, J.A., 2009. Biogenic amines and fish freshness assessment using a multisensor system based on voltammetric electrodes. Comparison between CPE and screen-printed electrodes. *Electrochimica Acta*, *54*(27), pp.7033-7041.

238. Kissinger, P. and Heineman, W.R. eds., 2018. *Laboratory Techniques in Electroanalytical Chemistry, revised and expanded*. CRC press.

239. Neves, M.M., Nouws, H. and Delerue-Matos, C., 2010. Carbon surfaces for the oxidative quantification of pravastatin: glassy-carbon vs. screen-printed carbon electrodes. *Journal of Food and Drug Analysis*, *18*(5), pp.353-357.

240. Renedo, O.D., Alonso-Lomillo, M.A. and Martínez, M.A., 2007. Recent developments in the field of screen-printed electrodes and their related applications. *Talanta*, *73*(2), pp.202-219.

241. Li, M., Li, Y.T., Li, D.W. and Long, Y.T., 2012. Recent developments and applications of screen-printed electrodes in environmental assays—A review. *Analytica chimica acta*, *734*, pp.31-44.

242. Beitollahi, H., Mohammadi, S.Z., Safaei, M. and Tajik, S., 2020. Applications of electrochemical sensors and biosensors based on modified screen-printed electrodes: a review. *Analytical Methods*, *12*(12), pp.1547-1560.

243. Murray, R.W., 1980. Chemically modified electrodes. *Accounts of Chemical Research*, *13*(5), pp.135-141.

244. Durst, R.A., 1997. Chemically modified electrodes: recommended terminology and definitions (IUPAC Recommendations 1997). *Pure and applied chemistry*, *69*(6), pp.1317-1324.

245. Foss Jr, C.A. and Martin, C.R., 1994. *Chemically Modified Electrodes*. colorado state univ fort collins dept of chemistry.

246. Song, Y., Xu, C., Kuroki, H., Liao, Y. and Tsunoda, M., 2018. Recent trends in analytical methods for the determination of amino acids in biological samples. *Journal of pharmaceutical and biomedical analysis*, *147*, pp.35-49.

247. Mirceski, V. and Gulaboski, R., 2014. Recent achievements in square-wave voltammetry (a review). *Macedonian Journal of Chemistry and Chemical Engineering*, *33*(1), pp.1-12.

248. Mirceski, V., Skrzypek, S. and Stojanov, L., 2018. Square-wave voltammetry. *ChemTexts*, *4*(4), pp.1-14.

249. Zoski, C.G. ed., 2006. *Handbook of electrochemistry*. Elsevier.

250. Jadon, N., Jain, R., Sharma, S. and Singh, K., 2016. Recent trends in electrochemical sensors for multianalyte detection–A review. *Talanta*, *161*, pp.894-916.

251. Jindra, J., 2010. The Long Way to Success: Jaroslav Heyrovský and the Nobel Prize. *Electroanalysis*, *22*(17-18), pp.1933-1936.

252. Kounaves, S.P., 1997. Voltammetric techniques. *Handbook of instrumental techniques for analytical chemistry*, pp.709-726.

253. Gupta, V.K., Jain, R., Radhapyari, K., Jadon, N. and Agarwal, S., 2011. Voltammetric techniques for the assay of pharmaceuticals—a review. *Analytical biochemistry*, *408*(2), p.179.

254. Scholz, F., 2015. Voltammetric techniques of analysis: the essentials. *ChemTexts*, *1*(4), pp.1-24.

255. Van Leeuwen, H., Cleven, R.F.M.J. and Buffle, J.A.C.Q.U.E.S., 1989. Voltammetric techniques for complexation measurements in natural aquatic media: role of the size of macromolecular ligands and dissociation kinetics of complexes. *Pure and Applied Chemistry*, *61*(2), pp.255-274.

256. Nicholson, R.S. and Shain, I., 1964. Theory of stationary electrode polarography. Single scan and cyclic methods applied to reversible, irreversible, and kinetic systems. *Analytical chemistry*, *36*(4), pp.706-723.

257. Elgrishi, N., Rountree, K.J., McCarthy, B.D., Rountree, E.S., Eisenhart, T.T. and Dempsey, J.L., 2018. A practical beginner's guide to cyclic voltammetry. *Journal of chemical education*, *95*(2), pp.197-206.

258. Geiger, W.E. and Barrière, F., 2010. Organometallic electrochemistry based on electrolytes containing weakly coordinating fluoroarylborate anions. *Accounts of chemical research*, *43*(7), pp.1030-1039.

259. DuVall, S.H. and McCreery, R.L., 1999. Control of catechol and hydroquinone electron-transfer kinetics on native and modified glassy carbon electrodes. *Analytical Chemistry*, *71*(20), pp.4594-4602.

260. Nicholson, R.S., 1965. Theory and application of cyclic voltammetry for measurement of electrode reaction kinetics. *Analytical chemistry*, *37*(11), pp.1351-1355.

261. Bond, A.M. and Feldberg, S.W., 1998. Analysis of simulated reversible cyclic voltammetric responses for a charged redox species in the absence of added electrolyte. *The Journal of Physical Chemistry B*, *102*(49), pp.9966-9974.

262. Espinoza, E.M., Clark, J.A., Soliman, J., Derr, J.B., Morales, M. and Vullev, V.I., 2019. Practical aspects of cyclic voltammetry: How to estimate reduction potentials when irreversibility prevails. *Journal of The Electrochemical Society*, *166*(5), p.H3175.

263. Geiger, W.E., 2011. Reflections on future directions in organometallic electrochemistry. *Organometallics*, *30*(1), pp.28-31.

264. Birke, R.L., Kim, M.H. and Strassfeld, M., 1981. Diagnosis of reversible, quasi-reversible, and irreversible electrode processes with differential pulse polarography. *Analytical Chemistry*, *53*(6), pp.852-856.

265. Kissinger, P.T. and Heineman, W.R., 1983. Cyclic voltammetry. *Journal of Chemical Education*, *60*(9), p.702.

266. Mirceski, V., Komorsky-Lovric, S. and Lovric, M., 2007. *Square-wave voltammetry: theory and application*. Springer Science & Business Media.

267. De Souza, D., Machado, S.A. and Pires, R.C., 2006. Multiple square wave voltammetry for analytical determination of paraquat in natural water, food, and beverages using microelectrodes. *Talanta*, *69*(5), pp.1200-1207.

268. Dias, L.G., Meirinho, S.G., Veloso, A.C., Rodrigues, L.R. and Peres, A.M., 2017. Electronic tongues and aptasensors. In *Bioinspired Materials for Medical Applications* (pp. 371-402). Woodhead Publishing.

269. Geisler, J. and Thompson, T., 2015. Choosing the Best Detection Method: Absorbance vs. Fluorescence, 2015.

270. De Caro, C. and Haller, C., 2015. UV/VIS spectrophotometry-fundamentals and applications. *Mettler-Toledo International*, pp.4-14.

271. Caro, C., 2015. UV/VIS Spectrophotometry–Fundamentals and Application. *Mettler-Toledo Publication*.

272. Azároff, L.V., 1980. X-ray diffraction by liquid crystals. *Molecular Crystals and Liquid Crystals*, *60*(1-2), pp.73-97.

273. Kibasomba, P.M., Dhlamini, S., Maaza, M., Liu, C.P., Rashad, M.M., Rayan, D.A. and Mwakikunga, B.W., 2018. Strain and grain size of TiO2 nanoparticles from TEM, Raman spectroscopy and XRD: The revisiting of the Williamson-Hall plot method. *Results in Physics*, *9*, pp.628-635.

274. Irfan, H., Racik K, M. and Anand, S., 2018. Microstructural evaluation of CoAl2O4 nanoparticles by Williamson–Hall and size–strain plot methods. *Journal of Asian Ceramic Societies*, *6*(1), pp.54-62.

275. kalita, o.c.p., doley, p. and kalita, a., 2017. 2. Uses of transmission electron microscope in microscopy and its advantages and disadvantages by op choudhary, pc kalita, pj doley and a. kalita. *life sciences leaflets*, *85*, pp.8

276. Zaefferer, S., 2011. A critical review of orientation microscopy in SEM and TEM. *Crystal Research and Technology*, *46*(6), pp.607-628.

277. Amrine Jr, J.W. and Manson, D.C.M., 1996. 1.6. 3 Preparation, mounting and descriptive study of eriophyoid mites. *World crop pests*, *6*, pp.383-396.

278. McMullan, D., 1995. Scanning electron microscopy 1928–1965. *Scanning*, *17*(3), pp.175-185.

279. Chen, X.Y., Huh, H.S. and Lee, S.W., 2008. Hydrothermal synthesis of antimony oxychloride and oxide nanocrystals: $Sb_4O_5Cl_2$, $Sb_8O_{11}Cl_2$, and Sb_2O_3. *Journal of Solid State Chemistry*, *181*(9), pp.2127-2132.

280. Ba Hashwan, S.S., Fatin, M.F., Ruslinda, A.R., Md Arshad, M.K., Hashim, U. and Ayub, R.M., 2015. Functionalization of Multi Wall Carbon Nanotubes Using Nitric Acid Oxidation. In *Applied Mechanics and Materials* (Vol. 754, pp. 1156-1160). Trans Tech Publications Ltd.

281. Jamal, A., Rahman, M.M., Faisal, M. and Khan, S.B., 2011. Studies on photocatalytic degradation of acridine orange and chloroform sensing using as-grown antimony oxide microstructures. *Materials Sciences and Applications*, *2*(06), p.676.

282. Jamal, A., Raahman, M.M., Khan, S.B., Abdullah, M.M., Faisaal, M., Asiri, A.M., Aslam, A., Khan, P. and Akhtar, K., 2013. Simple growth and characterization of α-Sb_2O_4: Evaluation of their photo-catalytic and chemical sensing applications. *J. Chem. Soc. Pak*, *35*(3), p.570.

283. Jamal, A., Raahman, M.M., Khan, S.B., Abdullah, M.M., Faisaal, M., Asiri, A.M., Aslam, A., Khan, P. and Akhtar, K., 2013. Simple growth and characterization of α-Sb_2O_4: Evaluation of their photo-catalytic and chemical sensing applications. *J. Chem. Soc. Pak*, *35*(3), p.570.

284. Zuber, A., Purdey, M., Schartner, E., Forbes, C., Van der Hoek, B., Giles, D., Abell, A., Monro, T. and Ebendorff-Heidepriem, H., 2016. Detection of gold nanoparticles with different sizes using absorption and fluorescence based method. *Sensors and Actuators B: Chemical*, *227*, pp.117-127.

285. Ahmed, D.S., Haider, A.J. and Mohammad, M.R., 2013. Comparesion of functionalization of multi-walled carbon nanotubes treated by oil olive and nitric acid and their characterization. *Energy Procedia*, *36*, pp.1111-1118.

286. Abuilaiwi, F.A., Laoui, T., Al-Harthi, M. and Atieh, M.A., 2010. Modification and functionalization of multiwalled carbon nanotube (MWCNT) via fischer esterification. *The Arabian Journal for Science and Engineering*, *35*(1), pp.37-48.

287. Buchholcz, B., Haspel, H., Boldizsár, T., Kukovecz, Á. and Kónya, Z., 2017. pH-regulated antimony oxychloride nanoparticle formation on titanium oxide nanostructures: a photocatalytically active heterojunction. *CrystEngComm*, *19*(10), pp.1408-1416.

288. Rabiei, M., Palevicius, A., Monshi, A., Nasiri, S., Vilkauskas, A. and Janusas, G., 2020. Comparing methods for calculating nano crystal size of natural hydroxyapatite using X-ray diffraction. *Nanomaterials*, *10*(9), p.1627.

289. Cheraghali, R., 2011. Effect of dry & wet oxidation of multi walled carbon nanotubes on their structures. *International Journal of Academic Research*, *3*(2).

290. Sharma, S., Singh, N., Tomar, V. and Chandra, R., 2018. A review on electrochemical detection of serotonin based on surface modified electrodes. *Biosensors and Bioelectronics*, *107*, pp.76-93.

291. Mohd Bakhori, N., Yusof, N.A., Abdullah, J., Wasoh, H., Ab Rahman, S.K. and Abd Rahman, S.F., 2020. Surface enhanced CdSe/ZnS QD/SiNP electrochemical immunosensor for the detection of Mycobacterium tuberculosis by combination of CFP10-ESAT6 for better diagnostic specificity. *Materials*, *13*(1), p.149.

292. Nineza, C., 2010. Application of surface modified electrodes in the study of selected pharmaceutical drugs-antimalarials, analgesics, antibiotics and herbal preparations (Doctoral dissertation, University of Nairobi, Kenya).

293. Wang, J., 1991. Modified electrodes for electrochemical sensors. *Electroanalysis*, *3*(4-5), pp.255-259.

294. Okpara, E.C. and Fayemi, O.E., 2019. Comparative study of spectroscopic and cyclic voltammetry properties of CuONPs from citrus peel extracts. *Materials Research Express*, *6*(10), p.105056.

295. Fayemi, O.E., Adekunle, A.S. and Ebenso, E.E., 2015. Metal oxide nanoparticles/multi-walled carbon nanotube nanocomposite modified electrode for the detection of dopamine: comparative electrochemical study. *J. Biosens. Bioelectron*, *6*(4), pp.10-4172.

296. Laviron, E.J.J., 1979. General expression of the linear potential sweep voltammogram in the case of diffusionless electrochemical systems. *Journal of Electroanalytical Chemistry and interfacial electrochemistry*, *101*(1), pp.19-28.

297. Fayemi, O.E., Adekunle, A.S. and Ebenso, E.E., 2015. Metal oxide nanoparticles/multi-walled carbon nanotube nanocomposite modified electrode for the detection of dopamine: comparative electrochemical study. *J. Biosens. Bioelectron*, *6*(4), pp.10-4172.

298. Wu, Y., Deng, P., Tian, Y., Feng, J., Xiao, J., Li, J., Liu, J., Li, G. and He, Q., 2020. Simultaneous and sensitive determination of ascorbic acid, dopamine and uric acid via an electrochemical sensor based on PVP-graphene composite. *Journal of Nanobiotechnology*, *18*(1), pp.1-13.

299. Tashkhourian, J., Nezhad, M.H., Khodavesi, J. and Javadi, S., 2009. Silver nanoparticles modified carbon nanotube paste electrode for simultaneous determination of dopamine and ascorbic acid. *Journal of Electroanalytical Chemistry*, *633*(1), pp.85-91.

300. Zuo, X., Zhang, H. and Li, N., 2012. An electrochemical biosensor for determination of ascorbic acid by cobalt (II) phthalocyanine–multi-walled carbon nanotubes modified glassy carbon electrode. *Sensors and Actuators B: Chemical*, *161*(1), pp.1074-1079.

301. Gu, B., Liu, Z., Wang, X. and Dong, X., 2016. RF magnetron sputtering synthesis of carbon fibers/ZnO coaxial nanocable microelectrode for electrochemical sensing of ascorbic acid. *Materials Letters*, *181*, pp.265-267.